

GRAIN GROWTH AND MECHANICAL PROCESSES
IN TWO-PHASED SYNTHETIC MARBLES AND NATURAL FAULT GOUGE

by

David LeClair Olgaard

B.S., Cornell University
(1978)

SUBMITTED TO THE DEPARTMENT OF
EARTH, ATMOSPHERIC, AND PLANETARY SCIENCES
IN PARTIAL FULFILLMENT
OF THE REQUIREMENTS
FOR THE DEGREE OF

DOCTOR OF PHILOSOPHY

at the

© MASSACHUSETTS INSTITUTE OF TECHNOLOGY

May 1985

Massachusetts Institute of Technology 1985

Signature of Author _____
Department of Earth, Atmospheric, and Planetary Sciences

Certified by _____
Brian Evans
Thesis Supervisor

and _____
William F. Brace
Thesis Supervisor

Accepted by _____
Theodore R. Madden
Chairman, Department Committee

MASSACHUSETTS INSTITUTE OF TECHNOLOGY
WITHDRAWN
MAY 30 1985
FROM
MIT LIBRARIES

GRAIN GROWTH AND MECHANICAL PROCESSES
IN TWO-PHASED SYNTHETIC MARBLES AND NATURAL FAULT GOUGE

by

David LeClair Olgaard

submitted to
the Department of Earth, Atmospheric, and Planetary Sciences
on May 1, 1985 in partial fulfillment of the
requirements for the degree of Doctor of Philosophy in
Geophysics

ABSTRACT

The formation and behavior of fault gouge and fine-grained rocks are fundamental to the understanding of several earth processes including solid-state metamorphism and fault- and shear-zone development. Thermomechanical processes in fine-grained natural fault-gouge and in synthetic marbles have been investigated using several characterization and fabrication techniques commonly used by materials scientists.

Unaltered quartz fault gouge was collected from two mining-induced seismic shear-fractures. This gouge was studied to determine that portion of the total energy released during an earthquake allocated to creating new surfaces. Electron microscopy showed that: 1) The particles ranged in size from the original grain size of the country rock to less than 0.05 μm , and 2) Large particles were conchoidally fractured and slightly rounded, while submicron-sized particles were highly angular and commonly showed basal plane cleavage. Specific surface areas of 0.7 to 2.0 m^2/g were measured for the two samples by X-ray sedimentation and nitrogen absorption (BET) techniques. The surface energy was found to be 1 to 10% of the total energy released during an earthquake, and therefore on the order of the seismic energy.

In order to further our understanding of the behavior of fine-grained rocks at high temperatures, synthetic marbles were fabricated by hot isostatically pressing fine powders into dense composites. A standardized two-step process was developed to produce high density starting materials with reproducible grain-boundary morphologies, dislocation densities, grain sizes, and other microstructures. The effect of second phases, i.e. both particles and pores, on thermally-induced grain growth and ductile deformation behavior was clearly evident.

Grain growth experiments were performed at 700° to 900°C, and 300 to 400 MPa confining pressure for up to 24 hours. Grain growth in the synthetic marbles behaved according to a normal growth law for pore-drag or fluid-boundary controlled growth. When non-reacting alumina particles were dispersed in the calcite matrix, a stable, limiting grain size was reached which depended upon the size and volume fraction of the alumina particles. The dependence of the limiting grain-size on volume fraction was weaker than predicted by the more generally accepted models, but agreed with the results from several other studies on both metals and ceramics and with models which restricted the relative locations of the dispersed particles. Mica plates affected the limiting grain-size in a manner similar to alumina particles; however, the "effective" grain size was difficult to measure. A grain-boundary fluid phase was identified in all samples containing water ("wet") in which grain growth was measured.

Separate experiments showed that the kinetics of grain growth were affected by variations of porosity, the presence of distilled water, the addition of a MnCl_2 solution, and, in a few cases, copper-jacket contamination. Pores were dispersed both intra- and intergranularly. The intergranular pores increased in size as the grain size increased. Pores interacted with grain boundaries in ways similar to particles' interactions, although the pores were more mobile. The major difference between the behavior of wet and dry synthetic marbles was due to contamination by the copper jacket in the dry experiments. The presence of a solution containing the substitutional cation Mn^{++} drastically increased the rate of grain growth.

Grain growth data for Solenhofen limestone was compared to that for the synthetic marbles. The rate of grain growth in Solenhofen depended on the confining pressure and was lower than the synthetic marbles in all cases. This behavior was presumably due to the presence of clay and quartz particles and pores in Solenhofen limestone.

Several experiments were performed to explore the mechanical behavior of synthetic marbles at 700°C, and 100 MPa confining pressure, at strain rates of 10^{-3} , 10^{-4} , and 10^{-5} s^{-1} , and at strains of up to 50%. Our experiments showed that: 1) Additions of 5% of 1.0 μm alumina particles increased the flow stress by 10% or more in the fine-grained specimens. 2) Wet specimens were a few percent weaker than similarly treated dry ones. 3) The flow stress depended inversely on grain size, with a decrease in the dependence with increasing grain size. 4) The amount of grain flattening was found to be grain-size dependent. 5) The data are more consistent with a strain-accommodation mechanism involving dynamic recrystallization than with grain boundary sliding; however, several inconsistencies remain to be resolved. 6) The synthetic marbles are significantly weaker than either Solenhofen limestone or Carrera marble deformed in the power-law creep regime. 7) The transition from power-law creep to superplasticity, previously recognized in Solenhofen limestone, was not immediately apparent in the synthetic marbles.

Several thermomechanical processes known to occur in fine-grained natural rocks have been explored using synthetic marbles. The results of this study support the use of synthetic rocks to understand solid-state static and dynamic metamorphic processes in the earth.

Thesis Supervisors: Brian Evans, Assistant Professor of Geophysics
William F. Brace, Cecil and Ida Green Professor of
Geology

DEDICATION

To my brother Roger,
through enthusiasm, optimism, and example, he taught
me to reach higher and to grasp every opportunity to
live a little.

"Luke--tell me. What do you love most in the world?..."

"In the entire world?"

"Yes!"

It was dawn before he came up with the answer.

"Triples."

The Great American Novel
by Philip Roth

TABLE OF CONTENTS

	<u>page</u>
TITLE PAGE	i
ABSTRACT	ii
DEDICATION	v
TABLE OF CONTENTS	vi
INTRODUCTION	1
CHAPTER 1. THE MICROSTRUCTURE OF GOUGE FROM A MINING-INDUCED SEISMIC SHEAR ZONE	5
Introduction	5
Description of the Shear Zones	7
Microscopy	8
SEM observations	9
TEM observations	10
Specific Surface Area Measurements	13
X-ray sedimentation	13
Gas adsorption	15
Results and discussion	16
Estimates of the Surface Area Energy	18
Summary	20
Bibliography	22
Tables	24
Figure Captions	26
Figures	27
CHAPTER 2. EFFECTS OF ALUMINA PARTICLES AS A SECOND PHASE IN CALCITE GRAIN-GROWTH EXPERIMENTS	33
Introduction	33
Review of Models for Particle-Grain Boundary Interactions	34
Experimental Method	36
Results	39
Grain growth and the establishment of a pinned state	39
Microstructure: Observations and comparisons	41
D_{\max} dependence on d and f	43
Discussion	46
Comparison with other experiments	46
Comparison of data to models	47

	<u>page</u>
Summary and Conclusions	50
Bibliography	52
Tables	54
Figure Captions	60
Figures	62
CHAPTER 3. RECRYSTALLIZATION AND GRAIN GROWTH OF PURE CALCITE AND CALCITE/MICA SYNTHETIC MARBLES	72
Introduction	72
Recrystallization in geologic materials	74
Mechanisms and models	76
Primary recrystallization, grain growth and secondary recrystallization	76
Particle-limited grain size	78
Experimental Method	79
Results	82
Densification and primary recrystallization	82
Microscopic observations	83
Kinetics of grain growth	85
Inhibition of grain growth by mica particles	86
Effects of pores on grain growth	88
Enhancement and suppression of grain growth by water and ionic impurities	90
Synthetic marbles vs. Solenhofen limestone	91
Discussion	93
Kinetics of grain growth	93
Comparison with alumina particle data and theoretical models	97
Straining prior to grain growth	98
The effects of pores and other ionic impurities	99
Application of results to grain growth in Solenhofen limestone	101
Applications to paleopiezometry	103
Summary and Conclusions	104
Bibliography	106
Tables	110
Figure Captions	118
Figures	120
CHAPTER 4. EFFECTS OF VARIATIONS IN GRAIN SIZE, SECOND-PHASE PARTICLE CONTENT AND WATER ON THE MECHANICAL PROPERTIES OF SYNTHETIC MARBLE	133
Introduction	133
Experimental Method	135
Results	140
Optical and transmission electron microscopy	141
Stress-strain behavior	144

	<u>page</u>
Discussion	147
Flow stress dependence on alumina particles and water	147
Flow stress dependence on grain size	148
Strain accommodation	150
Comparision to Solenhofen limestone	152
Summary	154
Recommendations for Future Work	155
Bibliography	157
Table	159
Figure Captions	160
Figures	162
Bibliography	182
APPENDIX 1 . THE DEPENDENCE OF D_{max} ON d AND f WHEN ALL GRAINS LIE ON GRAIN BOUNDARIES	177
Figure Caption	179
Figure	180
APPENDIX 2 CALCULATION OF THE NUMBER DISTRIBUTION CURVES FOR GRAIN SIZE FROM X-RAY SEDIMENTATION DATA	181
Figure Captions	185
Figures	186
APPENDIX 3 TECHNIQUE USED TO IDENTIFY THIN INTERGRANULAR FILMS ...	191
Table	194
Figure Captions	195
Figures	196
BIBLIOGRAPHY FOR APPENDICES	198
BIOGRAPHICAL NOTE	199
ACKNOWLEDGEMENTS	201

INTRODUCTION

The thermomechanical behavior of fine-grained materials is of fundamental interest to geoscientists. Fine-grained fault gouge forms during brittle rupture and slip along both newly formed and pre-existing faults and is intimately related to seismicity and strain-energy release rate. Fine-grained rocks are commonly associated with the most highly strained regions of deep-seated ductile shear zones and are believed to be responsible for strain localization by grain-size sensitive deformation processes. To investigate the relationship of grain size to both brittle and ductile deformation, as well as other static processes, rock mechanics have traditionally used natural specimens with differing grain sizes, mineralogies, porosities, and second phases. Recently, there has been growing interest in fabricating synthetic rocks from fine powders using sintering and hot-pressing techniques developed by ceramists. The advantages of investigating grain-size sensitive processes with synthetic rocks as opposed to natural ones are that their grain size, second phase content, and porosity can be controlled and varied independently. The purposes of the present study were: 1) to apply techniques commonly used by metallurgists and ceramists to characterize fine-grained geologic materials; 2) to explore the thermal and mechanical behavior of fine-grained synthetic rocks; and 3) to compare the behavior of these synthetic rocks to natural rocks.

Unaltered fault gouge was collected from two mining-induced shear fractures and was analyzed, as discussed in Chapter 1, in order to determine that portion of the total energy released during an earthquake allocated to creating new surfaces. Several techniques were used to

characterize the shapes and microstructures, and to determine the specific surface area of the fault gouge. It was determined that the surface energy could be 1 to 10% of the total energy released during an earthquake and, therefore, of the same order as the seismic energy. The microscopy and particle sizing techniques developed during this study were applied to characterize the initial powders used to fabricate the synthetic marbles described in Chapters 2, 3, and 4.

Chapters 2 through 4 present the results of the first study devoted exclusively to the fabrication and high-temperature static and dynamic behavior of synthetic rocks. Calcite is an important rock-forming mineral that is intimately involved in many ductile shear zones. Several other scientists have conducted experimental studies at high temperatures and pressures on both coarse- and fine-grained natural marbles. In fact, it was in fine-grained Solenhofen limestone that superplastic behavior was first experimentally documented in a natural rock. Additionally, the accessibility of temperatures and pressures required to produce relatively dense calcite aggregates and to induce many thermally-activated microstructural transformations made calcite a favorable choice for our experiments.

Chapters 2 and 3 are devoted to the effects of minor second phases on grain growth. The initial experiments, described in Chapter 3, involved developing a standard fabrication technique, determining the kinetics of grain growth in pure calcite marbles, and determining the effects of minor amounts of mica particles on both the kinetics of grain growth and the particle-limited calcite grain size. In Chapter 2, a standardized, two-step fabrication technique which produced the highest-density samples and the most reproducible microstructures is

described. Chapter 2 also discusses the effects of variations in the size and concentration of nearly rigid alumina particles on the stable, particle-limited grain size. Although the limiting grain-size varied systematically with the alumina particle-size and volume fraction, the dependence of the calcite grain size on the volume fraction of alumina was weaker than expected. Another significant observation was that a grain-boundary "melt" phase, identified in wet specimens using TEM, probably affected the mechanism(s) of grain growth.

In Chapter 3, several parameters known to affect grain growth and recrystallization are described. Many observations of the effects of pores were made during the development of the standardized fabrication technique. Porosity had a significant effect on the kinetics of grain growth, and attempts to eliminate or even control its effects proved to be much more difficult than anticipated. The emphases of Chapter 3, though, are the effects on grain growth of mica particles, water, copper contamination, and a MnCl_2 solution. These results are compared to the grain growth behavior of Solenhofen limestone, as observed by others. The rate of grain growth in the pure-calcite synthetic marbles was always faster than in the Solenhofen limestone, presumably because of the presence of detrital second phases and pores in the latter. However, other researchers have found that the growth rate could be increased in Solenhofen by applying a higher confining pressure which presumably reduced the porosity. When contamination problems were eliminated from the dry experiments, distilled water did not significantly increase the rate of grain growth. However, the rate was significantly increased by the presence of a MnCl_2 solution.

Chapter 4 describes a series of experiments designed to test the mechanical behavior of these synthetic marbles. The effects of second-phase particles, water, and grain size on the steady-state flow stress are presented and compared to similar experiments performed by others on Solenhofen limestone and Carrera marble. We observed that:

- 1) nearly rigid particles increased the strength of synthetic marbles;
- 2) the presence of water slightly decreased the strength;
- 3) there was a significant decrease in strength with increasing grain size, particularly in the finer-grained marbles; and
- 4) the transition to a more grain-size sensitive flow behavior, documented in Solenhofen limestone, was not recognized in the synthetic marbles in multiple strain-rate experiments.

The results of this study indicate that several parameters including grain size, second-phase particles, and water need to be considered in order to predict the behavior of rocks in the earth, particularly when processes occurring along grain boundaries are involved.

Each of the four chapters is intended to be read as a separate unit. Each chapter includes a general introduction, procedure, results, discussion, and a final summary. The last three chapters describe several experiments applicable to the understanding of solid-state metamorphism of natural rocks, performed on hot-pressed synthetic marbles.

CHAPTER 1

THE MICROSTRUCTURE OF GOUGE FROM A MINING-INDUCED SEISMIC SHEAR ZONE

INTRODUCTION

The three principal sinks for the strain energy released during faulting are heat, seismic waves, and microstructural defects formed during crushing. New surfaces are the principal defects produced at shallow crustal depths; therefore the "defect" energy will be mostly surface energy. Energy flux as heat or seismic radiation is known to an order of magnitude (Lachenbruch and Sass, 1980; Scholz, 1980), but estimates of surface energy range over several orders of magnitude (compare Engelder et al., 1975 and McGarr et al., 1979). The surface energy is given by:

$$E_A = S_T \Gamma \quad (1)$$

where S_T is the total surface area created during faulting and Γ is the specific surface energy. For most common minerals, e.g. quartz, Γ is known to within a factor of two (Brace and Walsh, 1962). A reasonable estimate of E_A will therefore depend on the accuracy of the measurement of S_T . S_T is poorly known for two reasons:

- 1) fault gouge contains particles too small to be measured accurately with conventional methods; and
- 2) fine particles may rapidly change their size, shape, and mineralogy during weathering, making S_T unobtainable a short time after the faulting event.

To make an accurate estimate of S_T fault gouge, is needed from the site of a very recent earthquake. Most earthquakes emanate from depths of several kilometers or more; thus sampling can only be done by deep drilling or mining. In deep South African gold mines, mining-induced faults produce fresh fault gouge that can be sampled almost immediately following the faulting event. Since the tectonic setting and seismicity of these faults have been extensively studied (McGarr et al., 1979; Gay and Ortlepp, 1979; McGarr et al., 1975) not only can S_T be measured, but the ratio of surface energy to the total energy can also be determined with confidence. In this study, scanning and transmission electron microscopy (SEM and TEM), X-ray sedimentation, and gas adsorption were used to measure S_T and to study particle size and shape in the submicron-size region. The results follow the description of the methods.

It seems appropriate at this time to clarify a few key terms. Normally fault zones are not simple planar features but are instead made up of multiple shear fractures. Fault gouge, defined by Engelder (1974), is "shattered rock so severely deformed that the few surviving grains are almost surrounded by a fine-grained matrix of crushed grains. Gouge is restricted to shear fractures and larger slip planes within the fault zone." The initial grain size of the country rock was chosen as the upper limit of particle size, and minor effects due to the cementing matrix or secondary minerals have been ignored. The widths and displacements quoted below are averages for individual shear fractures and are not necessarily those of the fault zone as a whole.

DESCRIPTION OF THE SHEAR ZONES

Fault gouge was collected by W.D. Ortlepp and S.M. Spottiswoode from two shear fractures in the Witwatersrand quartzite at a depth of 2 km in a gold mine operated by East Rand Proprietary Mines, Ltd., Boksburg, South Africa. The "old" gouge, exposed to the mine atmosphere for six years, is from a fracture in shear zone "A" (Figure 1) of Gay and Ortlepp (1979) which has been associated with an earthquake of magnitude 2.1 that occurred on September 23, 1970 (Ortlepp, 1978). The seismic signature of this earthquake is remarkably similar to that of other small- to medium-sized earthquakes (McGarr et al., 1979). The "fresh" gouge, exposed for three days, is from a small mining-induced fracture (Figure 2) of a different attitude, and therefore probably of a different age than shear zone "A" (Ortlepp, written comm., 1980). The Witwatersrand quartzite is nearly pure quartz and has an average grain size of about 0.5 mm. It is essentially dry, has negligible porosity, and has not been chemically altered prior to exposure in the mine.

Gay and Ortlepp (1979) and McGarr et al. (1979) have described shear zone "A" in detail. It strikes subparallel to and dips steeply away from the working face, has normal displacement, and does not follow a pre-existing fault. The zone is composed of en echelon shears connected by subsidiary conjugate shears and extension fractures. Gouge developed along all three types of fractures but is confined mostly to the main fractures, which are 10 to 50 mm wide and have offsets as large as 100 mm but averaging 50 to 60 mm. The zone covers an area of approximately 600 m² (Ortlepp, written comm., 1980) and dies out into diffuse conjugate shears and extension fractures. McGarr et al.

(1979) calculated an average driving stress for seismic failure of between 40 and 70 MPa. The 70 MPa value is from overcoring strain-relief measurements at a depth of 3.1 km. The 40 MPa value was calculated from experimental data of Spottiswoode (1978). The validity of a term called the crushing energy (McGarr et al., 1979) that was used to calculate the latter value has been questioned by Wong (1982).

MICROSCOPY

The fault gouge was analyzed with a scanning electron microscope (SEM) and a 100 kV transmission electron microscope (TEM). The objectives of the microscopy investigations were:

- 1) to characterize the size, shape, and surface morphology of the particles;
- 2) to determine the smallest particle size;
- 3) to investigate styles of fracturing, whether conchoidal or cleavage; and
- 4) to determine the degree of alteration by comparing the fresh and the old gouge.

Optical microscopy has been used to describe quartz fault gouge formed in naturally (Gay and Ortlepp, 1979) and experimentally (Engelder et al., 1975; Engelder, 1974) deformed rocks. Optical microscopy was not used here, except to examine evidence of alteration in the two samples. Both the fresh and the old samples showed minor amounts of orange iron oxide stain. This stain was more common on particles from the old gouge but was not abundant enough to indicate significant chemical alteration that may affect surface area measurements. Gay and Ortlepp (1979) analyzed quartz gouge from shear zone "A" with an SEM and

described 1) intensely comminuted areas between undeformed grains along shattered grain boundaries and in open spaces between grains, 2) a significant decrease in particle size from the initial grain size, and 3) cleavage, which is rare in quartz. Engelder and McKee (1973) and Engelder (unpublished micrographs, 1981) analyzed experimentally deformed fault gouge with a TEM and described conchoidal fractures and an aggregate of poorly-sorted well-rounded particles ranging in size from 4 μm to less than 0.06 μm . Engelder and McKee (1973) attributed these features to brittle fracture and mechanical abrasion during fault slip.

SEM observations

Observations from approximately 50 micrographs of fault gouge (e.g. Figures 3a and 4a and b) indicate that the gouge is made of a wide range of particle sizes and shapes. The smallest particles seen in the SEM were less than 0.1 μm in size, near the limit of resolution. It proved to be very difficult to determine the size distribution from these micrographs alone.

The particle shapes appear to increase in flakiness and angularity with decreasing size. Gouge particles greater than 1 μm resemble similar-sized particles of mechanically crushed Ottawa silica sand (compare Figures 3a and b). Conchoidal fractures are the dominant style of breaking with cleavage absent in the silica sand (Figure 3b) and occurring only to a minor extent in the gouge (Figure 3a). Most of the larger particles that appear platy in two-dimensional micrographs were found to be nearly equant when viewed in stereo pairs or when the sample was tilted. In contrast to the large particles, the submicron-sized particles are mainly highly angular plates, slivers, and irregular

fragments with high aspect ratios (length/width) (Figure 4). Conchoidal and cleavage fractures are both common. Engelder and McKee (1979) attributed contrasts in the degree of roundness to variations in mechanical abrasion during slip. Jones (1981) observed that in experimentally crushed Westerly granite, slightly rounded, equant grains formed in samples with localized faults, but more angular particles with high aspect ratios formed in samples crushed with no displacement. These observations imply that in the natural gouge, the large particles are rounded by abrasion during fault slip, and the submicron ones are relatively unaffected.

Kanaori et al. (1980) described surface textures of quartz, observed with an SEM, from gouge zones of various ages. They classified four groups of textures according to degree of corrosion by groundwater. None of these textures were observed for either the fresh or the old sample. It is unlikely, therefore, that any variations in size, shape, or surface area were caused by groundwater corrosion after the seismic event.

The energy dispersive X-ray (EDX) analyzer of the SEM was used to determine the mineralogy of the small, cleavage fragments. Only minor amounts of potassium, aluminum, and iron were detected. Therefore, it is unlikely that all of the cleavage fragments are accessory minerals such as muscovite.

TEM observations

The TEM was used to determine 1) the extent and orientation of cleavage in the submicron-sized particles, and 2) the size and crystallinity of the smallest gouge particles. Micrographs were taken of

approximately 30 images and 10 diffraction patterns. Many more images and diffraction patterns were analyzed in the microscope.

Cleavage is uncommon in quartz and only occurs in natural rocks deformed at very high strain rates (Carter, 1968). Cleavage in quartz gouge particles is significant not only because it established the deformation as being very rapid but also because flakes have much higher surface areas to volume ratios than cubes.

Two TEM micrographs of fresh gouge particles, typical of the electron transparent particles, are shown in Figure 5. The very thin, parallel plates in both particles are separated by cleavage fractures. The TEM diffraction pattern of the particle in Figure 5b was indexed as [0001] projection in quartz. The cleavage is therefore parallel with the basal plane. All diffraction patterns, taken randomly, were indexed as quartz [0001] projections. These results contradict the accepted fracture behavior of quartz both because cleavage fractures are normally rare and because when cleavage does occur, it is usually rhombohedral and less commonly basal plane (Carter, 1968; Deer et al., 1963).

The thickness of the thin cleavage plates is not easily measured directly but can be estimated from the contrast in the micrograph. The particle in Figure 5a is made up of at least eight to ten thin plates. At its thickest point, the particle is nearly opaque to transmitted electrons. Therefore the thickness of the particle at this point is near the extinction distance of quartz, estimated to be 0.15 μm from Ardell et al. (1974) for a 100 kV TEM. The average plate thickness in Figure 5a is then approximately 0.015 μm .

From the TEM micrographs (Figure 5) it can be seen that the cleavage is penetrative and that the plates have undergone relative rotations and translations. For a large fraction of the particles, edges and corners of the plates within a particle are superposable (Figure 5a). The alternating light and dark "moir" fringes in the particles (Figures 5a and b) and the dispersed or multiple point electron diffraction spots (Figure 5b inset) are both due to slight orientation misalignments between overlapping crystal plates (Hirsch et al., 1977). Since cleavage is only common in quartz deformed at very high strain rates, the separation of these plates probably occurred during the earthquake associated with the formation of the fault zone. The surface area of each plate must be considered when determining the total surface area created during faulting.

Whether thicker particles are as pervasively fractured as those in Figure 5 is difficult to ascertain. Almost all particles observed with the TEM show cleavage along their electron transparent edges and may also be pervasively fractured.

The second purpose of the TEM investigation was to determine the size of the smallest particles. Since the specific surface area is inversely proportional to the particle diameter, determining the lower limit of particle size is critical to any estimate of absolute surface area. The smallest particles observed with the TEM are 0.05 μm to 0.01 μm in diameter. These diameters are near the limit of resolution of bright field imaging. There is an important difference, though, between the limiting diameters seen in the TEM and the SEM. The particles near 0.1 μm in diameter are relatively numerous, but the particles less than

0.05 μm in diameter are very scarce, suggesting that 0.01 μm is near the lower limit of particle size, coincidentally, near the thickness of the cleavage plates described earlier. The crystallinity of the smallest particles was impossible to determine directly since electron diffraction patterns could not be obtained from particles less than 0.5 μm in diameter. But the shape, edges, and surface morphology of the smallest particles were similar to these larger particles, implying that they too are crystalline.

SPECIFIC SURFACE AREA MEASUREMENTS

An estimate of the surface energy consumed in creating fault gouge depends on an accurate measurement of the total area of new surface. Conventional optical microscopic methods of measuring particle dimensions are inappropriate for the gouge (Figures 3 to 5) because particles less than 1 μm in size are not resolvable.

An attempt was made to quantitatively determine the surface area from SEM and TEM micrographs, but this proved to be impractical. Besides being extremely tedious to measure dimensions of a statistically significant number of particles, it was difficult to obtain enough micrographs at different magnifications for a representative sampling of the particle distributions. Therefore, two techniques commonly used to measure powder sizes and surface areas, X-ray sedimentation and gas adsorption, were used.

X-ray sedimentation

The principle of the X-ray sedimentation technique is that the density of X-rays projected through a powder-liquid solution is

proportional to the weight of powder in the beam. This proportionality and Stokes' Law of particle settling are used to produce a cumulative mass percent vs. Stokes diameter sedimentation curve (Allen, 1981). The technique is useful for particle sizes between 100 μm and 1 μm ; the upper limit may vary between instruments, but the lower is the accepted limit for gravitational sedimentation techniques (Herdan, 1960).

The size fractions between 500 and 100 μm (solid circles and triangles), classified by sieving (Table 1), and the sub-100 μm fraction (bold lines), classified by X-ray sedimentation, are plotted in Figure 6. The data between 50 and 1 μm are reasonably close to a log-normal distribution, defined as a straight line in Figure 6. The non-linearity of the data for particles greater than 50 μm in diameter is probably a result of overlapping two classification techniques. Since the particles are not spheres, the sieve and Stokes diameters will not necessarily agree.

Since the surface area per unit volume is inversely proportional to the particle size, an attempt was made to estimate the contribution to S of the submicron fraction. The dashed lines through the 1 to 0.1 μm sizes in Figure 6 are projections of least-squares fits through the sedimentation data between 50 and 1 μm . The projections are based on qualitative estimates made with the SEM. A series of micrographs of different magnifications showed consistent ratios of fine to coarse sizes, suggesting a log-normal distribution down to at least 0.1 μm (compare Figures 3 and 4). TEM observations, as noted above, suggest a lower size limit of about 0.01 μm .

Included in Figure 6 are optically-determined size distributions of fault gouge from shear zone "A" (Spottiswoode, 1978) and from the Muddy

Mountain thrust fault (Nevada) in the Aztec sandstone and the Bonita normal fault (New Mexico) in the Mesa Rica sandstone (Engelder, 1974). The thin solid line is an average of three samples of gouge from shear zone "A"; the error bars indicate the range of data (Spottiswoode, 1978).

Over comparable size ranges, the data agree reasonably well, even though the size distributions were measured by different methods. Differences due to age, alteration, source rock, and displacement are not distinguishable.

The specific surface area ($S=S_T/M$, where M is the total mass of fault gouge in the fault zone) is defined by Herdan (1960) as:

$$S = \frac{K}{\delta} \left(\sum \frac{w_i}{x_i} \right) \quad (2)$$

where K is a geometric shape factor (see footnote of Table 2), δ is the particle density, equal to $2.65 \times 10^3 \text{ Kg/m}^3$ for quartz, w_i is the weight fraction over a certain size interval, and x_i is the average size in that interval. Values of S calculated from the data in Figure 6 are given in Table 2 and will be discussed below.

Gas adsorption

The principle of the single point gas adsorption (BET) method is that the quantity of adsorbate required to cover the surface of a solid with a monolayer of molecules is proportional to the surface area of the solid (Allen, 1981). Nitrogen was used as the adsorbate, but because the surface areas were low relative to materials normally investigated, a few measurements were made using krypton--considered more accurate for low surface areas. The difference in S using the two gases proved to be

small, and did not warrant the use of krypton for all measurements. Other factors that could affect the results are given in Allen (1981).

The advantage of this method over microscopic or sedimentation methods is that the surface area is measured directly without any size distribution extrapolations or shape assumptions. The method is limited by the fact that only those surfaces separated by at least two molecular diameters, about 6 for nitrogen, are accessible to gas molecules.

The surface areas for three fractions, <500 μm , <250 μm , and <100 μm sieve diameters, were measured for both the fresh and old samples (Table 1). If account is made for the weight percentages of each fraction, the fraction less than 100 μm contributes almost all of the surface area. The few percent contributed by the larger sizes could in part be due to scatter in the measurements, to clumping of small particles, or to small particles adhering to larger particles (Figures 3a and 4) and thus being removed with the large particles during sieving.

Results and discussion

The specific surface areas, S , of the fault gouge are given in Table 2, along with measured or assumed values from other studies. The areas calculated using the nitrogen adsorption method agree with those from the X-ray sedimentation method (projected to 0.1 μm) for particles with fairly high aspect ratios ($K \approx 20$ to 25). This value for K is consistent with the shapes observed in the SEM and TEM micrographs for particles less than 1 μm in diameter, indicating that the projection of the X-ray sedimentation data to 0.1 μm is valid. Therefore, reasonable values of S for the fresh and old samples are approximately 0.7 and 2.0 m^2/gm , respectively.

The difference of a factor of 2 to 3 between the two samples is not unreasonable, considering that they were collected from different fracture systems. Spottiswoode (1978) calculated S for three samples collected from different areas of shear zone "A" and noted a variation of S of almost a factor of 2 (Table 2). The effects of variations in fault parameters such as width, displacement, seismic moment, fault area, and earthquake magnitude are beyond the scope of this study since these parameters are not known for the fracture system from which the fresh sample was collected. It is assumed that the error in the measurements of S is also about a factor of 2 for each method.

The value of S calculated by Spottiswoode (1978) for the Witwatersrand quartzite gouge from shear zone "A" agrees with the value for the Aztec sandstone gouge from the Muddy Mountain thrust (Engelder, 1974) (Table 2). However, both values are significantly lower than those from this study (Table 2). The main reason for this large disagreement is that optical microscopy methods omit the submicron-sized particles which contribute significantly to S. Other problems with optically determined values of S are only the largest dimension is usually measured and surface irregularities are unaccounted for.

The surface area calculated from the 1 μm cube assumption of Lachenbruch and Sass (1980) agrees with the X-ray sedimentation and nitrogen adsorption values (Table 2). But the SEM and TEM observations show that this assumption is not valid because the particles actually vary widely in size and shape. Therefore, the agreement is fortuitous. Engelder et al. (1975) assumes that the gouge generated from experimentally crushing 200 μm spheres consisted of quartz particles averaging 25 μm in diameter. The value of S for particles of this size

is an order of magnitude less than the values obtained in this study. Engelder et al. (1975) and Engelder and McKee (1973) also reported an indurated gouge consisting of micron- and submicron-sized particles with, therefore, a much larger surface area. The thin indurated layer represented 5% of the gouge thickness and only formed under certain experimental conditions.

Other contributions to S that may be unaccounted for by the microscopy, sedimentation, and even the nitrogen adsorption methods are the thin cleavage plates observed in the TEM. Consider that the 4% by weight of the old gouge that is less than $1 \mu\text{m}$ in size (Figure 6) is pervasively fractured into plates of dimensions $0.015 \mu\text{m} \times 0.5 \mu\text{m} \times 1.0 \mu\text{m}$, representing an increase in S of $2 \text{ m}^2/\text{gm}$.

ESTIMATES OF THE SURFACE AREA ENERGY

The amount of energy consumed in creating the new surfaces is important for an understanding of the partitioning of the energy released during faulting. The energy density W_A , energy per unit volume of gouge, is

$$W_A = S\delta\Gamma \quad (3)$$

where Γ is the specific surface energy of quartz from Brace and Walsh (1962). Considering only the old gouge, $S = 2.0 \text{ m}^2/\text{gm}$, and choosing $\Gamma = 0.7 \text{ J/m}^2$, and $\delta = 2.65 \times 10^3 \text{ Kg/m}^3$,

$$W_A = 3.7 \times 10^6 \text{ J/m}^3$$

This can be compared to the total energy released during an earthquake,

E_T :

$$\frac{E_A}{E_T} = \frac{W_A}{E_T} \frac{A}{u} \quad (4)$$

where A is the area of the fault face and u is the width of the gouge zone. From Brune (1968),

$$E_T = A d \bar{\delta} \quad (5)$$

where d is the average fault displacement and $\bar{\delta}$ is the average stress on the fault. Combining (3) and (4),

$$\frac{E_A}{E_T} = \frac{W_A}{\delta} \frac{u}{d} \quad (6)$$

McGarr et al. (1979) report typical mine values of $\bar{\delta} = 40$ to 70 MPa, $u = 10$ to 50 mm, and $d = 50$ to 60 mm for shear zone "A". Therefore,

$$\frac{E_A}{E_T} = 0.01 \text{ to } 0.09$$

This agrees with Jones (1981) who determined that 4 to 8 percent of the total energy was used to create new surface in experimentally-deformed crushed Westerly granite.

The seismic efficiency has been estimated by McGarr et al. (1979) to be .36 to 3.6%. Therefore, the surface energy may be of the same order as the seismic energy.

Based on the above estimates of the surface area, 10 percent, at most, of the total energy may be allocated to creating new surface. If TEM results are considered and the submicron fraction of the gouge is

made up of plates 0.015 μm thick, the energy used to create surface area may be a factor of two higher, but no more.

SUMMARY

The microstructure of unaltered granular fault gouge from the site of a known seismic event has been investigated with SEM and TEM, and the specific surface area has been measured using two small-particle analysis techniques.

The main observations and conclusions are:

- 1) All particles are irregularly shaped. The larger ones tend to be slightly rounded and equant, while the sub-micron-sized ones are more angular and have higher aspect ratios.
- 2) Gouge particles range in size from the initial grain size of the quartzite (0.5 mm) to less than 0.05 μm . X-ray sedimentation data indicate that the particles follow a log-normal size distribution between 1 and 50 μm . SEM observations suggest that this distribution may extend to 0.1 or less. Shape and size similarities, observed with the TEM, between the smallest and other larger particles (e.g. Figure 5) suggest that the smallest particles are crystalline.
- 3) No surface alteration effects were found in any of the quartz grains. The surfaces were smooth and freshly fractured. The only alteration detected was a minor amount of orange iron oxide stain on the surface of some of the particles.
- 4) The submicron particles are commonly broken into basal plane cleavage fragments, which have a thickness at least as small as 0.015 μm . From the TEM micrographs, it appears that the thin

cleavage plates have rotated and translated with respect to one another. If all of the submicron material were broken into these plates, the specific surface area would be approximately doubled.

- 5) Specific surface areas from both X-ray sedimentation and nitrogen adsorption measurements are 0.7 and 2.0 m²/gm for the fresh and old gouge, respectively. Each of these values has an uncertainty of about a factor of 2.
- 6) If the assumptions made in equations 3 to 6 for shear zone "A" are correct and the area between the cleavage plates is included, then the surface energy is 2 to 20 percent of the total energy released during an earthquake, and therefore of the same order as the seismic energy. If these results apply to all earthquakes, then most of the energy released during faulting is, evidently, converted into heat.

BIBLIOGRAPHY

- Allen, T., Particle size measurement, Chapman and Hall, London, 678p., 1981.
- Ardell, A.J., J.M. Christie, and J.W. McCormick, Dislocation images in quartz and the determination of Burgers vectors, Phil. Mag., 29, 1399-1411, 1974.
- Brace, W.F., and J.B. Walsh, Some direct measurements of the fracture energy of quartz and orthoclase, Am. Mineral., 47, 1111-1122, 1962.
- Brune, J.N., Seismic moment, seismicity, and rate of slip along major fault zones, J. Geophys. Res., 73, 777-784, 1968.
- Carter, N.L., Dynamic deformation in quartz, in Shock metamorphism of natural materials, edited by B.M. French and N.W. Short, Mono Book Corp., Baltimore, 453-474, 1968.
- Deer, W.A., R.A. Howie, and J. Zussman, Rock forming minerals, Vol. 4, Framework silicates, Longman, London, 435p., 1963.
- Engelder, J.T., Cataclasis and the generation of fault gouge, Bull. Geol. Soc. Am., 85, 1515-1533, 1974.
- Engelder, J.T., J.M. Logan, and J. Handin, The sliding characteristics of sandstone on quartz fault-gouge, Pure and Appl. Geophys., 113, 69-86, 1975.
- Engelder, J.T., and T.R. McKee, Electron microscopical study of indurated quartz gouges, Proc. 31st Ann. Mtg. Electron Microscopy Soc. Am., 214-215, 1973.
- Gay, N.C., and W.D. Ortlepp, Anatomy of a mining-induced fault zone, Bull. Geol. Soc. Am., 90, 47-58, 1979.
- Herdan, G., Small particle statistics, Butterworth, London, 418p., 1960.
- Hirsch, P.B., A. Howie, R.B. Nicholson, D.W. Pashley, and M.J. Whelan, Electron microscopy of thin crystals, Kreiger, New York, 563p., 1977.
- Jones, L.M., Field and laboratory studies of the mechanics of faulting, Ph.D. thesis, Massachusetts Institute of Technology, 106p., June, 1981.
- Kanaori, Y., K. Miyakoshi, T. Kakuta, and Y. Satake, Dating fault activity by surface textures of quartz grains from fault gouges, Engrg. Geol., 16, 243-262, 1980.
- Lachenbruch, A.H., and J.H. Sass, Heat flow and energetics of the San Andreas fault zone, J. Geophys. Res., 85, 6185-6222, 1980.
- McGarr, A., S.M. Spottiswoode, and N.C. Gay, Relationship of mine tremors to induced stresses and to rock properties in the focal region, Bull. Seismol. Soc. Am., 65, 981-993, 1975.
- McGarr, A., S.M. Spottiswoode, N.C. Gay, and W.D. Ortlepp, Observations relevant to seismic driving stress, stress drop, and efficiency, J. Geophys. Res., 84, 2251-2261, 1979.
- Ortlepp, W.D., The mechanism of a rockburst, Proc. 19th U.S. Rock Mechanics Symp., Reno, NV, 476-483, 1978.

- Scholz, C.H., Shear heating and the state of stress on faults, J. Geophys. Res., 85, 6174-6184, 1980.
- Spottiswoode, S.M., Fault gouge, driving stress, and seismic efficiency, Unpublished report, 1978. (Most of the data is quoted in McGarr et al., 1979.)
- Wong, T.-F., Shear fracture energy of Westerly granite from post-failure behavior, J. Geophys. Res., 87, 990-1000, 1982.

TABLE 1. Fractional weight percent from seive analysis and surface areas determined by the gas adsorption method

Sample	Wt %	S m ² /gm
<u>Fresh:</u>		
<100 μm	46	1.07
<250 μm	70	0.80
<500 μm	100	0.75
<u>Old:</u>		
<100 μm	75	2.28
<250 μm	88	2.10
<500 μm	100	2.03

TABLE 2. Surface area estimates of fault gouge

Method	Dimensions (L x B x T) ¹	K ²	S (m ² /gm)		Reference
			Fresh	Old	
X-ray sedi- mentation	Sphere	6.0	0.20		
"	Cube	8.3	0.27		
"	4 x 2 x 1	14	0.46		
"	6 x 3 x 1	19	0.63		
"	10 x 5 x 1	29	0.96		
N ₂ adsorption			0.75		From Table 1
Optical microscopy		11.0	0.15 - 0.27 ³		Spottiswoode (1978)
"		11.0	0.18 ⁴		Spottiswoode (1978)
Assumed size and shape	1 μm cubes		2.3		Lachenbruch & Sass (1980)
"	25 μm spheres		0.09		Engelder <i>et al.</i> (1975)

¹L = length; B = breadth; T = thickness

² $K = [1.57 + C(a/m)^{4/3} (n + 1)/n] / [a/mn^{1/2}]$, where a and C are angularity constants taken as 0.43 and 3.1 respectively, m = B/T and n = L/B (Herdan, 1960).

³Witwatersrand quartzite from shear zone "A".

⁴Aztec sandstone, surface area calculated by Spottiswoode (1978), using data from Engelder (1974).

FIGURE CAPTIONS: CHAPTER 1

- FIGURE 1. Inclined shear fracture from which old gouge was sampled. It is located near the east end of the main fracture and was exposed almost seven years prior to sampling.
- FIGURE 2. Near vertical shear fracture from which fresh gouge was sampled. It is located near the western extremity of the main fracture and was exposed only three days prior to sampling. Scale bar = 1 meter.
- FIGURE 3. SEM micrographs of crushed quartz: (a) fresh fault gouge; and (b) mechanically crushed silica sand.
- FIGURE 4. SEM micrographs of (a) fresh fault gouge; and (b) old fault gouge.
- FIGURE 5. TEM micrographs of fresh gouge particles showing (a) individual cleavage plates; (b) moiré fringes and associated diffraction pattern.
- Figure 6. X-ray sedimentation results plotted on a log-probability graph. Particle sizes below 1.0 μm are projected; those above 100 μm are from sieve analysis. Results are compared to optical microscopy analyses of quartz fault gouge by Spottiswoode (1978) and Engelder (1974).

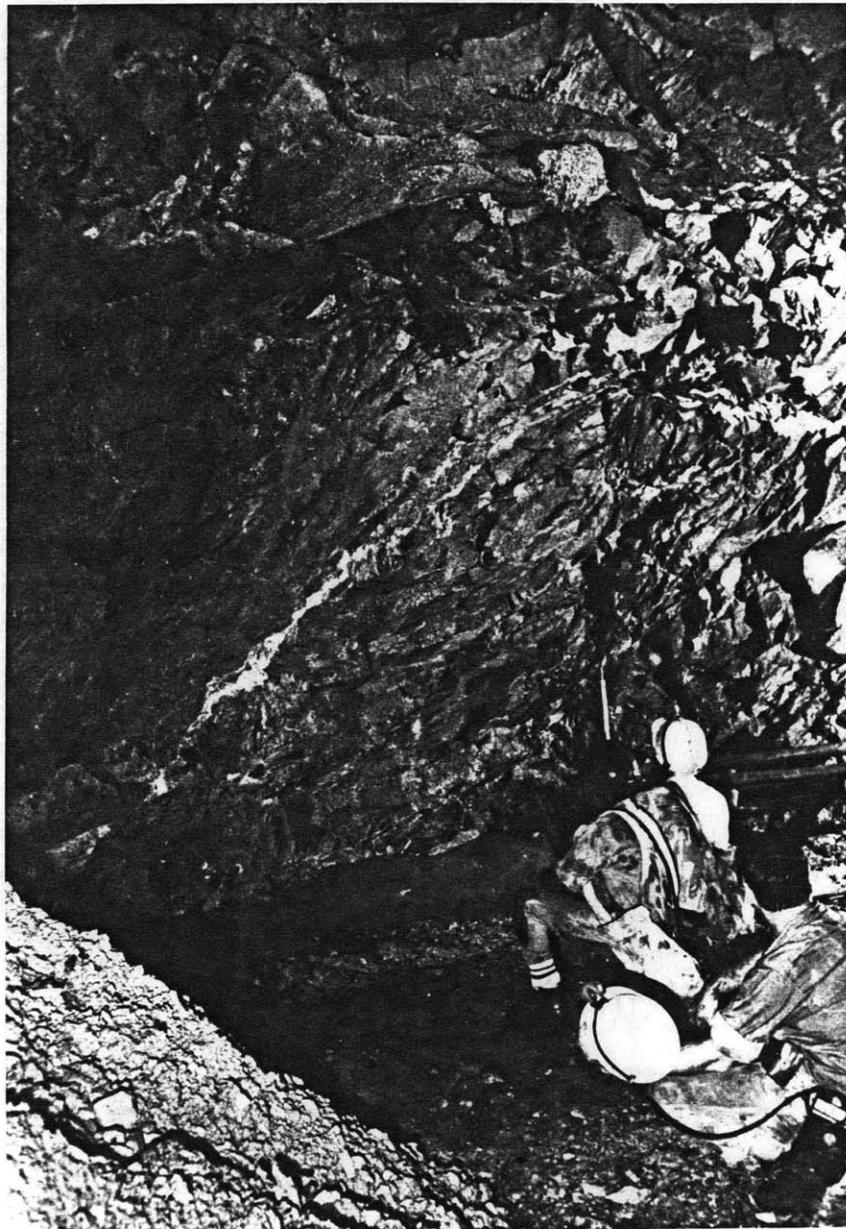
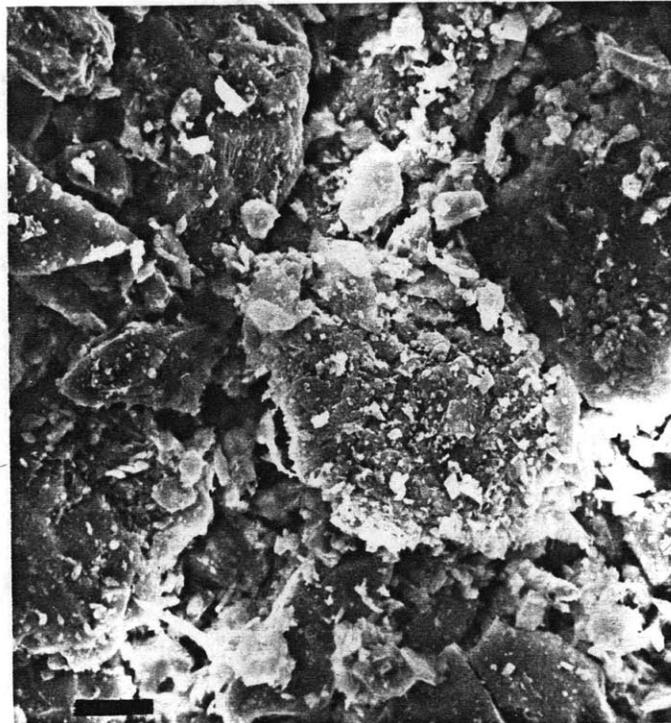


Figure 1



Figure 2



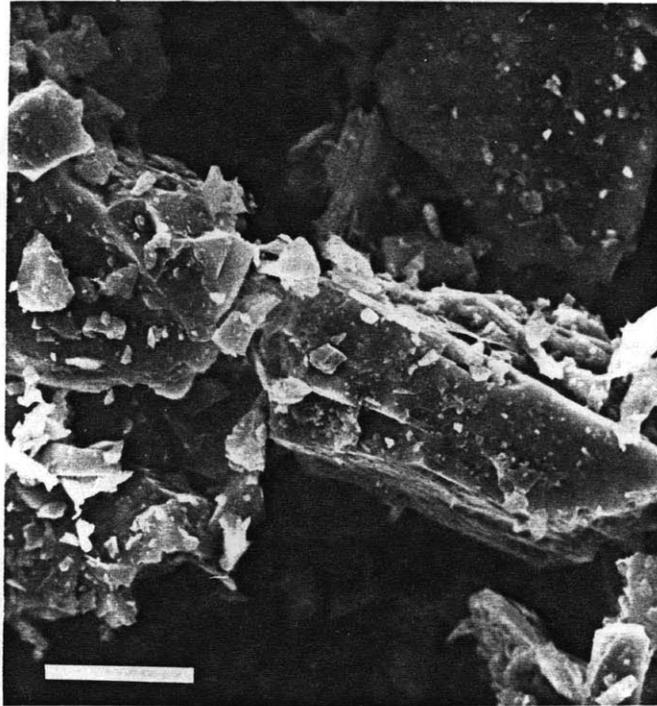
a 10 μm



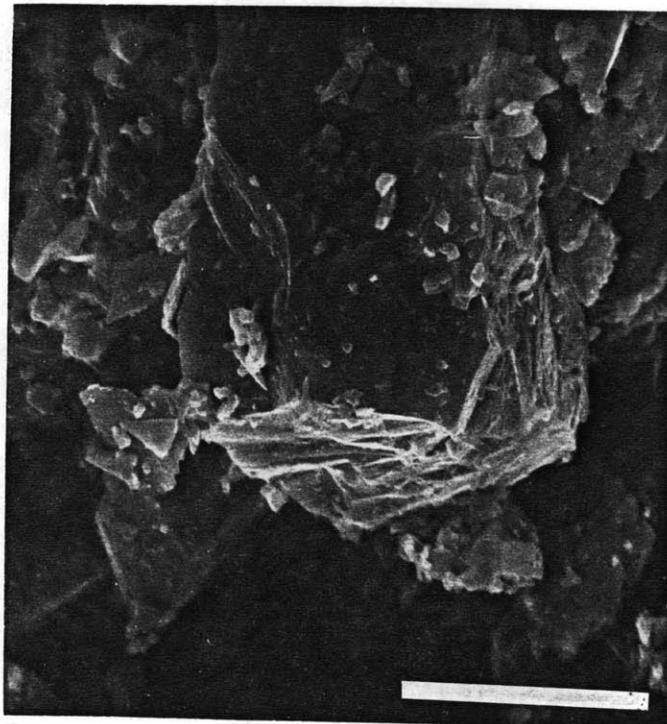
b

10 μm

Figure 3

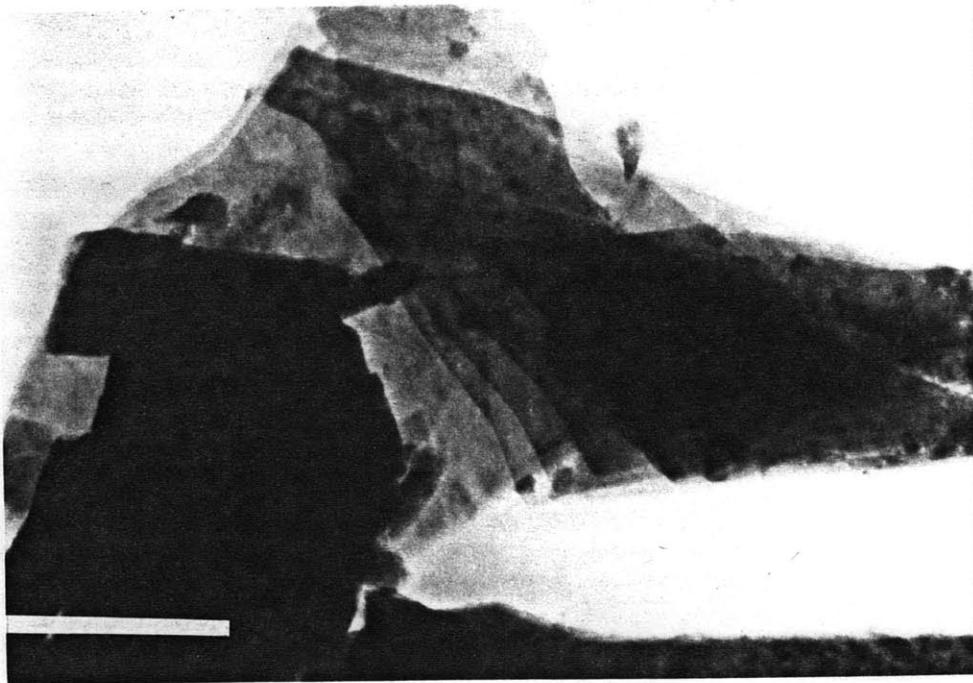


a 10 μm

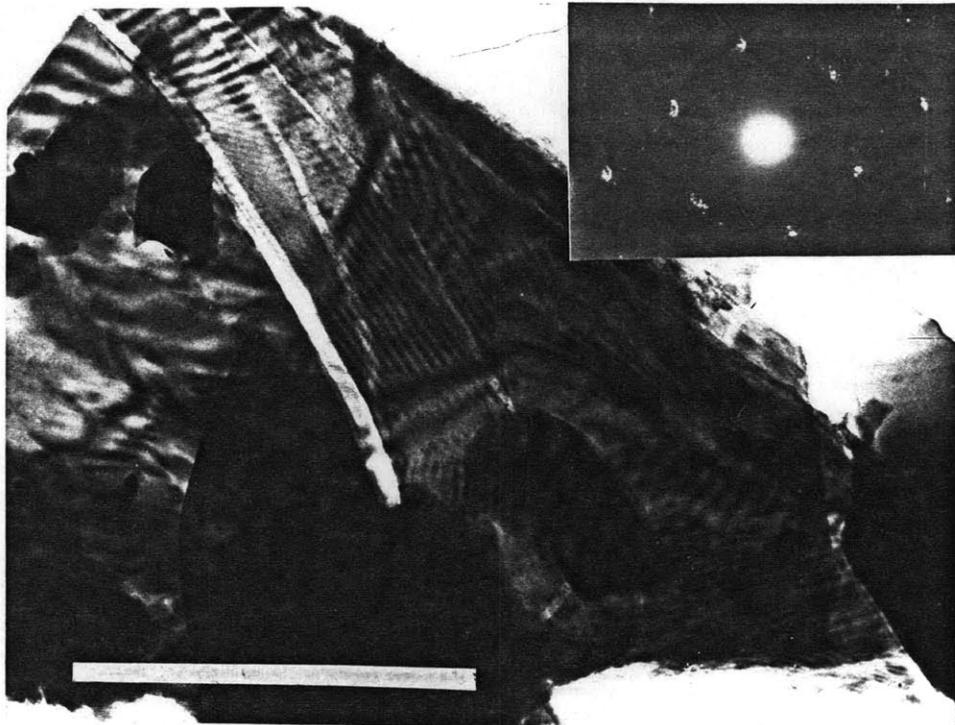


b 10 μm

Figure 4

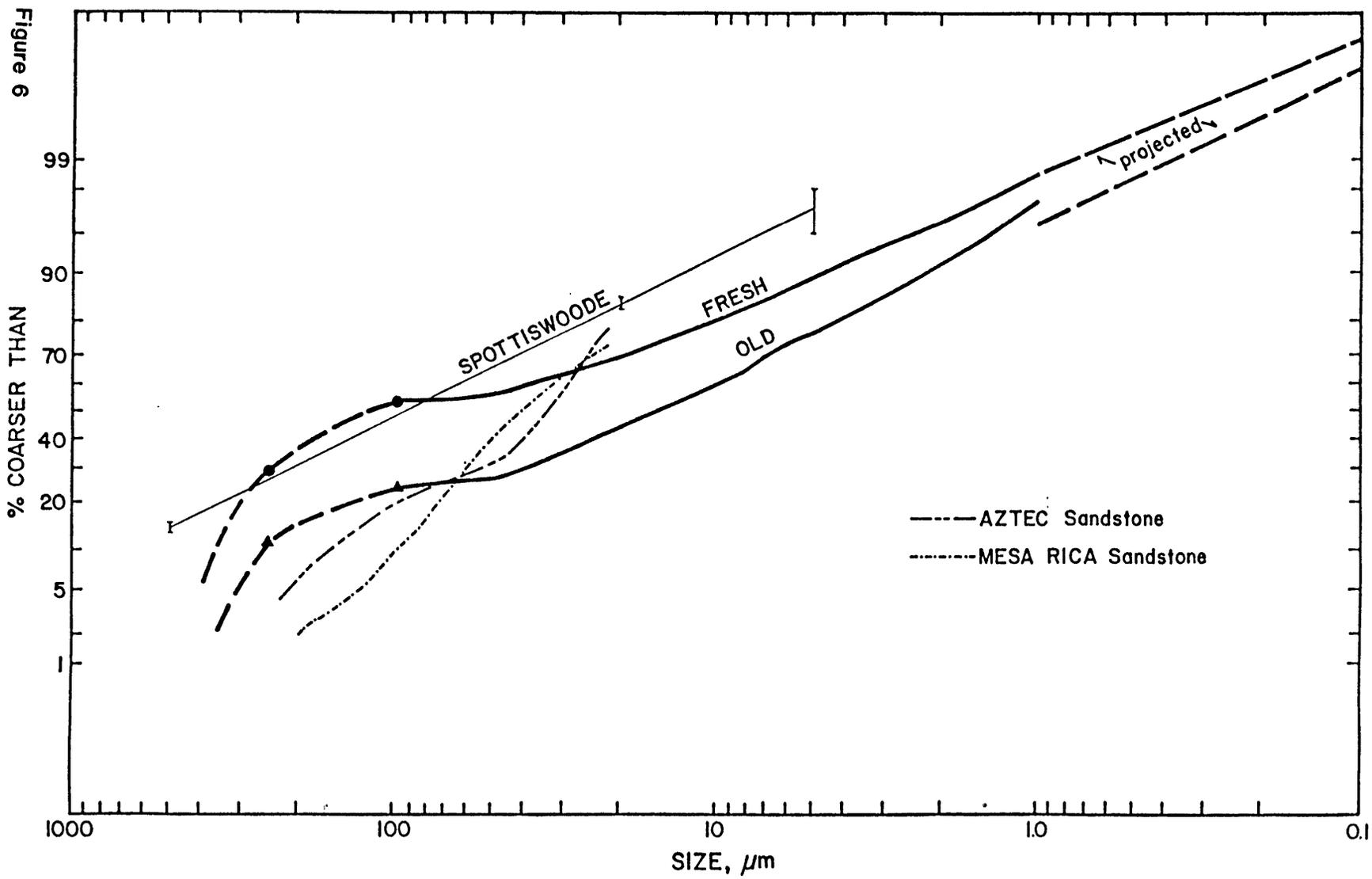


a 0.5 μm



b 0.5 μm

Figure 5



CHAPTER 2

EFFECTS OF ALUMINA PARTICLES AS A SECOND PHASE
IN CALCITE GRAIN-GROWTH EXPERIMENTS

INTRODUCTION

In studying polycrystalline materials, ceramists and metallurgists have long recognized the influence of grain size on physical properties, such as creep strength, ductility, and fracture toughness. Several theories have been developed to predict how second phases interact with grain boundaries during grain growth. Considerable experimental research has focused on developing methods of controlling grain size by the precipitation of inclusions or by the direct addition of insoluble particles.

Grain size is an important parameter in petrology as well. The microstructural behavior of rocks during metamorphism appears to be similar to that of metals and ceramics during hot working and high temperature annealing. Therefore, it is probable that finely-dispersed particles, usually present even in so-called monomineralic rocks, would influence the development of microstructures and thereby influence the physical properties of rocks as well. A recent trend among experimental petrologists and structural geologists has been to fabricate synthetic rocks by hot isostatically pressing fine powders into dense aggregates (e.g. Schwenn and Goetze, 1978; Caristan et al., 1981; Chopra and Kohlstedt, 1983; and Karato and Paterson, 1984). In this way, the size and concentration of second phase particles as well as the porosity, the

initial grain size distribution and the impurity and defect contents can be controlled. While investigating recrystallization and grain growth in synthetic marbles, we measured the limiting grain size of the calcite mineral matrix and its dependence on the size and concentration of dispersed second phase particles. The experiments were performed on CaCO_3 aggregates containing 0-10 volume percent of Al_2O_3 particles (0.3-5.0 μm) at temperatures and pressures high enough to promote rapid densification, recrystallization, and grain growth. Although the limiting grain size varied with both particle size and volume fraction of the second phase particles, the dependence of grain size on either parameter was weaker than predicted by most models.

REVIEW OF MODELS FOR PARTICLE-GRAIN BOUNDARY INTERACTIONS

Several equations (Table 1) have been derived to relate the size and concentration of second-phase particles to the limiting grain size of the matrix by equating the driving force for grain boundary movement to the restraining force due to the particles. Zener (1948) was the first to consider the dependence of the minimum radius of curvature, R , of a pinned boundary on a random dispersion of rigid, insoluble, equal-sized spherical particles of diameter, d , and volume fraction, f . By assuming that the only driving force for grain growth is the interfacial tension of the grain boundary, Zener (1948) derived the expression $R=2/3(d/f)$ ($d=2r$) (Eqn. 1, Table 1). Smith (1948) suggested that the average grain size when growth stopped, the limiting grain size, D_{max} , was virtually equal to the radius of curvature, or $D_{\text{max}} \approx d/f$. Several modifications have been made to this relation (Table 1) by considering more complicated particle-boundary interactions or less idealized geometries. Haroun and

Budworth (1968) measured grain sizes and found that they were nearly an order of magnitude less than the boundary radii of curvature (Eqn. 2). To account for the importance of a heterogeneous size distribution of matrix grains, Gladman (1966) introduced the variable Z , equal to the ratio of the radius of a growing grain to that of its neighbors (Eqn. 3). Hellman and Hillert (1975) examined the approximations involved in Zener's derivation and introduced a correction factor β , whose value is dependent upon the restraining force between a spherical boundary and a particle, as a function of their relative position (Eqns. 4 and 5 for uniform and non-uniform particle sizes, respectively). The value of β was found to be near unity for small f , but appreciably smaller for f greater than 10%. Louat (1983) included the effect of grain boundary flexibility, and the variability and frequency of resisting forces due to the trailing and leading particles (Eqn. 6). In each of these models, the limiting grain size was found to be proportional to d/f . A review of most of these models has been made by Nes et al. (1984).

In all of the above models, it is assumed that the particles are randomly dispersed and that growth stops when the average boundary is pinned. If restrictions are placed on the locations of the particles, other relationships are derived from purely geometrical considerations. Anand and Gurland (1975) derived an expression for the case where all particles lie on grain boundaries (Eqn. 7). Haroun and Budworth (1968) and Haroun (1980) also considered a slightly different geometry in which every boundary is required to intersect and be pinned by at least one particle (Eqns. 8 and 9 for uniform and non-uniform particle sizes, respectively). The relationships derived from these equations are proportional to $d/f^{1/2}$. A similar relationship was obtained from a

computer simulation by Srolovitz et al. (1984), although they believed that the $1/f^{1/2}$ dependence was due to an oversimplification of the detailed topology. Hellman and Hillert (1975) estimated that for volume fractions greater than 10%, the majority of the particles would be located at four-grain junctions (corners). If all particles were located at grain corners, the limiting grain size would be proportional to $d/f^{1/3}$ (Eqn. 10). A similar relationship is derived in Appendix 1 (Eqn. 11).

Several experimental studies have been conducted using both precipitates and insoluble particles, to test the validity of these theories. The objectives of our study were to measure the dependence of the stable grain size, D_{\max} , of synthetic marbles on the diameter, d , and the volume fraction, f , of a well characterized dispersion of insoluble, rigid alumina particles and to compare our results to the theories and to the results of some of the experimental studies. The results of our study can be applied to understanding the thermal history of metamorphosed rocks, and the involvement of other processes such as deformation that affect grain-boundary migration.

EXPERIMENTAL METHOD

The study involved four steps: 1) initial characterization and mixing of the powders; 2) fabrication of dense, fine-grained synthetic marbles; 3) heat-treatment of the marbles until a limiting grain size was reached; and 4) grain-size measurements and microstructure descriptions using transmitted light and scanning and transmission electron (SEM and TEM) microscopes.

Reagent grade CaCO_3 powder was mechanically mixed with various volume fractions (0 -.10) of four commercial Al_2O_3 grinding powders (0.1, 1.0, 5.0, and 9.5 μm) in ethanol for four hours. The powders were sized by X-ray sedimentation before mixing and by single-point N_2 adsorption (BET) both before and after mixing. The grain size distribution curves calculated from the X-ray sedimentation data (Appendix 2) are plotted in Figure 1 and average particle sizes from both methods are listed in Table 2. The relative agglomeration of the particles was estimated from the ratio of the X-ray sedimentation and BET sizes (Table 2).

The powder mixtures were then densified and recrystallized by a series of cold and hot isostatic presses. The mixtures were initially die-pressed into cylinders at 150 MPa, and were then hydrostatically cold-pressed at 150 MPa, producing a sample with a relative density of approximately 80% (relative to the single crystal value). In an internally-heated, argon confining-medium, pressure vessel (Fig. 2) the mixtures were hot-pressed at 650°C (550°C for one pure sample) $\pm 10^\circ\text{C}$ over the length of the sample; 500 ± 5 MPa confining pressure, P_c ; 2 ± 1 MPa $\text{H}_2\text{O} + \text{CO}_2$ pore pressure, P_p , for one hour ± 5 min. A typical temperature (T) and confining pressure (P_c) vs. time history is shown in Figure 3. This fabrication process produced relatively dense (>96%) polycrystalline synthetic marbles with fine but uniform grain sizes (Table 3) that were an order of magnitude larger than the initial powder sizes (Table 2).

Each of these hot-pressed cylinders was cut into disks 3 mm thick, and stacked with disks of the sixteen other mixtures (see Table 3). All mixtures were then heat-treated together at 800°C, P_c equal to 300

MPa, and P_p equal to 2 MPa for 1, 10, or 24 hours. This heat treatment induced normal grain growth of the matrix which proceeded until a state of metastable equilibrium was reached, where the boundaries were effectively pinned by the dispersed particles. Two 24-hour experiments were performed as a check on the reproducibility of the data.

In ultra-thin sections (5-10 μm thick) the grain sizes (Table 3) were measured with a transmission optical microscope using the linear intercept method described by Underwood (1970). Following Exner (1972), the average grain diameter, D , was calculated from the average linear intercept length, L , by setting D equal to $3L/2$, the conversion for equi-sized spheres. For other more realistic shapes, the conversion factor differs only slightly (Underwood, 1970 and Exner, 1972).

TEM specimens of selected samples were prepared by ion thinning. SEM specimens were polished to 0.1 μm . Grain-boundary structures were carefully examined for the following features: the presence or absence of intergranular films; the distribution of the particles and pores between the matrix and the grain boundaries; particle agglomerates; and the distribution and density of dislocations.

The presence of melt was of particular interest to us, since the mechanisms (and therefore the kinetics) of grain growth are altered by the presence of a fluid phase along the boundary (Yan *et al.*, 1977). According to Wyllie and Tuttle (1960) and Wyllie and Boettcher (1969), our 800°C experiments were conducted slightly above the melting point of the $\text{CaCO}_3 + \text{H}_2\text{O} + \text{CO}_2$ system. For this reason, one experiment was conducted at 900°C (definitely above the melting point) with P_c equal to 300 MPa and P_p equal to 2 MPa for 10 hours. The initial material was die-pressed only in order to insure complete saturation of

the sample with CO₂ and H₂O. The grain boundaries were examined for the presence of amorphous or very fine-grained material, using dark-field TEM imaging techniques (Clarke, 1979 and 1980; Lou, et al., 1978). These boundaries were then compared to grain boundaries in the fabricated and heat-treated samples. The technique and criteria used to establish the presence or absence of a melt are discussed more thoroughly in Appendix 3.

RESULTS

Grain growth and the establishment of a pinned state

The heat-treatment conditions were chosen so that a limiting grain size, D_{\max} , was reached within 24 hours in all of the two-phase mixtures. The grain-growth curves for both pure calcite and for two-phase mixtures are shown in Figure 4. Each data point represents the average of all of the optical measurements on a single sample. The error bars represent the spatial inhomogeneity in D . Standard deviations were measured for selected samples, including both small and large grain sizes, and were approximately $\pm 12\%$. The reproducibility of the data from these experiments was reflected by the difference between the two 24 hour points. Other errors including observer bias and preferred orientation were minimal ($\pm 2\%$). In all cases but one, D from the 10 and 24 hour experiments are nearly equal. The only exception was 0.2% of the '0.1' data where D for 24 hours was anomalously large. In the larger volume fraction samples, D_{\max} may have been reached during the initial fabrication stage.

Other supporting evidence that D_{\max} was reached in our experiments follows from Srolovitz et al. (1984), and Hillert (1965), who have demonstrated by computer simulation and by calculation, respectively, that grain growth should follow a normal growth law, even in the presence of a rigid second phase, until D has nearly reached D_{\max} . Then the growth rate should decrease rapidly as D asymptotically approaches D_{\max} . In Figure 4a, the pure data are compared to the normal grain growth law $D^n - D_0^n = Kt$ where D_0 is the initial grain size, K is a temperature-dependent constant, and n is a constant depending upon the rate controlling step for grain growth. Theoretically, n is equal to 2 in single-phase, ultra-pure materials and equal to 3 in materials where growth is controlled by several processes including impurity and pore drag or a liquid, grain-boundary phase (Brook, 1976). In practice, n equal to 2 is rarely observed and is more commonly found to be equal to 3 or more. Anderson et al. (1984) have shown by computer simulation that $n > 2$ is expected even when no second phases are present. Our data fit the n equals 3 curve reasonably well, as expected, since our microscopic observations showed traces of intergranular porosity and evidence for a boundary film. Comparing the growth curves from the various mixtures to the pure data and to the normal growth law indicate that neither the pores nor the grain boundary film affected D_{\max} but that the particles caused a significant deviation from normal growth behavior. This deviation occurred well before 10 hours in most cases, and before 24 hours in all but the smallest volume fractions of the '0.1' samples. Therefore we have assumed that D_{\max} was reached within 10 hours. The 10 and 24 hour data have been averaged below. This growth evidence, combined with the lack of anomalously large

grains, indicated that secondary recrystallization or abnormal grain growth had little effect on the pinned state and D_{\max} .

Microstructure: Observations and comparisons

Optical, SEM, and TEM micrographs, illustrating the particle matrix interactions and other microstructures, are shown in Figures 5, 6, and 7. In the pure calcite specimens, the heat-treatment did not significantly alter the microstructure except for the pronounced increase in grain size (Figures 5a and 6a). The grains, both before and after the heat-treatment, were equi-axed with smooth, gently curved boundaries. No anomalously large grains appeared after any heat-treatment interval. Twins and cracked boundaries, present in nearly all specimens, probably formed during the sample quench due to the extremely large thermal expansion anisotropy of calcite.

With alumina present in low to moderate concentrations, the grains were also equiaxed before the heat-treatment, but many boundaries were dimpled by particles (Figure 5b). The particles, which were randomly dispersed by the mixing process, were present in the interior of grains as well as along grain boundaries. After the heat-treatment, the microstructures did not change noticeably; however, in plane section, nearly every boundary intersected at least one particle (Figure 6b and c).

For high concentrations of alumina (Figures 5c and 6d), the average grain size was quite small. The matrix size distribution was bimodal with a few large grains surrounded by groups of fine grains, suggesting abnormal grain growth. This structure may have resulted from the initial size distribution of the calcite powder where grains larger than twice

the average were common (Figure 1) (Hillert, 1965). Thus the smallest grains may have represented a first-generation structure that was erased by abnormal growth of a few large grains. These large grains were either present initially or nucleated during primary recrystallization. In the pure and low-to-moderate particle concentration samples, this growth stage may have proceeded to completion before the heat-treatment, creating the uniform sizes shown in Figures 5a and b. Heat-treatment of the high-concentration samples produced a more uniform microstructure and an increase in the average grain size (Figure 6d).

Microstructures produced during the final stages of densification and primary recrystallization are shown in Figures 5d and e. Particles occurred along grain boundaries and in the interior of grains and were often associated with dislocations (Figure 5d). Pores were lenticular along grain boundaries and equiaxed in grain interiors. Free dislocations were also common, as were low-angle boundaries and triple-junction pores (Figure 5e). The fine black spots were caused by the electron beam. In samples heat-treated at 800°C, the dislocation density was reduced and low-angle grain boundaries and lenticular pores were rare (Figure 7a).

An intergranular "glassy" phase was detected along most grain boundaries. The phase consisted of very fine grains (<10 nm) imbedded in a "glassy" matrix (Figure 7b). Diffraction patterns from this "glassy" region showed distinct rings made up of multiple points (Figure 7b, inset). We interpret this "glassy" phase to be a quenched melt which partially crystallized to very fine grains as the specimen cooled. Potential complications due to the ion-thinning, the carbon coat, and the cracked boundaries precluded identification of films less than 10 nm

wide. An intergranular film was identified above 700°C; no film was detected below 600°C (Figure 7c); and observations at intermediate temperatures were inconclusive.

Although there was no evidence that particles had been dragged by migrating grain boundaries, clusters or agglomerates of two or more particles were common in some samples (Figure 5f) making the determination of the "effective" particle size difficult. From SEM observations, agglomerates were common in the '0.1' and '1.0' mixtures (Figure 6e) but were rare in the '5.0' and '9.5' mixtures (Figure 6f).

D_{\max} dependence on d and f

The dependence of the limiting calcite grain size, D_{\max} , on the particle size, d, and volume fraction, f, of the alumina particles is shown in Figure 8 for all mixtures listed in Table 3. D_{\max} was chosen as the average D from the one 10-hour and two 24-hour experiments since $D_{10} \approx D_{24}$. As before, the error bars represent the combined spatial inhomogeneity in D from each of the three experiments. The value of d was calculated from the sedimentation results using the summation method proposed by Flowers (1979) (Appendix 2). This "effective" size is believed to be more representative of the inhibiting strength of a distribution than the average particle diameter (Table 2). The volume fraction, f, was measured to better than 0.1% accuracy. The error bars for d/f represent one standard deviation in d, determined from the particle size distribution curves (Figure 1). Errors in f due to non-uniform mixing of the powders were possible but, from microscopy, were believed to be small and therefore were not included. If either the BET diameter or the average X-ray sedimentation diameter had been used

instead, all data points would have been shifted to the left in Figure 8, but the relative fit would not have been improved (Appendix 2). A correlation with d/f was sought because most of the models listed in Table 1 predict a linear dependence of D on d/f .

The thin solid lines, which were fit to the data for a constant d by the method of least squares, represent the equation:

$$D_{\max} = C(d/f^m) \quad (12)$$

where m and C are constants. The shaded region between the bold lines was arbitrarily chosen to envelop the points 10% of '1.0' and .02% of '0.1'. For dispersions of constant second phase diameter, m was significantly less than 1 (contrary to most predictions) and varied between 0.34 and 0.55 (Table 4). Unlike the linear dependence of $\log D_{\max}$ on $\log f$, no simple dependence existed between D_{\max} and d . The '0.1', '1.0', and '5.0' data are reasonably represented by the shaded region but the '9.5' data are uniformly low. In fact, the data indicate that the "effective" particle size for the '9.5' set was less than that for the '5.0' set; a result not supported by any of the particle size measurements. Particle clustering probably accounted for most of the mismatch between the '0.1' and '1.0' and the '5.0' sets, but no explanation is offered for the mismatch of the '9.5' set.

Soluble impurities are known to decrease boundary mobilities in oxides (Yan et al., 1977), even in very small concentrations, and may have accounted for the anomalous '9.5' data. Unlike the other alumina powders, the '9.5' powder included 5% impurities, primarily TiO_2 and SiO_2 , with 0.1% or more of Zr_2O_3 , Fe_2O_3 , MnO_2 , CaO , and MgO . If these impurities completely dissolved in the calcite matrix, the

impurity concentration in the 1.0% samples would be 0.05%. A similar concentration of Fe_2O_3 in MgO for example (Yan et al., 1977, Figure 7), lowered the boundary mobility by nearly an order of magnitude. But by lowering the boundary mobility only, impurities would only affect the initial development of the microstructures and the rate of grain growth. Although the kinetics of the '9.5' data were more sluggish than the pure data (Figure 4), they were similar enough to the '5.0' data to indicate that the rate of growth had not been significantly reduced. Given the heat-treatment conditions, SiO_2 would react with the CaCO_3 to form CaSiO_3 (Harker and Tuttle, 1956). If insoluble precipitates formed, they would add to the second phase concentration and thereby contribute to limiting the grain sizes. The effects of impurities on grain growth in synthetic marbles have been recognized in other experiments. Attempts to induce grain growth in dry calcite jacketed in copper under conditions similar to those used here were only moderately successful (Gee 1982). In recent experiments where the dry calcite was isolated from the copper jacket by silver foil, grain growth occurred at a rate only slightly slower than in the "wet" experiments (see Chapter 3). As an ionic impurity, copper would lower the boundary mobility, and as oxide particles it would pin the boundaries. It is not apparent from the grain growth curves (Figure 4) whether the anomalously low D_{max} values were a kinetic or a pinning effect.

An alternative explanation derives from the relative sizes of the calcite and alumina powders. Before the fabrication and heat-treatment steps, the particle sizes of the '9.5' powder and, to a lesser extent, of the '5.0' powder were significantly larger than the initial size of the calcite powder (Table 2 and Figure 1). During primary recrystallization

and the initial stages of grain growth, a single alumina particle may have impeded the movement of two or more calcite boundaries, and thereby decreased the "effective" particle size. Such a condition has not been examined, and in fact, the theories listed in Table 1 were based on the assumption that $d \ll D$. Multiple boundary pinning would not be expected in the '0.1' and '1.0' sets, since no large particles existed in either.

A liquid grain-boundary phase may have altered the kinetics of grain growth but it is unlikely that it affected D_{\max} significantly. Grain growth in the presence of a liquid has been examined by Greenwood (1955) for dispersed grains and by Lay (1968) for closely packed grains. Lay (1968) showed that grain growth followed a cubic law in support of the results shown in Figure 4. Previous studies on wet and dry synthetic marbles (Evans and Olgaard, 1980, and Gee, 1982) and several experiments on ceramics (see review by Yan *et al.*, 1977) indicate that liquid phases enhance grain growth. Therefore liquid phases should decrease the time required to reach a limited grain size.

DISCUSSION

Comparison with other experiments

Several experimental studies have been conducted on both metals and ceramics to determine the effects of second phases on grain growth and to check the validity of the theories relating second phases to a limiting grain size. The second phases used have been of two types: 1) precipitates, which have limited solubility in the matrix and coarsen with time at high temperatures; and 2) particles, which remain immobile, rigid and constant in size. Data from eight studies are summarized in

Table 4 and are compared to our data in Figure 9. The lines in Figure 9 represent least-square fits to particular data sets. For the data of Hsu (H), Flowers and Karas (FK), and Koul and Pickering (KP), a single line was fit through each set. For the present study (O) and Tweed *et al.* (THR) the lines were fit through points of constant d . For Green (G), Lange and Hirlinger (LH), Anand and Gurland (AG) (matrix diameter is for subgrains, not grains), and Hellman and Hillert (HH) the lines were fit through points of constant f . By fitting lines to the data in this way, the dependence of D_{\max} on d was determined from G, LH, HH, and AG and on f from O and THR. For the first case, $D = K'd^p$, p (f constant) varied between 0.7 and 2, clustering near 1, in agreement with all of the models listed in Table 1. For the second case, $D = C'f^{-m}$, m (d constant) varied between 0.33 and 0.55. For those experiments where neither d nor f were held constant the dependence of D_{\max} on d/f varies between 0.9 and 1.4.

Comparison of data to models

Assuming that D_{\max} depends linearly on d , all of the data were plotted in Figure 10 as D_{\max}/d vs. f and compared to the models listed in Table 4. A least-squares fit was made through all of the data from each study. The error bars represent the range of D/d listed for a given f . A least squares fit through the data of this study had a slope of 0.7 but was not plotted because of the very low correlation coefficient.

No general relationship was found to fit all of the data.. The H, AG, and KP data lines have a slope near 1, and fit both the Hellman and Hillert (Eqn. 4) and the Zener (Eqn. 1) models rather well. The FK data also has a slope near 1 but more closely fits the Haroun and Budworth

model, although a line of almost any slope could be drawn through the data. The rest of the data have a much weaker dependence of D_{\max} on f with slopes ranging between 0.27 and 0.55, correlating more closely with equations 7-11. The fact that the '0.1' and '1.0' data have higher D_{\max}/d values than predicted, supports the observation that particles clustered into agglomerates. The reason for the high D_{\max}/d values for the THR data is unknown. Although the particles were plate-like in shape, with maximum:minimum length ratios of 1:6, shape effects would not cause this large a difference (Wold and Chambers, 1968; Nes et al., 1985). Tweed et al. (1983) did not note any clustering of particles although they recognized that the oxide distribution was not completely uniform. The HH, LH, G, and the '5.0' and '9.5' data are within the range of equations 7-11, although the LH and '9.5' data are below. Equation 8 was derived in order to explain the observation that the inclusions of the AG samples were dispersed on the subgrain walls. Although their data fit equation 8 reasonably well, the least-squares fit shown in Figure 10 shows a near linear dependence of D_{\max}/d on f . Therefore, their data supports the theories that assume a random second phase dispersion.

Assuming that there were no concentration-dependent effects, such as solute solubility or particle clustering, most of the data show a much weaker dependence of D_{\max} on f than predicted by the Zener-type theories. This weak dependence may indicate that the second phases were preferentially located along grain boundaries and at triple junctions, and therefore the assumption of a random dispersion may not always be valid. In the studies where the second phase precipitates were mobile and coarsened with time (AG, KP, G, LH, HH, H, and FK), one would expect

that the boundary concentration would increase as pores are swept up by the migration front. Micrographs from LH, G, and AG support this idea. Micrographs from H showed that precipitates were well dispersed intra- and intergranularly, however, all three variables, D_{\max} , d , and f , changed with heat-treatment temperature. Micrographs from THR and from our study indicated that the particles were randomly dispersed before and after grain growth. Systematic errors in the experiment, which would cause the data to artificially agree with the weak dependence of D_{\max} on f laws, were unlikely. The discrepancy in the '0.1' and '1.0' data could be explained if particle clustering were concentration dependent. However, little or no clustering was observed for any concentration. The data for the largest d/f values in Figure 8 indicate that D may not have reached a pinned state ('0.1', 0.02%; and '1.0', 0.2% vs. Pure) but this explanation is unlikely for the '5.0' or '9.5' data.

Finally, for the smallest d/f values, initial boundary migration associated with primary recrystallization may have created an initial grain size for normal grain growth that was already larger than the predicted limit (e.g. '1.0' 5 and 10%; and '9.5', 10%). Even if allowances were made for all three of these arguments, they could not explain the '5.0' data where little or no clustering was observed; D_{\max} for the 1% specimen was less than D_{\max} for the pure specimen; and grain growth was observed in the 10% specimens.

SUMMARY AND CONCLUSIONS

Two phase synthetic marbles were hot-pressed with varying sizes and concentrations of alumina particles in order to test the models for grain-growth inhibition by second phases. Growth curves for the two-phase marbles vs. the pure calcite showed that a limiting grain size was obtained in all cases. Both optical and electron microscopy indicated that the particles were randomly dispersed intra- and intergranularly, and that the boundary structures were consistent with normal grain growth occurring during the heat-treatment. A liquid film, presumably a partial melt, was present along many grain boundaries during the heat-treatment. This film may have accelerated grain growth kinetics but should not have affected the limiting grain size.

The results showed that the stable grain size had a weaker dependence on volume fraction than predicted by the "Zener-type" models. This dependence was consistent with other models derived from computer simulation or from special boundary-particle configurations (Srolovitz et al., 1984, Anand and Gurland, 1975, Haround and Budworth, 1968, and Hellman and Hillert, 1975 and Appendix 1). No consistent dependence was found for D_{\max} on d . This was believed to be due to particle clustering, impurities, and/or the matrix/particle-size ratios. Data from other studies showed a consistent linear dependence of D_{\max} on d , in agreement with all of the models, and showed a dependence of D_{\max} on f^{-m} , for m equal to 0.3 to 1.3. The data analyzed was within the range of the models, but no single model could explain all of the data satisfactorily.

In the earth, dispersed second phases are always present, and millions of years are available for grain growth. Even at low metamorphic temperatures, grain size would be expected to be in equilibrium with the size and concentration of second phases, unless external driving forces were introduced. Such external driving forces may have arisen from plastic strain, thermal stresses, phase transformations, and chemical interactions. The magnitude of these external driving forces would be reflected in the relationship between D_{\max} , d , and f .

The present understanding of second phase size and concentration is inadequate to explain many observations. Other variables such as the prior mechanical history and the second phase mobility and dispersion characteristics are also very important.

BIBLIOGRAPHY

- Anand, L., and J. Gurland, The relationship between the size of cementite particles and the subgrain size in quenched and tempered steels, Metall. Trans. A, 6A, 928-931, 1975.
- Anderson, M.P., D.J. Srolovitz, G.S. Grest, and P.S. Sahni, Computer simulation of grain growth - I. Kinetics, Acta Met., 32, 783-791, 1984.
- Brook, R.J., Controlled grain growth, in Treatise on Materials Science and Technology, edited by F.F.Y. Wang, 9, 331-364, Academic Press, New York, 1976.
- Caristan, Y., R.J. Harpin, and B. Evans, Deformation of porous aggregates of calcite and quartz using the isostatic hot-pressing technique, Tectonophysics, 78, 629-650, 1981.
- Clarke, D.R., On the detecting of thin intergranular films by electron microscopy, Ultramicroscopy, 4, 33-44, 1979.
- Clarke, D.R., Observation of microcracks and thin intergranular films in ceramics by transmission electron microscopy, J. Am. Ceram. Soc., 63, 104-106, 1980.
- Evans, B., and D.L. Olgaard, Static recrystallization of pure calcite and two-phase assemblages of calcite/biotite and calcite/phlogopite, EOS Trans. Amer. Geophys. Union, 61, 1131, 1980.
- Exner, H.E., Analysis of grain- and particle-size distributions in metallic materials, Int. Metall. Rev., 17, 25-42, 1972.
- Flowers, J.W., Grain growth inhibition by spherical particles with a distribution of sizes, IEEE Trans. Magn., 15, 1601-1603, 1979.
- Flowers, J.W., and S.P. Karas, Coalescence of sulfides during secondary growth in 3% Silicon-Iron, J. Appl. Phys., 38, 1085-1086, 1967.
- Gladman, T., On the theory of the effect of precipitate particles on grain growth in metals, Proc. R. Soc. London, 294A, 298-309, 1966.
- Green, D.J., Critical microstructures for microcracking in $\text{Al}_2\text{O}_3\text{-ZrO}_2$ composites, J. Am. Ceram. Soc., 65, 610-614, 1982.
- Greenwood, G.W., The growth of dispersed precipitates in solutions, Acta Met., 4, 243-248, 1956.
- Haroun, N.A., Theory of inclusion controlled grain growth, J. Mater. Sci., 15, 2816-2822, 1980.
- Haroun, N.A., and D.W. Budworth, Modifications to the Zener formula for limitation of grain size, J. Mater. Sci., 2, 326-328, 1968.
- Hellman, P., and M. Hillert, On the effect of second-phase particles on grain growth, Scand. J. Metallurgy, 4, 211-219, 1975.
- Hillert, M., On the theory of normal and abnormal grain growth, Acta Met., 13, 227-238, 1965.
- Koul, A.K., and F.B. Pickering, Grain coarsening in Fe-Ni-Cr alloys and the influence of second phase particles, Acta Met., 30, 1303-1308, 1982.
- Lange, F.F., and M.M. Hirlinger, Hindrance of grain growth in Al_2O_3 by ZrO_2 inclusions, J. Am. Ceram. Soc., 67, 164-168, 1984.
- Lay, K.W., Grain growth in $\text{UO}_2\text{-Al}_2\text{O}_3$ in the presence of a liquid phase, J. Am. Ceram. Soc., 51, 373-376, 1968.
- Lou, L.K.V., T.E. Mitchell, and A.H. Heuer, Impurity phases in hot-pressed Si_3N_4 , J. Amer. Ceram. Soc., 61, 392-396, 1978.

- Louat, N., The inhibition of grain-boundary motion by a dispersion of particles, Philos. Mag. A, 47, 903-912, 1983.
- Nes, E., N. Ryum and O. Hunderi, On the Zener Drag, Acta Met., 33, 11-22, 1985.
- Paterson, M.S., The melting of calcite in the presence of water and carbon dioxide, Am. Mineral., 43, 603-606, 1958.
- Schwenn, M.B., and C. Goetze, Creep of olivine during hot-pressing, Tectonophysics, 48, 41-60, 1978.
- Smith, C.S., Grains, phases and interfaces: an interpretation of microstructure, Trans. AIME, 175, 15-51, 1948.
- Srolovitz, D.J., M.P. Anderson, G.S. Grest, and P.S. Sahni, Computer simulation of grain growth-III. Influence of a particle dispersion, Acta Met., 32, 1429-1438, 1984.
- Tweed, C.J., N. Hansen, and B. Ralph, Grain growth in samples of aluminum containing alumina particles, Metall. Trans. A, 14A, 2235-2243, 1983.
- Wyllie, P.J., and A.L. Boettcher, Liquidus phase relationships in the system CaO-CO₂-H₂O to 40 kilobars pressure with petrological applications, Am. J. Sci., 267-A, 489-508, 1969.
- Wyllie, P.J., and O.F. Tuttle, The system CaO-CO₂-H₂O and the origin of carbonatites, J. Petrology, 1, 1-46, 1960.
- Yan, M.F., R.M. Cannon, and H.K. Bowen, Grain boundary migration in ceramics, in Ceramic Microstructures - 76, edited by Fulrath and Pask, 276-307, Westview Press, 1977.
- Zener, C., private communication to C.S. Smith, Grains, phases and interfaces: an interpretation of micro-structure, Trans. AIME, 175, 15-51, 1948.

TABLE 1. Theoretical expressions for the dependence of D_{\max} on d and f .

1. $D_{\max} = R = 4/3(r/f) = 2/3(d/f)$ Zener (1948)

2. $R \sim 9D_{\max}$; $D_{\max} = 0.08(d/f)$ Haroun and Budworth (1968)

3. $r = \frac{6R_0 f}{\pi} (3/2 - 2/z)^{-1}$ Gladman (1966)
 $2R_0 \cong D_{\max}$, $z = \frac{D}{D_0}$ $\sqrt{2} < z < 2$
 $d \cong \frac{12D_{\max} f}{\pi} (3/2 - 2/z)^{-1}$

4. $2R_0 = D_{\max} = \left(\frac{4}{9} \frac{d}{\beta f}\right)$ Hellman and Hillert (1975)
 $\beta = 0.125 \ln 40(\rho/r)$

5. $D_{\max} = 4/9 \left(\Sigma \frac{\beta_1 f_1}{d}\right)^{-1}$ Hellman and Hillert (1975)

6. $R = \frac{4r}{3f} \left[16/\left[\ln \frac{2R}{r} \left(1 - 16/\ln \frac{Re^2}{r}\right)^2\right]\right]$ Louat (1983)
 converted assuming $R \cong 9 D_{\max}$
 $D_{\max} = \frac{2d}{9f} \left[16/\left[\ln \frac{12 D_{\max}}{d} \left(1 - 16/\ln \frac{6e^2 D_{\max}}{d}\right)^2\right]\right]$

7. $L = Cr/f^{1/2}$ $D = (3/4)Cd/f^{1/2}$ Anand and Gurland (1975)
 $C = 2.71$ (Zener model)
 $C = [5.52 - 7.36/z]^{1/2}$ (Gladman model)

8. $D_{\max} = 1.03 d/f^{1/2}$ Haroun and Budworth (1968)

TABLE 1. (cont'd.)

9. $D_{\max} = \left(f \sum \frac{x_i}{d_i^2} \right)^{-1/2}$	Haroun (1980)
10. $D_{\max} = 1.8 \frac{d}{f^{1/3}}$	Hellman and Hillert (1975)
11. $D_{\max} = 2.5 \frac{d}{f^{1/3}}$	Appendix 1

D_{\max} = limiting grain size expected during normal grain growth

R = radius of curvature of grain boundary

r = second phase radius

d = second phase diameter

f = volume fraction second phase

R_0 = 1/2 distance between parallel hexagonal faces of a tetrakaidekahedron

L = linear intercept length = (2/3) D

x_i = fraction of particles of diameter d_i

ρ = macroscopic curvature of boundary

Since most measurements of matrix grain size or particle size are of diameters, we have converted all equations to account for this. For clarity, both the expression as originally quoted by the author and as we have converted it are listed here. All future discussion will refer to the converted expressions.

TABLE 2. Al₂O₃ and CaCO₃ powder diameters

Grit Size	Mean diameter (μm)					
	X-ray Sedimentation ^{1,2}		TEM	BET ³ after before		Agglomeration factor ⁴
Al ₂ O ₃	d _F	d _X		d _{BET}		
0.1 ^a	0.290 σ ⁶ 0.13-0.63	0.103		0.059	0.57	1.75
1.0 ^a	0.404 0.22-0.74	0.210	0.38	0.25	0.26	0.84
5.0 ^b	2.53 1.33-4.82	1.20	0.72	1.26	0.96	0.91
9.5 ^c	4.73 3.51-6.38	3.92		1.4	1.4	2.8
CaCO ₃ ^d	2.81 ⁵	0.648 ⁵		0.8 ⁵	3.2	0.81

¹d_X = Equivalent spherical diameter at 50% number fraction.

²d_F = Flowers diameter, see Appendix 2.

³Equivalent spherical diameter calculated from specific surface area after and before mechanical grinding.

⁴Equal to d_X/d_{BET}; an estimate of the relative dispersion of second phases.

⁵Determined after powder was mechanically ground equivalent to mixing procedure.

⁶σ = one standard deviation

^a 0.1CR alpha and 1.0CR alpha Baikadox, Baikowski Int. Corp., Charlotte, NC

^b AOP5-1, Al₂O₃ powder, Mark V Lab, E. Granby, CT

^c 40-6009-095 Al₂O₃ powder, Buehler Ltd. Lake Bluff, IL

^d CaCO₃ AR, Mallinckrodt Inc., Paris, KY

TABLE 3. Grain growth data

Al ₂ O ₃ mixture		D ^c , average grain size				
grit size ^a d _F	f ^b	hot-pressed starting material	CA-13 t=1 hr.	CA-12 t=10 hrs.	CA-11 t=24 hrs.	CA-15 t=24 hrs.
0.1/0.29	0.0002	7.1	35.9	58.8	85.4	54.2
	0.001	7.7, 11.0	27.5	50.6	28.7	49.6
	0.002	11.0	21.2	27.2	47.0	45.2
	0.01	8.1, 10.3	13.4	18.2	14.2	18.2
1.0/0.40	0.002	8.2	26.6	58.8	65.1	63.2
	0.01	7.7	16.8	24.0	31.5	25.9
	0.02	9.0	15.6	19.2	17.3	18.0
	0.05	9.9	--	9.6	8.4	9.5
	0.10	6.9	--	7.8	7.7	7.8
5.0/2.53	0.01	9.0	13.4	27.0	27.8	41.0
	0.05	7.7	10.8	20.0	22.2	15.3
	0.10	8.5	--	13.8	12.0	11.8
9.5/4.73	0.01	5.6	11.9	27.0	22.4	26.0
	0.02	8.5	12.0	17.7	22.1	22.5
	0.05	6.0	--	8.4	9.0	9.3
	0.10	5.8	--	11.2	11.0	9.5
CaCO ₃	P-2	0	13.3	31.1	66.2	
	P-3	0	23.0			
	P-4	0	11.2			69.2
	P-10-1 ^d	0	12.3	17.4		84.6
	P-10-2 ^d	0	9.1	17.2	35.5	68.4

^a d chosen as d_F from Table 2

^b f = volume fraction second phase

^c D = 3L/2 where L equals the mean linear intercept length (Underwood, 1970)

^d Pure CaCO₃ powder initially hot-pressed at 550°C.

TABLE 4. Second phase-limited grain size data for metals and ceramics

Materials/Reference matrix/second phase	f vol. fraction	#points	D=C'(d/f)P [†]		r ^{2*}	D _{max} = Cd/f ^m #			
			C'	p		#points	C	m	r ²
Al ₂ O ₃ /ZrO ₂ Lange & Hirlinger (1984)	.01	2	10 ⁻²⁷	27	1				
	.025	2	2.6	1.1	1				
	.05	6	2.3	1.1	0.95				
	.075	6	1.8	.92	0.92				
	.10	6	1.6	1.0	0.99				
without .01 & .025						18	0.47	0.52	0.83
with .01 & .025						22	0.91	0.27	0.69
Al ₂ O ₃ /ZrO ₂ Green (1982)	.05	4	4.0	1.2	0.99				
	.10	4	2.0	2.3	0.82				
	.15	4	2.4	.97	0.98				
	.20	4	1.8	1.3	1.0				
	without abnormal g.g.						13	1.3	0.29
with abnormal g.g.						16	1.0	0.43	0.72
Ferrite/cementite Hellman & Hillert (1975)	.03	8	7.5	.69	0.97				
	.057	10	5.6	.59	0.95				
	.12	10	4.1	.78	0.95				
						28	1.15	0.48	0.74
particles and subgrains Carbon steels/cementite Anand & Gurland (1975)	.07	1	---	---	---				
	.12	4	3.7	0.73	1.0				
	.16	5	3.7	1.1	0.97				
	.19	4	2.9	1.3	0.96				
						14	0.67	0.89	0.79

TABLE 4. (cont'd.)

Materials/Reference matrix/second phase	d(μm)	#points	$D_{\text{max}} = \text{Cd}/\text{fm}^{\dagger\ddagger}$		
			C	m	r^2
CaCO ₃ /Al ₂ O ₃ present study	0.29	4	13.8	0.34	0.94
	0.40	5	5.0	0.55	0.99
	2.5	3	2.2	0.39	0.97
	4.7	4	0.58	0.49	0.96
Total		16	1.0	0.70	0.64
CaCO ₃ /mica (Chapter 3)	Total Experiment 2033	2	7.0	0.24	1.0
Alumina/Al ₂ O ₃ Tweed <i>et al.</i> (1983)		5	53.8	0.33	0.73
RSP steel/several conventional steel/several Hsu(1984)		6	0.87	0.90	0.95
		6	0.07	1.22	0.98
Fe-Ni-Cr alloys/Carbides Koul & Pickering (1982)		5	1.25	0.78	0.77
3% Si-Fe steel/MnS Flowers & Karas (1967)		5	0.001	1.34	0.37

* r^2 = coefficient of determination

†equation used to plot data in Figure 9

‡equation used to plot data in Figure 10

FIGURE CAPTIONS: CHAPTER 2

- FIGURE 1. X-ray sedimentation results for calcite and alumina particles. The data were collected as mass percent, M , and has been converted to number percent, $\#$. (See Appendix 2 for calculations and original curves.)
- FIGURE 2. Experimental assembly inside pressure vessel. $H_2O + CO_2$ pore pressure was added through the thermocouple hole. The uncertainty in the temperature over a maximum sample length of 70 mm was $\pm 10^\circ C$. The schematic is approximately 1/2 true scale.
- FIGURE 3. A typical temperature, T , and confining pressure, P_c , history for the experiments.
- FIGURE 4. Calcite grain growth curves for the various calcite + alumina mixtures. The normal growth law ($D^n - D_0^n = Kt$) for various values of n has been plotted for comparison with the pure data. Where no error bars are shown, uncertainty was less than the size of the symbol. A stable grain size, D_{max} , was reached within 10 hours in almost all cases. Symbols are for volume percent of alumina.
- FIGURE 5. Optical and TEM micrographs of samples heat-treated at 550° or $650^\circ C$ and 500 MPa confining pressure for one hour. Fraction (e.g. 1/10) represents grit size (μm)/volume fraction (%). Optical: a) pure $CaCO_3$; b) moderate concentration of alumina; c) high concentration of alumina. TEM: d) particle interactions with boundaries and dislocations. (Spots are due to electron-beam damage.); e) dislocations, low-angle boundaries, and pores; f) particles clustering along grain boundaries.
- FIGURE 6. Optical and SEM micrographs of samples heat-treated at $800^\circ C$ and 300 MPa for 24 hours. Symbols are the same as in Figure 5. Optical: a) pure $CaCO_3$; b) moderate concentration of alumina; c) low concentration of alumina showing particle-boundary interactions; d) high concentration of alumina. SEM: e) clustering of fine particles; f) little or no clustering of coarse particles.
- FIGURE 7. TEM micrographs showing boundaries with and without a grain boundary film. a) Bright-field image showing dislocations, a low angle boundary, and a circular pore. b) Dark-field image showing very fine particles in a "glassy" matrix along grain boundaries or cracks. Inset: selected-area-diffraction pattern from grain-boundary region; c) Bright-field (left) and dark-field (right) micrographs of low-temperature specimens showing the absence of melt. Note lens-shaped pores.

- FIGURE 8. D_{\max} vs. d/f (Equation 12) for the synthetic marbles. Shaded region chosen to bound points 10% of '0.1' and 0.2% of '1.0'. "Pure" point shows range of the pure data at 24 hours.
- FIGURE 9. D_{\max} vs. d/f for the synthetic marbles compared to data the from other studies on metals and ceramics listed in Table 4. See text for the label identification (letters are authors last initials). Data for constant f used for D_{\max} dependence on d ; data for constant d used for D_{\max} dependence on f .
- FIGURE 10. Comparison of D_{\max}/d vs. $1/f$ data for the synthetic marbles and the other composites (Table 4) to the models listed in Table 1. Numbers refer to equation numbers. Letters stand for authors last initials, as in Figure 9. Error bars represent the range in D_{\max}/d for a given f .

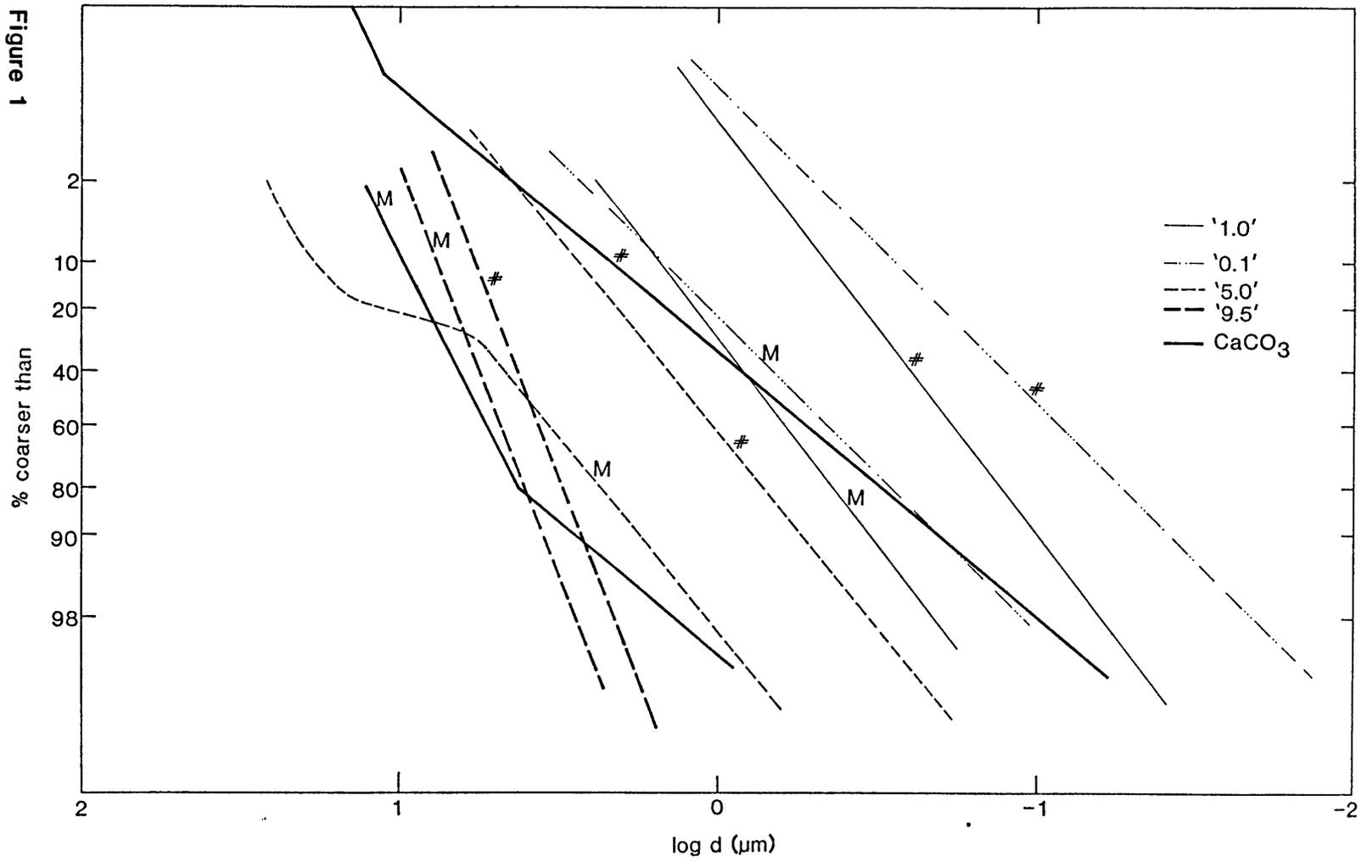


Figure 1

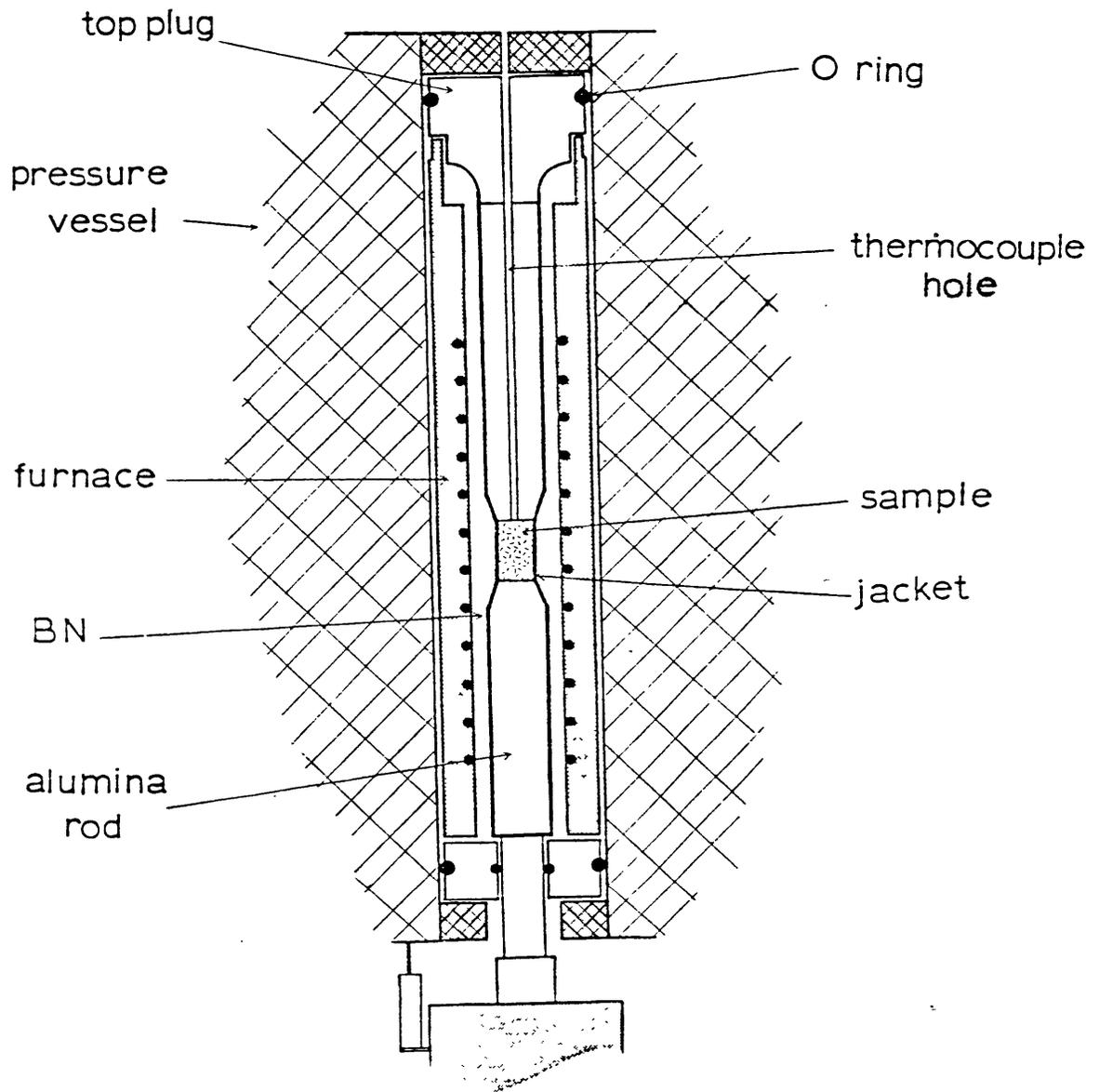
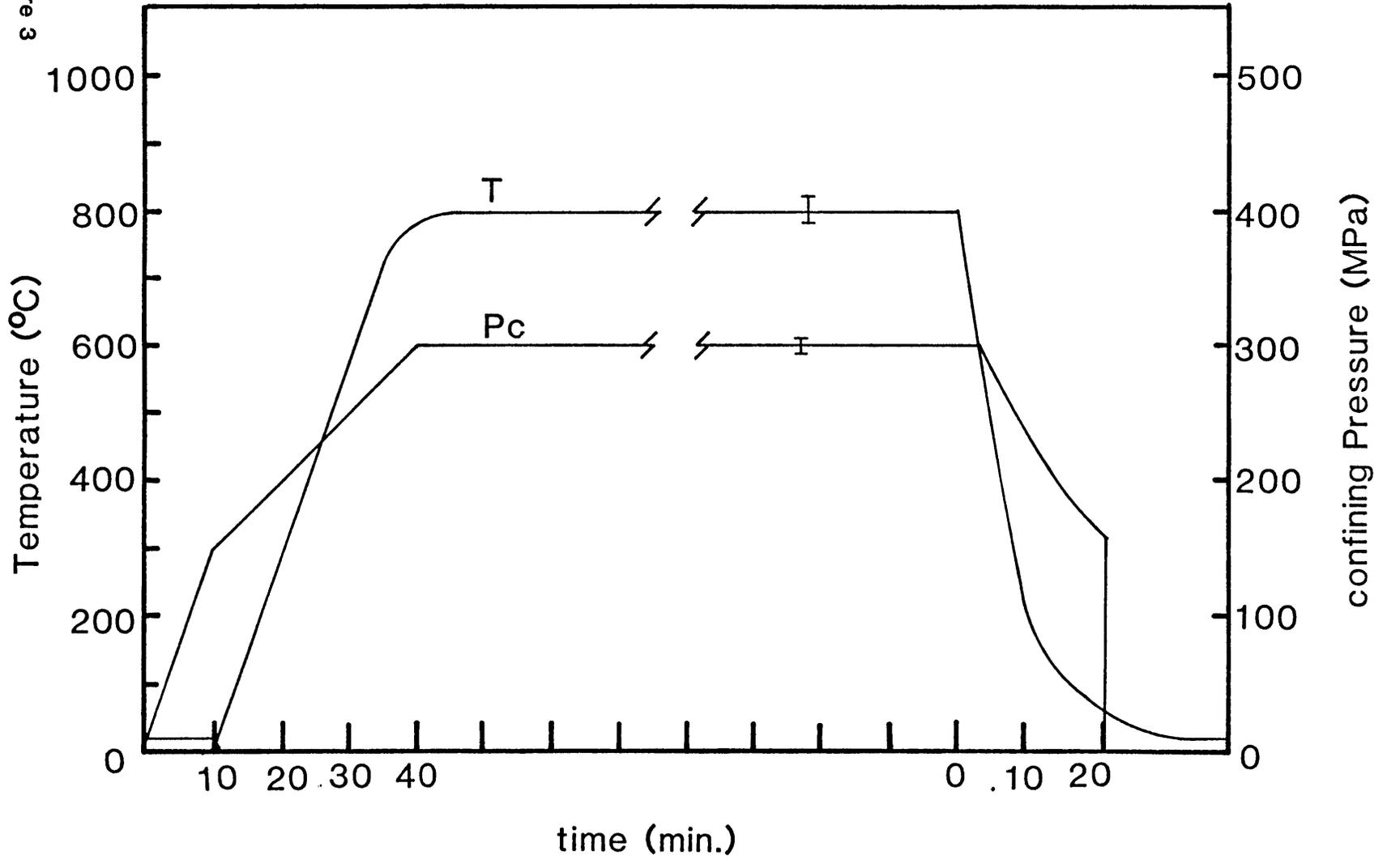


Figure 2

Figure 3



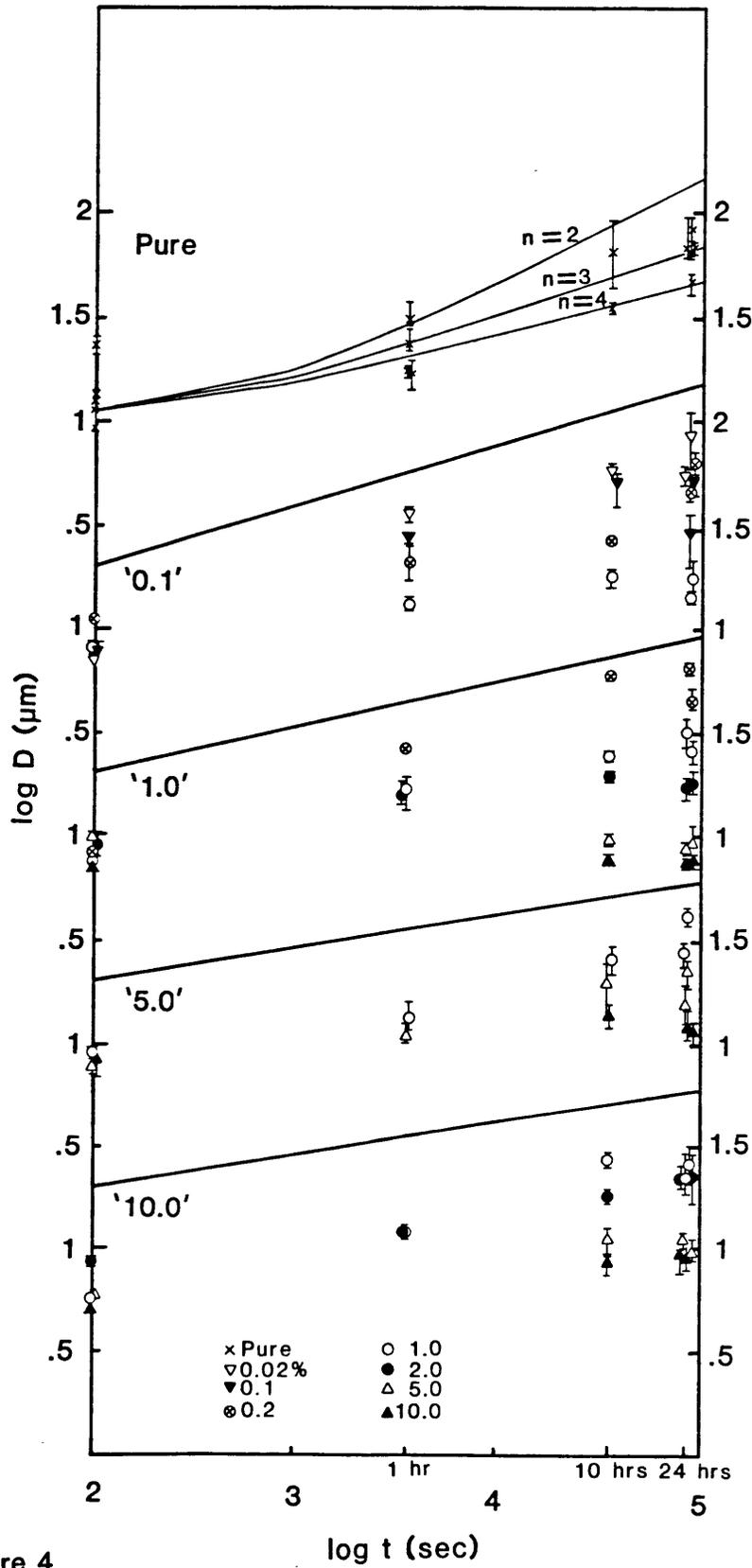


Figure 4

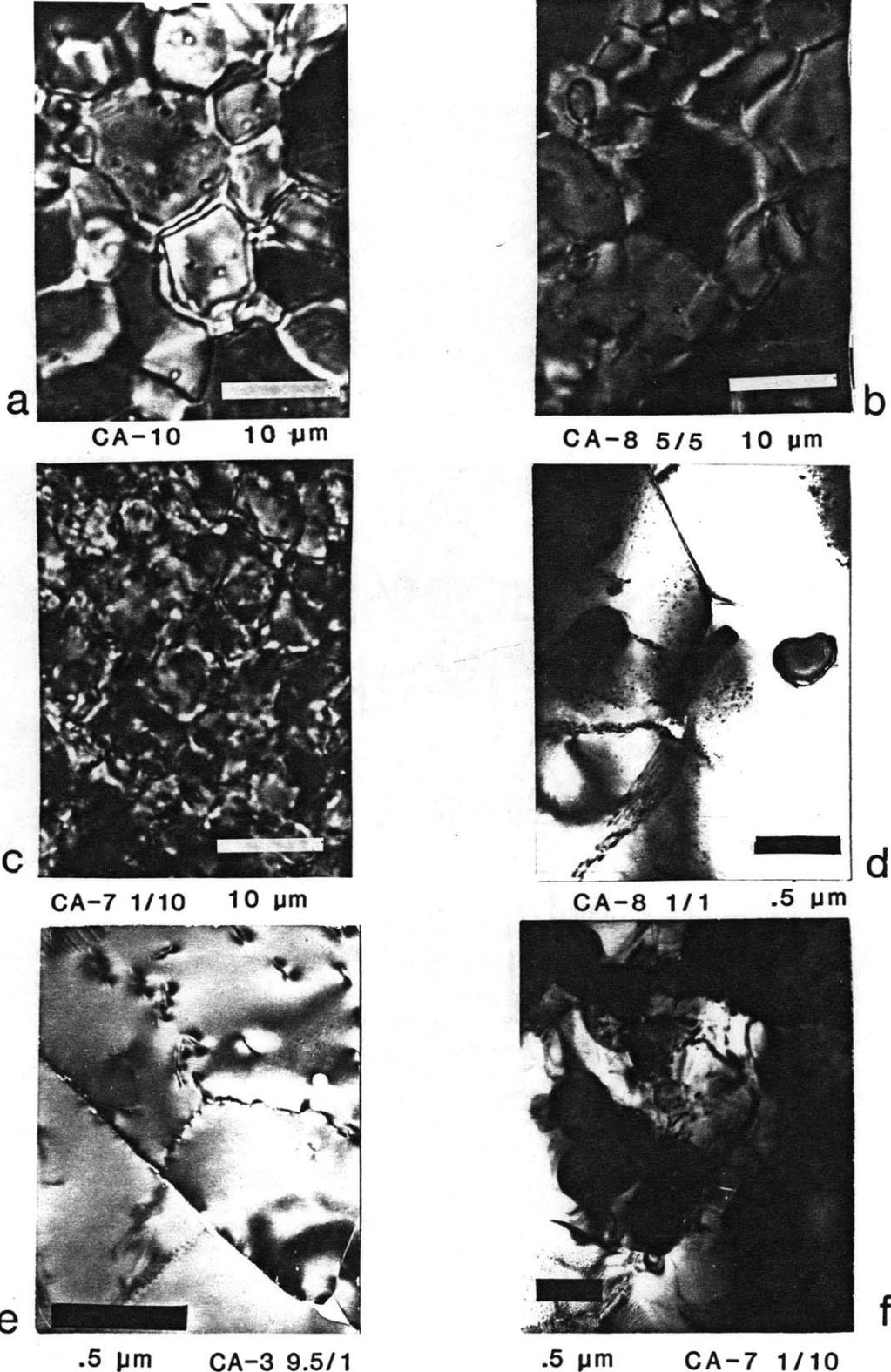


Figure 5

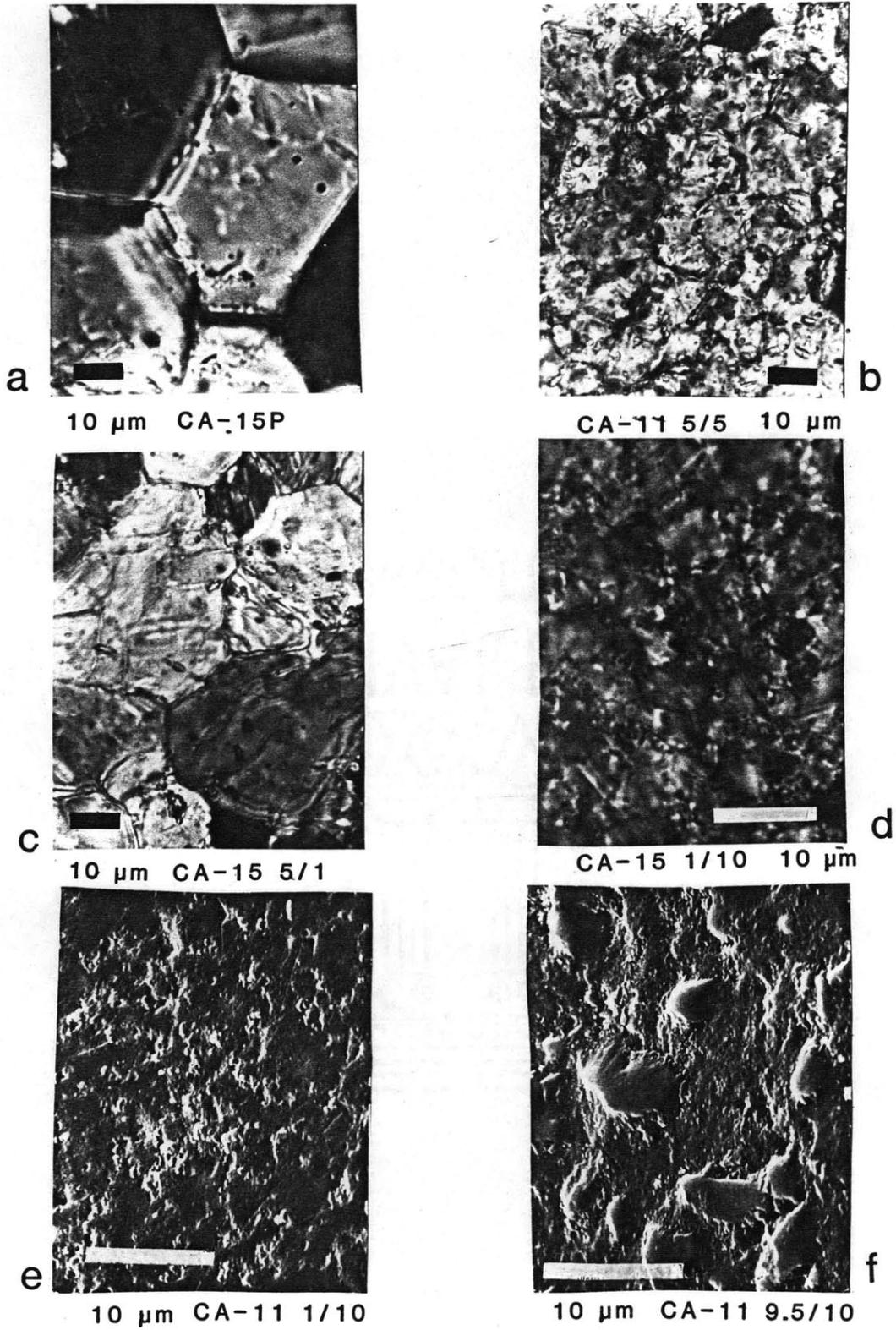
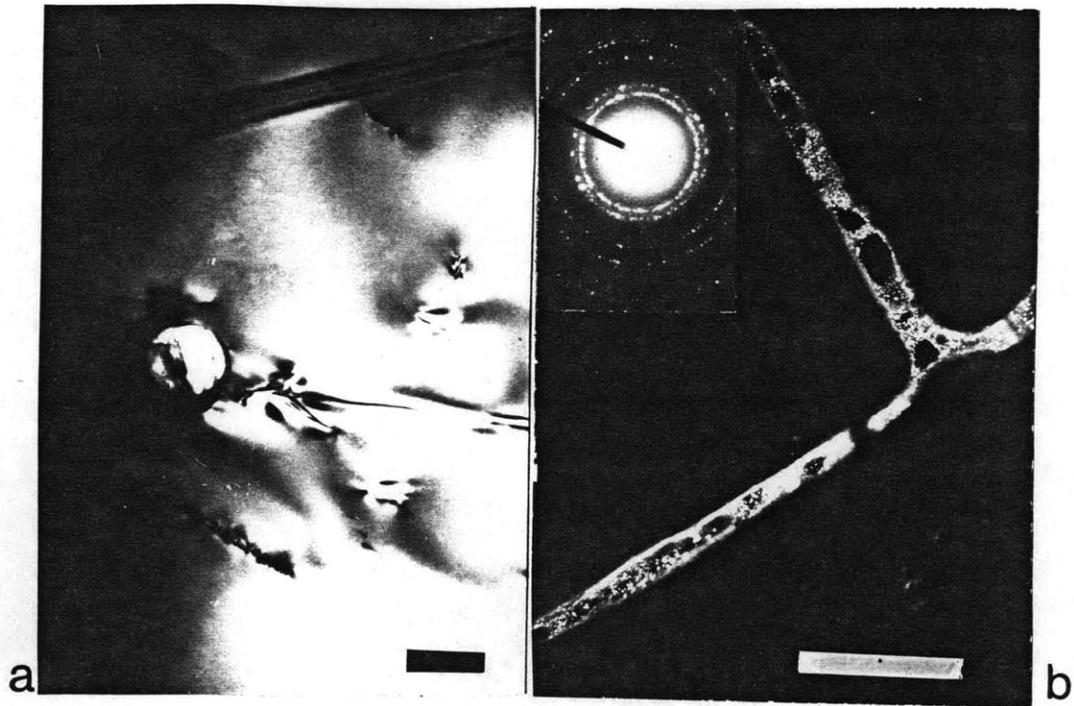


Figure 6



CA-11 5/5

.5 μ m

CA-11 1/10

.5 μ m



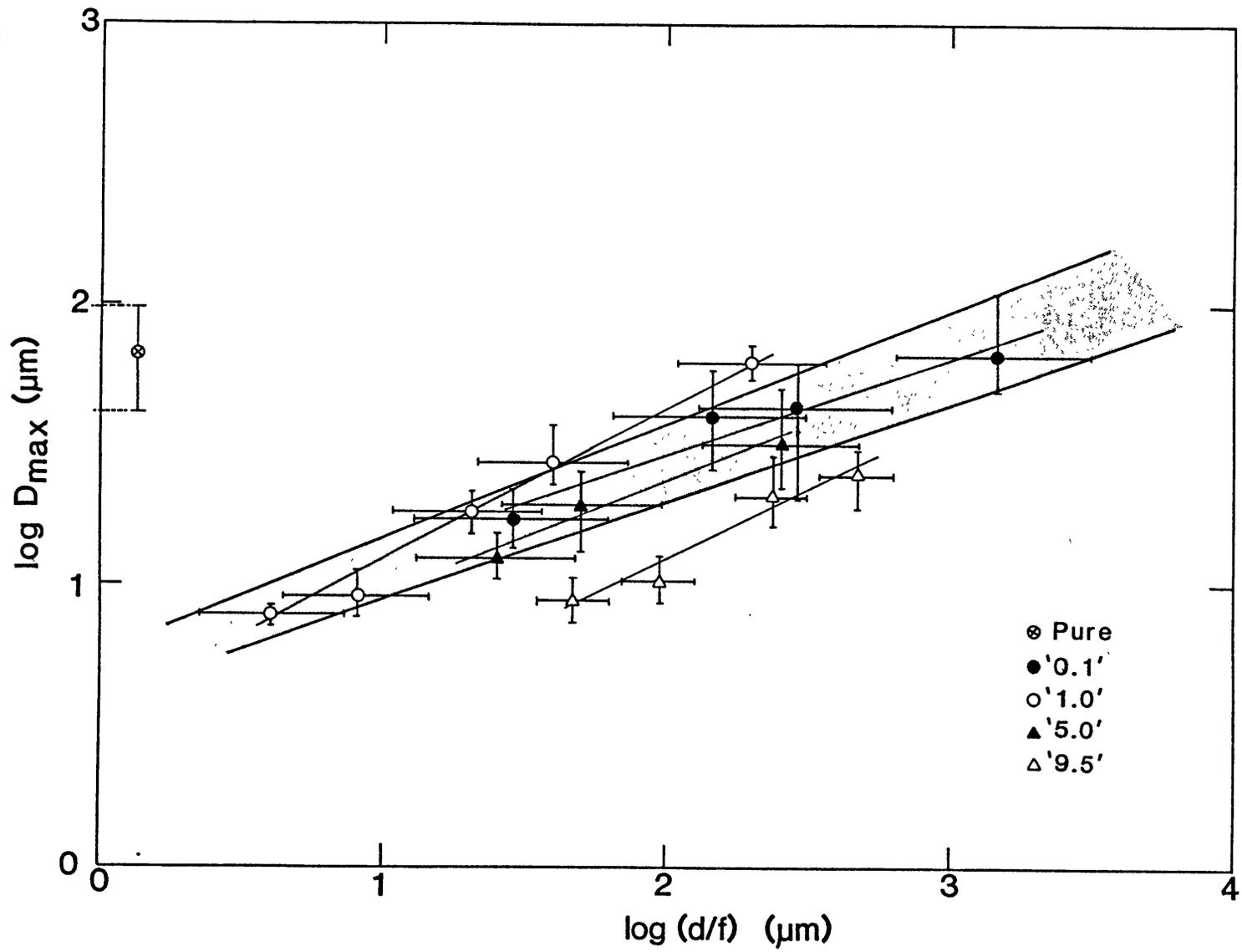
c

.5 μ m

CA-10

Figure 7

Figure 8



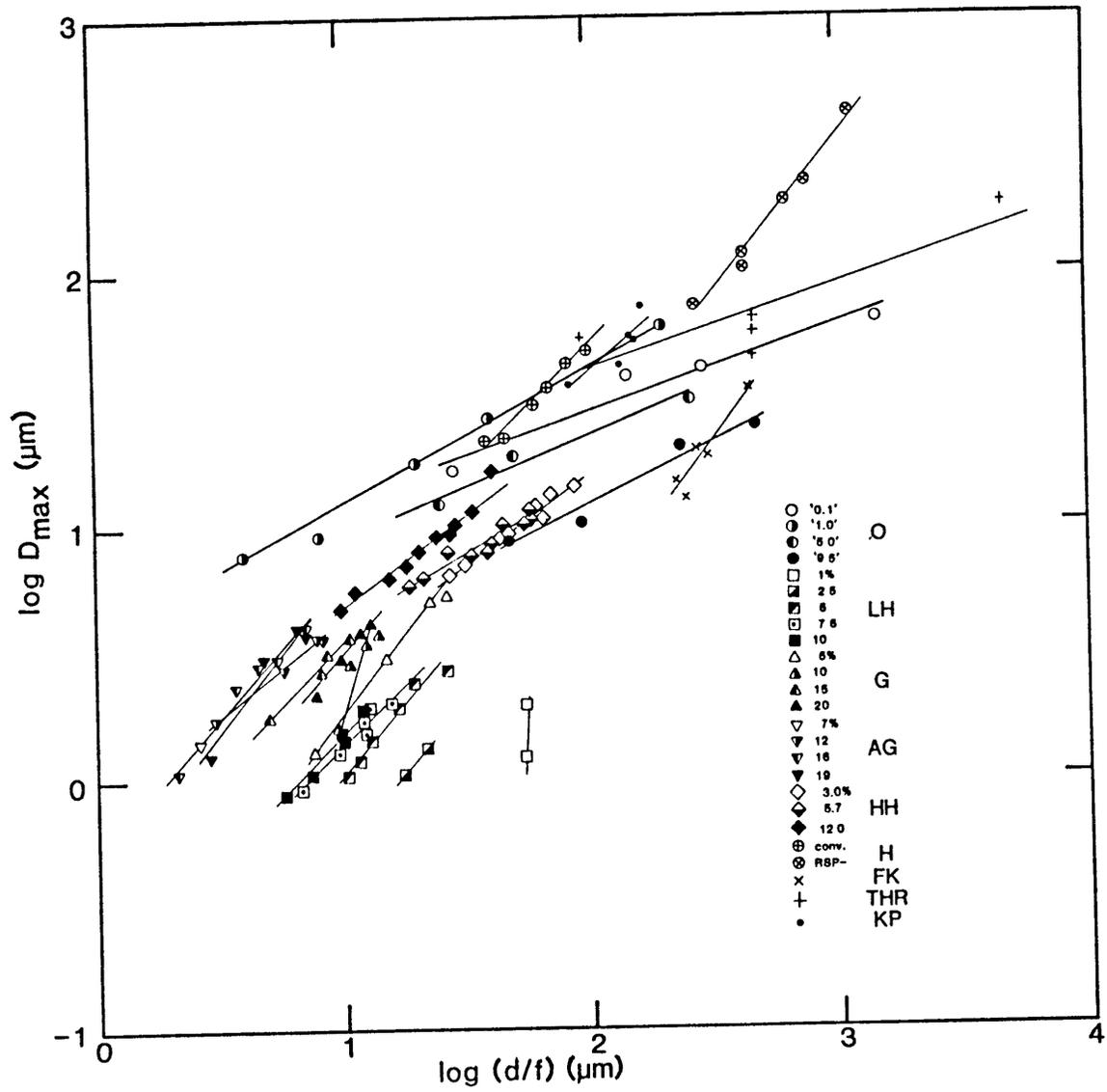


Figure 9

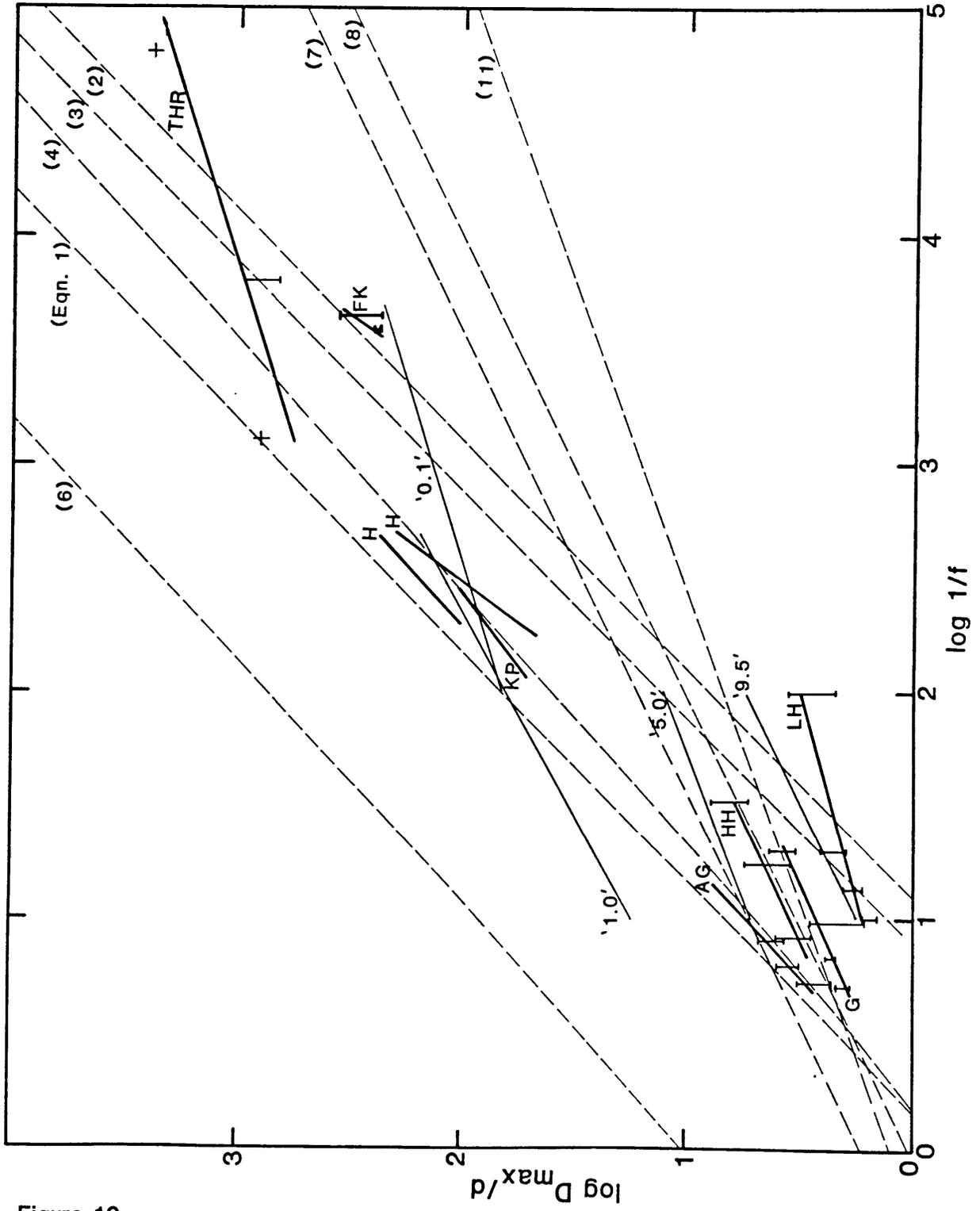


Figure 10

CHAPTER 3

RECRYSTALLIZATION AND GRAIN GROWTH OF PURE CALCITE
AND CALCITE/MICA SYNTHETIC MARBLES

INTRODUCTION

Deformation-induced microstructures, such as dislocation density, subgrain size, and dynamically recrystallized grain size, have been used to estimate paleostresses in deformed rocks (e.g. Mercier et al., 1977; Briegel and Goetze, 1978; Weathers et al., 1979; and Christie and Ord, 1980). However, as all of these authors recognized, the correlation between stress magnitudes estimated from different microstructures is often poor and several major uncertainties need to be resolved before these paleopiezometers can be used with confidence (White, 1979; Twiss, 1977). Of the three microstructures, dynamically recrystallized grain size seems to be the most resistant to transient stress conditions; thus it shows the most promise for recording major deformation events. A major problem with the grain size paleopiezometer is that grain-boundary migration may be affected by second phases such as particles, pores, fluids, and ionic impurities.

Ceramists and metallurgists recognize three distinct microstructural transformation processes that alter grain size: primary recrystallization, normal grain growth, and secondary recrystallization, also called abnormal grain growth. Although dynamic recrystallization is the stress-activated form of primary recrystallization, the effects of second phases on grain boundary migration and thus on the development of

an equilibrium grain size are most easily determined by first studying normal grain growth.

A recent trend among experimental petrologists and structural geologists has been to fabricate synthetic rocks by hot isostatically pressing fine powders into dense aggregates (e.g. Schwenn and Goetze, 1978; Caristan et al., 1981; Karato and Paterson, 1984; Chopra and Kohlstedt, 1983; Zeuch and Green, 1984. Using this method, the size and concentration of second phases, the impurity-ion content, the water content, and the initial matrix grain-size distribution can be controlled.

In Chapter 2, the effects of rigid, insoluble, alumina particles on grain growth in synthetic marbles were analyzed. In this chapter, attention was focused on other second phases known to be important in natural calcite rocks. Natural rocks commonly contain accessory clay or mica minerals that are known to affect metamorphic textures. The role of water during metamorphism is not well understood but known to be important as a transport medium for chemical reactions, and to affect deformation mechanisms and rock strength. Impurity ions are known to affect grain growth in cermics and are also common in natural carbonates. In fact several cations including Mg^{++} , Mn^{++} , Sr^{++} , and Ba^{++} are known to freely substitute for Ca^{++} in calcite. The purpose of the present study was to examine the effects of mica particles, pores, and water on grain growth in synthetic marbles and to compare the results to grain growth in rocks.

Recrystallization in geologic materials

The importance of solid-state recrystallization as a metamorphic process in rocks was first recognized by Buerger (1930). He urged geologists to follow the lead set by metallurgists and consider the question of recrystallization by plastic flow and subsequent annealing. The first quantitative study was carried out by Buerger and Washken (1947) on compressed powders of anhydrite, fluorite, and periclase--the first "synthetic rocks". The first recrystallization studies on calcite aggregates were performed by Griggs et al. (1960). It would be impossible to summarize all of the studies of recrystallization and grain growth that have been done since these first ones or even the studies that have recognized the effects of second phases or impurities. Instead, only a few of the more recent field and experimental observations are given here.

Several field observations have been made on the effects of second phases, impurities, and other parameters on grain size in naturally recrystallized rocks. Hobbs et al. (1976) described quartzites where the grain size and preferred orientation were linked to the mica content. Christie and Ord (1980) also recognized a size dependence of quartz grains on second-phase concentration in a dynamically recrystallized mylonite. They estimated that the grain size was approximately equal to the spacing of mica plates. Etheridge and Wilkie (1979) discussed the possible effects that second phases and aqueous fluids might have on grain-size sensitive deformation mechanisms and the formation of mylonites. Spry (1969) discussed both experimental and field observations of the effects of temperature on recrystallization. Evans

et al. (1980) measured grain size and second phase content in deformed clasts from a stretched-pebble conglomerate and found that grain size correlated inversely with second-phase volume fraction. Knipe (1980) analyzed the effects of impurity atoms (other than OH^- in quartz) and discussed their implications for deformation studies.

Several experimental studies on geologically important materials have also recognized the importance of second phases. Wilson (1979) studied the effects of several impurities, the most notable being mica plates, on grain size in deformed polycrystalline ice and qualitatively found an inverse dependence of grain size on mica content. Hobbs (1968) observed that recrystallization of single crystal quartz did not take place unless trace amounts of OH^- were present in the quartz structure, although he did not specifically study the effect of OH^- on boundary migration rates. Tullis and Yund (1982) studied grain growth in three natural quartzites and in one limestone and found a pronounced effect of water on the kinetics of grain growth in the quartzites. They found that recrystallization in marble was not strongly affected by the presence of water and, contrary to the results of this study, that minor amounts of other phases had little effect on grain growth.

MECHANISMS AND MODELS

Primary recrystallization, grain growth and
secondary recrystallization

The effects of second phases and impurity ions on grain growth in synthetic marbles will be the main emphases of this paper. Primary and secondary recrystallization will also be briefly discussed since they may be activated during the initial fabrication of the sample. More thorough discussions of these processes are given by Shewmon (1969) and Kingery et al. (1976).

Primary recrystallization involves the transformation of a deformed matrix into an underformed one by the production and motion of grain boundaries. New grains tend to nucleate at inhomogeneities such as pre-existing grain boundaries in regions with anomalously high strains. The nuclei are unstable until they grow to a critical size where the decreased internal free-energy of the new grain due to elimination of defects equals the increased surface free energy due to the increased grain boundary area. For a continuously deforming sample, this critical size is the dynamically recrystallized grain size. During static recrystallization, grains above this critical size grow until they impinge on one another and a strain-free matrix results.

When a nearly strain-free matrix has developed, grain growth will become the dominating process. Grain growth involves the reduction in surface free energy by boundaries migrating toward their center of curvature. In two dimensions, hexagonal grains would have straight sides and would thus be considered stable. But in three dimensions no such stable grain shape exists which both satisfies interface tension

constraints at grain corners and fills the space completely. The closest shape is a tetrakaidecahedron (see Appendix 1, Figure 1) with bowed sides. Grains will thus continue to grow until boundaries are restricted by second phases or until a single grain remains. Rarely, if ever, has the latter case been observed.

Normal grain growth kinetics are usually described by an equation of the form:

$$D^n - D_0^n = Kt \quad (1)$$

where D and D_0 are the grain sizes at times t and $t=0$ respectively. The growth-rate factor, K , is temperature dependent and is related to the grain boundary mobility, and n is a parameter dependent on the rate-controlling mechanism. In a pure system, n is theoretically equal to 2 (Burke and Turnbull, 1952). In practice, n is more commonly observed to be 3 or more. Table 1, reprinted from Brook (1976), lists several rate controlling mechanisms and the expected values of n . The mechanism(s) cannot unambiguously be chosen from measured values of n and, in fact, over a wide temperature and grain-size range, the mechanism(s) will most likely change.

If grain growth were inhibited by second phases or impurities, a small fraction of grains could continue to grow if there were inhomogeneities in the distribution of the inhibiting agents. When these growing grains reach a critical size where they had many more sides than neighboring grains, they would grow rapidly at the expense of their neighbors by secondary recrystallization until they impinged upon each other. Hillert (1965) has shown that the critical size necessary to initiate secondary recrystallization was only twice the average size of

the matrix. If a grain attains this size inhomogeneity during the final stages of primary recrystallization, secondary recrystallization may initiate. But, as with the final step of primary recrystallization, when these large grains mutually impinge upon each other, normal grain growth will again proceed. The growth rate during secondary recrystallization is independent of their size and therefore n equals 1 in Equation 1 (Brook 1976).

Particle-limited grain size

Several equations (for a review see Chapter 2) relating particle size and concentration to the limiting matrix grain size can be generalized by the equation (Chapter 2):

$$D_{\max} = C(d/f^m) \quad (2)$$

where D_{\max} is the limited matrix grain diameter, d is the diameter of second phase particles, and f is the volume fraction of second phases. C is a constant of order one, and m is a constant dependent upon the assumptions of the dispersion parameters. For a completely random dispersion m equals 1; for particles preferentially concentrated at grain boundaries m equals 1/2; and for particles concentrated at triple junctions, m equals 1/3. In Chapter 2, equation 2 was compared to experimental data and it was found that m varied between 0.24 and 1.22. But, for alumina particles in a calcite matrix, m was between 0.34 and 0.55. In Figure 7 the data for the effect of mica particles on grain growth are compared to the alumina data of Chapter 2 and to four of the models given in Chapter 2, Table 1: 1) Zener (1948), 2) Hellman and Hillert (1975), 3) Anand and Gurland (1975), and 4) Appendix 1.

EXPERIMENTAL METHOD

The experiments involved four major steps: 1) grinding, classifying, and mixing the calcite and mica powders; 2) cold-pressing the mixtures into moderately dense cylinders and saturating them with water; 3) densification, recrystallization, and grain growth at high temperatures and pressures; and 4) grain size measurements and microstructure characterization using transmitted light and scanning and transmission electron (SEM and TEM) microscopes.

Reagent grade CaCO_3 powder was mechanically mixed with 0, 1, or 5 volume percent of biotite or phlogopite particles in ethanol for four hours. Fine-grained biotite and phlogopite were not commercially available and were therefore ground in our laboratory from large sheets by a series of steps including ball-milling, sieving, grinding in an agate mortar and pestle and settling in distilled water. Impurities introduced by these steps were removed by soaking in acetone, settling in the presence of a magnet, and sorting with the aid of a binocular microscope. The mica and calcite powders were sized by X-ray sedimentation, single-point N_2 adsorption (BET), (these two techniques were described in detail in Chapter 1), and by measurement with an optical microscope and TEM. The average particle sizes from all of these methods are listed in Table 2. Reasonable agreement was found between the sizing methods for the CaCO_3 powder, as was the case for the Al_2O_3 powders used in Chapter 2, but agreement for the mica powder was poor, probably because of the mica particles' plate-like shape.

The powder mixtures were then densified and recrystallized by a series of cold and hot isostatic presses. The procedure that resulted in the most reproduceable microstructures was described in Chapter 2. Only in the CA-series of experiments, Tables 3 and 4, was this procedure followed. All permanent procedural changes noted below resulted in improvements in the reproduceability of the data. Two variables appeared to be the major contributors to grain size variations in the sample; the "green" density (prior to hot pressing) at which the H₂O pore pressure, P_p , was added and the number of hydrostatic presses at temperatures below the heat-treatment temperature. In general, the highest densities were obtained if water was added after the first hydrostatic press to 150 MPa confining pressure, P_c . Complete saturation of the sample was still possible if water was then added and allowed to equilibrate at a slightly positive effective pressure ($P_e = P_c - P_p$). In a number of experiments, multiple hydrostatic presses were done at temperatures below the heat-treatment temperature due to small pressure seal leaks or furnace failures. The grain sizes were usually less in these experiments than in those without the extra pressure cycle(s). Temperature, pressure, and time uncertainties as well as the heating and cooling rates were as quoted in Chapter 2 unless otherwise noted.

Prior to and including experiment 2042 (except for 2033 and 2034), P_c and P_p were 400 MPa and 100 MPa, respectively. Following 2042, they were 300 MPa and 2 MPa, respectively. The effective pressure was essentially the same for these two conditions and no difference in the results was observed. A few exploratory experiments were performed to determine other factors which may affect grain growth in calcite and to compare the synthetic marble results to grain growth in Solenhofen

limestone. To determine the effects of a substitutional impurity on grain growth, a 0.6M MnCl_2 solution was added to the sample prior to the first hydrostatic press (CM-1). Mn is a common replacement ion for Ca in carbonates. CA-18 was designed to determine the effect of water on grain growth in calcite when contamination from the copper jacket was eliminated. In order to ensure dryness, the calcite powder was oven dried at 100°C under vacuum for 3 days before being die-pressed into wafers. The wafers were then dried for 20 hours at 300°C in a silver jacket prior to the hydrostatic press. For the Solenhofen limestone experiments, both lithographic and massive samples were cored perpendicular to the fabric and placed in the sample column along with the die-pressed wafers without any special treatment.

Grain sizes were measured as in Chapter 2 using the linear intercept method (Underwood, 1970). We report the data as the average grain diameter, D , which is $3/2$ times the average intercept length (Exner, 1972). Grain sizes were larger near the ends of the samples, presumably due to elastic mismatch between the rigid alumina pieces and the compressible calcite samples. Similar behavior was noted by Wenk et al. (1973). Therefore in 2037 and all subsequent experiments the samples were cut longitudinally and the grain sizes were measured away from the sample ends. It is likely that some of the anomalous measurements in pure samples prior to 2037 were a result of these end effects. SEM and TEM specimens were prepared and analyzed as in Chapter 2.

RESULTS

Several important observations have been made of the effects of mica particles and pores on grain growth in synthetic marbles. In the course of developing a technique of minimizing porosity variations, a number of observations were made of grain growth in the presence of up to 6% porosity. The ideal fabrication process would have produced dense aggregates where grain size and other differences in microstructure could be directly attributed to the added second phase particles. One of the more important results of this study was the development of a fabrication process for making samples with reproduceable porosities and grain sizes. Additionally, several observations were made of the effects of a grain boundary fluid phase (probably a melt), and of the effects of impurities on grain growth in synthetic marbles. These results are compared to growth data from several studies on Solenhofen limestone, a fine-grained natural analog.

Densification and primary recrystallization

Cold pressed aggregates, with a relative "green" density of 80% and a wide grain size distribution, transformed to nearly dense (>96%) synthetic marbles with unconnected pores and more uniform-sized, polygonal grains during the initial heat-up to 800°C. The transition from connected to unconnected porosity in these samples occurred at about 95% of the theoretical density (Bernab and Brace, 1982). Optical micrographs showing typical microstructures in specimens before and after recrystallization are shown in Figures 1b and 2a. The presumed onset of primary recrystallization occurred at less than 600°C during heat-up and

corresponded closely with the final stages of densification (Caristan et al., 1981). The onset of grain growth occurred between 550° and 650°C during heat-up; however, the growth kinetics were sluggish below 700°C. In the dry experiments, negligible grain growth occurred at 700°C, but significant growth occurred at 800°C. In the wet samples, the maximum relative densities measured were only 96 to 98% (Table 5); however, densities as high as 99.5% were measured in dry samples (Caristan, 1981). The effect of the mica particles on any of these stages is not known, but there is evidence from sample 2049, and from the Al₂O₃ data of Chapter 2, that normal grain growth began in the pure samples before the two-phased ones.

Microscopic observations

The progressive development of microstructures during recrystallization and grain growth is shown in Figures 1 and 2. The latter stages of primary recrystallization are characterized by relatively strain-free grains with smooth, gently-curving boundaries (Figure 2a). During the earliest stages of grain growth, the grain-size distribution was quite broad, due to the initial powder-size distribution (Figure 1a), and/or to secondary recrystallization prior to the onset of normal grain growth. After short heat-treatments at 800°C, the grain-size distribution had narrowed and polygonal grains with near equilibrium triple junctions (Figure 2b) had developed. In the absence of pores (Figure 2c), a five-fold increase in grain size occurred within 3.5 hours. The grain boundaries were very straight and in plane-section, almost all triple junctions were at 120° angles. The ideal fabrication process would have produced dense aggregates similar to these. When

pores were present, the grain sizes were smaller (Figure 2d). The pores were distributed in the interiors of grains, along grain edges, and at triple junctions. Secondary recrystallization may have accounted for part of the increase in grain size. The progressive development of grain size by secondary recrystallization is illustrated in Figure 3 from (Rossi and Burke, 1973). Boundaries of grains in the initial structure separate from pores by abnormal grain growth, thus creating a second generation structure of included pores (Figure 3a). A few of these second generation grains would then grow until a third generation structure developed with large grains containing a nucleus of fine pores surrounded by a pore-free annular region (Figure 3b). Mica particles were also distributed intra- and intergranularly (Figure 2f) and inhibited grain growth even more dramatically than similar concentrations of pores.

SEM and TEM analyses showed that the pores were lens-shaped on grain edges and nearly spherical at triple junctions (Figure 4a). Intragranular pores were typically smaller than their intergranular counterparts and were polygonal in shape. Plate-shaped mica particles were oriented with their shortest dimension normal to the boundary plane (Figure 4c), clustered in fluid phases at triple junctions (Figure 4b), and dispersed in grain interiors (Figure 4c and d). Grain boundaries were exceptionally smooth and were frequently open. Most dislocations were either non-interacting, straight and parallel, or gently curved and loosely tangled (Figure 4b-d). Dislocations commonly terminated at mica plates and were rarely arranged in low-angle boundaries. We believe that most of the dislocations and the cracked grain boundaries formed during the sample quench due to thermal stress; calcite has one of the largest thermal expansion anisotropies of any mineral (Rosenholtz and

Smith, 1949; Skinner, 1966). An alternative explanation for the cracked grain boundaries is given by Rutter (1974), who observed that at 400°C, samples of Carrera marble could be completely disaggregated along every grain boundary by simply increasing the pore pressure until it equaled the confining pressure. Although the unconnected porosity was no doubt equal to the confining pressure in our samples at the conditions of the experiments, this explanation is unlikely since we observed a definite correlation between disaggregation and grain size in both wet and dry samples.

As discussed in Chapter 2 and Appendix 3, an intergranular film was detected in the wet samples but was not detected in dry samples given the same heat treatment. The presence of such a film affects the boundary migration mechanisms and may also provide a means for dragging particles (Ashby and Centamore, 1968).

Kinetics of grain growth

The grain growth data for the pure calcite samples listed in Table 3 are shown in Figure 5. Each data point represents the average size for all measurements on a single sample. The error bars represent the spacial inhomogeneity in the average grain size. Where error bars overlap, only the maximum and minimum values of the combined points are shown. Standard deviations of mean intercept lengths for selected samples of both large and small grain sizes were approximately $\pm 12\%$. Other errors in the grain size measurement, including observer bias and preferred orientation, were minimal ($\pm 2\%$). Curves of the normal growth law (Eqn. 1) for n equal to 2, 3, and 4, with the constants K and D_0 chosen arbitrarily to fit the CA-series (Chapter 2), are also shown. It

is not possible to delineate a mechanism from the fit of the data to a single value of n (Table 1, reprinted from Brook, 1976) but n equal to 3 or more is suggested, consistent with microscopic observations of both pore-drag and a liquid grain-boundary film (Figure 4). There was considerable real variation in grain sizes due to uncertainties in several parameters at the onset of grain growth. Variations in the initial powder size or the cold-pressing procedure may have affected the amount of grain crushing or plastic strain at grain contacts, thereby altering primary and/or secondary recrystallization prior to normal grain growth. Differences in pore size and concentration would cause variations in boundary mobilities and thus affect K . Finally, experimental variations, such as temperature or pressure fluctuations and measurement inconsistencies (for example, measuring the grain size near sample ends), contributed to the uncertainties, but they were minimized as the fabrication technique was improved.

Inhibition of grain growth by mica particles

Figure 6 shows the effect of mica particles in concentrations of 1 and 5 vol. % on calcite grain growth. Several observations indicate that: 1) Grain growth was suppressed by dispersed mica particles in concentrations of 5, and to a lesser extent, 1 vol. %. 2). The variations in the average grain size at a given time were again attributed mainly to differences in porosity. For pure and two-phase mixtures within a single experiment, grain sizes were consistently large (e.g. 2023) or small (e.g. 2004 or 2053). 3) Grain sizes in mixtures with equal amounts of either phlogopite or biotite were similar, perhaps because they had similar shapes and similar size distributions. 4) A

limiting grain size, D_{\max} , of 15 to 25 μm , was reached within 2.5 hours for a 5% dispersion, and 20 to 40 μm within 5.5 hours for a 1% dispersion of mica particles.

In Figure 7 the effects of mica particles on D_{\max} , are compared to the three theoretical models summarized above and to the results from Chapter 2 for alumina particles. D_{\max} for 5% was chosen as the average of all D values for $t > 2.5$ hours excluding the three points below 15 μm where growth was probably inhibited by anomalously high porosities. For the 1% dispersions, D_{\max} was chosen as the average D for $t > 5.5$ hours. In Figure 7, two values for the effective particle size, d , are shown, the BET equivalent spherical diameter of 0.15 μm and the average maximum plate diameter from TEM micrographs of 1.3 μm . Independent of the choice of d , the value of m from the generalized pinning condition, equation 2, is equal to 0.24, lower than that predicted by any model or by the empirical fit to the alumina data (Chapter 2). An alternative estimate of m can be made by choosing D_{\max} from the experiment with the most extreme 1 and 5% values. In this way, uncertainties due to variations in porosity are minimized. The values from experiment 2005 are plotted and the value of m has increased to 0.38 which is within the expected range but well below Zener's prediction of $m = 1$.

The value for d was not well constrained. In the case of the Al_2O_3 particles (Chapter 2), d 's from X-ray sedimentation, BET, and TEM micrographs all agree within a factor of 2 (Appendix 2). But for the mica particles (Table 2), the three diameters differ by over three orders of magnitude. The TEM diameter is the most reasonable size since it agrees best with the alumina data (Figure 7) and also with the data from

several studies with metals and ceramics (Chapter 2, Figure 10). The BET and the X-ray methods underestimate the effective particle size.

Effects of pores on grain growth

Pores were observed to have a major effect on the kinetics of grain growth. Several microstructures indicative of pore-boundary interactions commonly observed in ceramics were also recognized in these synthetic marbles: 1) Clusters of pores left in the grain interiors (Figure 3) are suggestive of the sweeping of pores by grain boundaries (Rossi and Burke, 1973). 2) Distorted pores along grain boundaries are suggestive of pore drag (Hseugh et al., 1982). 3) Larger pores at triple-junctions than in grain interiors suggest pore coarsening (Francois and Kingery, 1965). And 4) smaller grain sizes in regions of higher porosity suggest reduced boundary mobilities and possibly a porosity limited grain size. In a general way, quantitative measurements of porosity and pore size (Table 5) support these qualitative observations. Porosities measured by immersion in CCl_4 range from <0.1% to 6.3% with a mean of 2.6%. There is a slight correlation between porosity and grain size relative to the reference line in Figure 5 (see Table 3). Samples with porosities less than the mean overlap the reference line, while those with porosities greater than the mean are below. Although there is a correlation between the 'pure' and two-phase grain sizes, the correlation is not reflected in the porosity measurements. Two-phase samples have equal to slightly lower porosities than the pure samples, but no trend relative to grain size is established.

Porosities measured from optical and SEM micrographs range from 2.7% to 15.5%. The optically measured porosities of the pure samples range from 2.7% to 11% with a mean of $6.2 \pm 0.7\%$. As before, porosities that are less than the mean correlate reasonably well with grain sizes that are greater than the average in Figure 6. Optically measured porosities in the two-phase samples range from 8.3% to 15.5% with a mean of $12 \pm 1.2\%$ and do not show any trend with grain size. Porosities measured from SEM micrographs are on the order of the optical porosities and also show no trend with grain size. In general, the porosities measured by point counting pores in both optical and SEM micrographs are higher than porosities measured by the other two methods. For the optical measurements, this discrepancy was due to the measurements not being corrected for section thickness and due to the difficulty in distinguishing mica particles from pores. For SEM measurements, the discrepancy was due to grain plucking during polishing.

The relative pore-size measurements show that the grain boundary pores are larger than the intragranular pores by a factor of 2 to 3. These data indicate that pores became separated from grain boundaries during the early stages of grain growth, but as the boundary curvature decreased, pores became attached and coarsened by the mechanism described by Kingery and Francois (1965) and Hsueh *et al.* (1982). By analogy with the precipitate coarsening experiments summarized in Chapter 2, a correlation similar to equation 2 is expected between pore size and concentration, and grain size. Such a correlation is only vaguely supported by the data.

Enhancement and suppression of grain growth by
water and ionic impurities

The importance of water in accelerating the kinetics of grain growth in calcite has been recognized by several authors (Tullis and Yund, 1982; Gee, 1982; Rutter, 1983). In the present study, several observations have been made of grain growth in wet and dry environments as well as in the presence of a 0.6M MnCl_2 solution (Figure 8).

In Chapter 2, it was shown that at 800°C and in the presence of water, grain growth occurred through a grain-boundary fluid, presumably a melt. Grain growth experiments on 'dry' synthetic marbles (Gee, 1982) showed that in the presence of a very small amount of water (room humidity) grain growth proceeded at a rapid rate. Gee's oven-dry samples showed little or no grain growth and were slightly discolored. In wet experiments there was a very thin reddish-brown coating on the sample near the copper jacket--calcite interface. In dry experiments, the coating was gray to black (perhaps CuO) and penetrated the sample. In the present study, a single grain growth experiment was performed on an exceptionally dry sample jacketed in silver instead of copper. There was no discoloration of the sample in this experiment and grain growth was nearly the same as in the wet samples. Therefore it is possible that grain boundary mobilities were higher in the presence of a fluid phase (Yan et al., 1977), but the effect on grain growth was partially offset by the higher porosities (4% vs 2%) in wet vs. dry samples. In the dry copper-jacketed samples, recrystallization and grain growth were probably suppressed by the formation of copper oxide particles (although there was no systematic variation in grain size away from the jacket) or to impurities dispersed throughout the sample. The poly-modal grain size

distribution in the dry samples may have been due to heterogeneous oxide or impurity dispersions.

The grain size in the sample with the 0.6M MnCl₂ solution was a factor of 3 or more larger than in any other sample that was heat-treated for one hour (Table 3), and in fact, larger than in any sample heat-treated at any temperature for any length of time ($T_{\max} = 900^{\circ}\text{C}$, $t_{\max} = 24$ hours). It was difficult to determine the mechanisms by which the MnCl₂ solution increased boundary mobility. An SEM EDAX elemental analysis showed no Mn⁺⁺ concentration gradient from the grain interior to the boundary. Although the original intention of this experiment was to study the mechanism of CIGM (chemically induced grain boundary migration), the order of magnitude increase in grain size obliterated any hope of documenting the process. However, there was little doubt that grain growth was significantly enhanced by the presence of the MnCl₂ solution.

Synthetic marbles vs. Solenhofen limestone

Grain growth data for Solenhofen limestone at temperatures above 800°C from Tullis and Yund (1982), Schmid et al. (1977), and the present study are compared to the grain growth data for the synthetic marbles at temperatures from 550°C to 900°C in Figure 9. The data from Schmid et al. (1977) are published and unpublished grain size measurements from experiments where, in all but one case, grain growth was concurrent with deformation. In Solenhofen limestone heat-treated at 700°C, Tullis and Yund (1982) found significant grain growth at 1500 MPa confining pressure, but not at 200 MPa. Schmid et al. (1977) and the experiments of the present study found little or no grain growth at 300 or 400 MPa.

Important observations from the data plotted in Figure 9 and 11 include:

1) In all cases, the grain growth constant, K , increased with increasing temperature. 2) For Solenhofen limestone, little or no grain growth occurred below 900°C at 300 MPa confining pressure, but at 1500 MPa grain growth was much more pronounced. 3) For a given temperature, the growth rate of the synthetic marble at 300 MPa was faster than Solenhofen limestone at 1500 MPa. 4) From Schmid's data, strain did not appear to influence the grain size. 5) At 1000°C and "room humidity" water content, pressure didn't appear to affect grain growth. 6) At all temperatures and 1500 MPa, a larger grain size was obtained when water was added.

Solenhofen Limestone contains 5 to 6% porosity (Rutter, 1972) and other second phases including detrital clay and quartz particles (Kern, 1979). The initial grain size was about 6 μm , but some very large grains (>30 μm) existed (Figure 10a), and the microstructure was not unlike that of the synthetic marbles before primary recrystallization (compare Figures 1b and 10a). After a 10-hour heat-treatment at 800°C and 300 MPa, the microstructure resembled the recrystallized synthetic marbles in that the boundaries were no longer sutured. However, little or no grain growth had occurred and the large grain size heterogeneity remained (Figure 10b). When significant grain growth occurred in Solenhofen limestone (Tullis and Yund, 1982; Schmid *et al.*, 1977, unpublished micrographs; and this study, at 900°C), the grain size distribution was more uniform, and the microstructures resembled the synthetic marbles of comparable sizes. Pores and other secondary grain boundary phases in Solenhofen limestone were recognized in TEM (Figure 10c). Other optical and TEM micrographs of Solenhofen limestone before and after grain growth

are shown by Tullis and Yund (1982), Grigg et al. (1960), and Barber and Wenk (1973 and 1979). The samples they analyzed had microstructures that were very similar to those used in our study.

Since a grain boundary film, presumably a melt, was detected in synthetic marbles heat-treated to 800°C (Chapter 2), a melt phase may also have existed in Solenhofen limestone at similar conditions. In Solenhofen limestone heat-treated at 1000°C, (Figure 10d, Schmid, unpublished micrograph and private communication) large fluid-filled pores formed and the rate of grain growth was significant.

DISCUSSION

Grain growth is an important solid state transformation process in the earth that may be affected by several parameters. Parameters that have been examined in this study include: 1) second phase particles that pin grain boundaries; 2) fluid-filled pores which may pin, separate from, or be dragged by migrating boundaries; 3) grain boundary fluids which enhance boundary migration; and 4) ionic impurities which may enhance or suppress boundary migration. Variations in the cold pressing procedure and in the degree of water saturation affected densification leading to variations in porosity, pore size, fluid content, grain size and internal strain. The effects of most of these variables were minimized by adding a moderate-temperature, high-pressure fabrication step.

Kinetics of grain growth

The fit of the data to Equation 1 for n equal to 3 (Figure 5) may imply a porosity drag or boundary-fluid controlled growth mechanism which is consistent with observed microstructures. The values of the other two

constants, D_0 , the starting grain size, and K , the rate constant for grain growth, are also dependent upon densification, recrystallization, and the mechanisms controlling grain growth (Burke and Turnbull, 1952; Brook, 1976). The value of D_0 for the synthetic marble was chosen as the smallest grain size in a recrystallized microstructure from the CA-suite of samples (550°C, 500 MPa, $D_0 = 10 \mu\text{m}$). The true initial grain size may have been somewhat less, but a sample fabricated at 50°C lower had a very different microstructure (Figure 1b). The large grain size heterogeneity in the original powder, the 10- to 20-fold increase in grain size from the average initial powder size, and the prevalence of intragranular pores and particles suggest that secondary recrystallization may have played a role in the development of the initial microstructure. D_0 may have varied depending upon the degree of secondary recrystallization which occurred. D_0 for Solenhofen limestone was chosen as the grain size measured before any heat-treatment. K is a temperature-dependent growth-rate constant that is functionally related to the grain boundary mobility. The value of K can be estimated from a $\log (D^3 - D_0^3)$ vs. $\log t$ plot (Figure 11) by assuming D_0 equal to $10 \mu\text{m}$ for synthetic marbles, and equal to $6 \mu\text{m}$ for Solenhofen limestone. The data from Tullis and Yund (1982), Schmid et al. (1977), and Schmid (private communication) have been included with our data. Estimates of K values are given in Table 6. In general,

the growth rate increased with temperature and confining pressure and was significantly lower for Solenhofen limestone than for the synthetic marbles. Also, the growth rate for the MnCl_2 solution was two orders of magnitude higher than for the synthetic marble. At high temperatures, the growth rate was less dependent on pressure (note the similarity in K between the 300 MPa and 1500 MPa data at 1000°C and "room humidity" water content). This decreased pressure dependence may indicate that boundary migration was no longer controlled by pore-drag.

K is nearly time-independent for the CA-X and the X0XX, 900°C data. For Solenhofen, there is a consistent trend of increasing slope (decreasing time-dependence of K) with increasing temperature. The K dependence on t may indicate that the mechanism for grain growth was different at the lower temperatures (Table 1), or, more likely, that the pinning effect of the second phases decreased with increasing temperature, T . K can be represented by the Arrhenius relation:

$$K = K_0 \exp(-Q/RT)$$

where K_0 and R are constants, and Q is the activation energy for the rate controlling mechanism for grain growth (Nichols, 1968 and Lay, 1968).

An Arrhenius plot for growth rate constants is shown in Figure 12. There is no conclusive evidence of a change in growth mechanism. The similarity in K for Schmid's data at 600 and 700°C probably indicates that no growth occurred at these low temperatures. The values of Q determined from the slopes of the lines are listed in Table 7. Q is similar for both the wet and the dry synthetic marbles and the Solenhofen limestone heat-treated under 300 MPa confining pressure. The Solenhofen

heat-treated under 1500 MPa is about 50% higher. The apparent pressure-dependence of Q has not been explored but may be related to differences in experimental procedures between the various studies, or to a pressure dependence of the activation volume for the migration process (Molodov et al., 1984). The Q values are also compared to those for carbon and oxygen diffusion in calcite single crystals between 500° and 800°C (Kronenberg, et al., 1984). The measured Q values are reasonable since Q for grain growth is usually assumed to be approximately equal to Q for grain boundary diffusion which is less than (on the order of one-half of) Q for lattice diffusion (Cotterill and Mould, 1976).

Yan et al. (1977) present mobility data for several oxides and show that, in general, the effect of a grain-boundary film is to increase the boundary mobility in those systems containing even a small amount of porosity. Bennison and Harmer (1983 and 1985) showed that in exceptionally clean, fully dense Al_2O_3 , both MgO and a liquid phase reduced K . Therefore, one would expect that if all impurities, particles, and pores were removed from the synthetic marbles, grain growth would be more rapid in the dry system than in the wet.

The boundary film was almost certainly a partial melt. According to Wyllie and Boettcher (1968) a melt for our system is composed of $CaCO_3$, $Ca(OH)_2$, and a small amount of dissolved H_2O . The melt composition was not analyzed but the ring spacings from TEM diffraction patterns corresponded to lattice spacings from the two minerals (Appendix 3). Whether the melt completely wet the grain boundary was not known. Films as narrow as 10 nm were identified along many boundaries but the effects of grain boundary cracks, carbon coating, and ion-thinning damage

were not fully assessed (Appendix 3 and Chapter 2). The grain boundary film may have provided a mechanism for particle drag. Clusters of both mica (Figure 3b) and alumina (Chapter 2) particles were commonly observed at triple junctions in heat-treated samples. Although it is believed that most of the clustering was due to a non-uniform initial dispersion, some "coarsening" could have resulted if particles were mobile. According to Ashby and Centamore (1968), the particles may have been loose or only weakly bonded to the calcite boundaries since they were mechanically mixed in and not grown in situ. If a fluid phase completely surrounded the particles (Figure 3b), they may have been undeformable, but otherwise have moved like pores. Therefore boundaries could drag the particles and the 'effective' second phase size would increase by a mechanism similar to that given by Kingery and Francois (1965) for pores.

Comparison with alumina particle data and theoretical models

The effects of mica plates on grain growth in synthetic marbles were similar to the effects of equant alumina particles (Chapter 2). Plates were found along grain boundaries, at triple junctions, and included in grain interiors (Figure 3). In general, the intragranular particles were smaller than those on grain boundaries. The main difference between the mica and the alumina was the particle shape (Table 2 and Chapter 2). All TEM observations of plates on grain edges showed that the plates were oriented with their shortest axis perpendicular to the boundary plane. Therefore the "effective" particle diameter was equal to the maximum plate dimension. Wold and Chambers (1968) have discussed the effect of particle shape on its pinning ability and have shown that discs of

similar dimensional ratios to that of the mica plates would not drastically affect D_{\max} . As with the alumina, there was a much weaker dependence of D_{\max} on f than predicted by the Zener-type models (Figure 7), indicating that the particles were not randomly dispersed but were concentrated at grain edges and triple junctions. Other possible causes of this weak dependence have been discussed in Chapter 2.

Straining prior to grain growth

At least two processes that occurred prior to the onset of grain growth, densification and thermal expansion, created large anisotropic stresses that plastically strained the matrix. Because the particles-pinning-boundaries models have been derived by assuming that normal grain growth is driven only by the boundary curvature, it is instructive to calculate a residual dislocation density that would result in a driving pressure equal to that due to a boundary of a specified curvature. From Zener (1948) the driving pressure for grain growth, P_{gg} , is given by:

$$P_{gg} = \Gamma/R \quad (3)$$

where R is the boundary radius of curvature, and R equals αD where $\alpha \approx 1$ (Smith, 1948) or $\alpha \approx 9$ (Haroun and Budworth, 1968). Γ is the interfacial energy per unit area which is approximately equal to 0.1 J/m^2 (Janczuk et al., 1983, and Hay, unpublished data). Stored dislocations result in driving forces given by:

$$P_{\delta} = 1/2\mu b^2\delta \quad (4)$$

(e.g. Takeuchi and Argon, 1976), where μ is the shear modulus (25 GPa), b

is the burger's vector (.63 nm) and δ is the dislocation density. If D is chosen equal to D_0 (10 μ m), the dislocation density that would contribute an equal driving pressure is given by combining Equations 3 and 4:

$$P_{gg} = P_{\delta} = \Gamma/\alpha D = 1/2\mu b^2\delta \quad (5)$$

If α equals 9, δ equals $2 \times 10^{11} \text{ m}^{-2}$ ($2 \times 10^7 \text{ cm}^{-2}$). If α equals 1 (Smith, 1948 and Ashby, 1980), δ equals $2 \times 10^{12} \text{ m}^{-2}$. Dislocation densities equal to 3 to $8 \times 10^{11} \text{ m}^{-2}$ were measured in synthetic marbles heat-treated at 800°C and then quenched to room temperature. We believed that most of these dislocations were introduced by thermal stresses. (Following Wong and Brace, 1979, an 800°C temperature change could result in internal stresses as high as 1200 MPa!) Slightly higher densities were estimated in our samples heat-treated at lower temperatures indicating that some recovery occurred. Therefore it is reasonable, at least in the early stages of grain growth, that boundary migration was driven by a combination of the interfacial energy and the internal strain energy. The result would be a matrix with a grain size that was larger than predicted.

The effects of pores and ionic impurities

Pores had a major effect on the grain-growth kinetics and, perhaps, on the limiting grain size. There was a slight correlation of porosity with grain size. The porosity was not constant between experiments, and proved to be the largest single contributor to scatter in the data. Several pore-boundary interactions observed in ceramics during final stage sintering were also observed in these synthetic marbles. For

example, pores separated from grain boundaries especially during the early stages of grain growth. Also, pores which remained attached to boundaries migrated from grain edges to triple-junctions and coarsened while those which separated from boundaries remained stable in size and shape.

Other impurities also affected calcite grain growth in wet and dry environments (Figure 9). Grain growth in dry synthetic marbles was suppressed by a reaction with the copper jacket. Whether the effect was due to ionic Cu or copper oxide particles is uncertain, but silver did not have the same effect. However, grain growth in wet marbles was significantly enhanced by the presence of a 0.6M MnCl_2 solution (Figure 8). A partial list of additives that both enhance and suppress grain boundary migration in oxides is given by Brook (1976, p. 350). Chai (1974) examined hydrothermal particle coarsening of calcite in the presence of various cations. At 650°C and 200 MPa, Chai (1974) found over an order of magnitude increase in the growth rate of calcite in a 2N CaCl_2 solution compared to distilled water; in this case, growth enhancement was due to an excess of Ca ions and not to other cation impurities. Cation impurities may also enhance migration of boundaries by a process called CIGM (chemically induced grain-boundary migration) (Cann and Balluffi, 1978). Hay and Evans (1984) and Evans and Hay (1984) have reported results from CIGM experiments in calcite bicrystals and have discussed the possible applications of this process to the development of metamorphic microstructure. Although the original intention of the present experiment was to study the mechanism of CIGM in polycrystalline calcite, the order of magnitude increase in grain size prevented documentation of the process. However, it is clear that grain

growth was significantly enhanced by the presence of the MnCl_2 solution.

Application of results to grain growth in Solenhofen limestone

The effects of second phases on grain growth in synthetic marbles can be used to interpret the temperature and pressure dependences of grain growth in Solenhofen limestone (Figure 10). At confining pressures of 300 MPa or less, there was only a slight increase in grain size in Solenhofen below 900°C and, in fact, in only one sample (CA-18), heat-treated for 10 hours, was the grain size significantly larger than the grain size of the synthetic marble heat-treated for 1 hour at 550°C and 500 MPa. Since a melt phase was identified in the synthetic marbles at 800°C, it follows that significant grain growth in Solenhofen may depend on the presence of a melt. A similar observation has been made by Rutter (1983) at 100 MPa hydrostatic pressure. Without a melt, the slight increase in grain size observed in heat-treatments at as low as 600°C may have been due to slight adjustments of grain boundaries until they were pinned by the porosity of 5 to 6% and the other second phases (Figure 11c). With melt, the mobility of these second phases may have been significantly increased, as was observed for pores and possibly particles in the synthetic marbles. As the temperature increases, the melt fraction would also increase causing a decrease in the effective "drag" of the second phases on grain boundaries.

Several explanations are possible for the dramatic increase in growth rate at 1500 MPa. 1) In the dry samples of Tullis and Yund (1982), the pore pressure was initially less than the confining pressure and therefore pore shrinkage would have occurred. If pores were

significantly undersaturated the 5-fold increase in pressure would cause a similar decrease in pore volume (5% to 1%), thereby substantially decreasing the inhibiting effect of the pores. 2) As grain-grain contacts deformed during the shrinkage, dislocation densities would increase in these deforming regions according to:

$$\sigma_1 - \sigma_3 = A\mu b\delta^{1/2} \quad (6)$$

where $\sigma_1 - \sigma_3$ is the differential stress, A is a constant of order 1, and μ and δ are as given above (e.g. Takeuchi and Argon, 1976). A 5-fold increase in differential stress at grain-grain contacts would result in a 25-fold increase in dislocation density in these regions. An overall increase in the internal strain energy would result which would provide an additional driving pressure for boundary migration (Eqn. 3). 3) Tullis and Yund (1982) considered the effect of pressure on the solubility of CaCO_3 in H_2O but, as they pointed out, solubility data does not exist above 700°C and 140 MPa (Sharp and Kennedy, 1965). 4) The driving force for boundary migration is pressure dependent. And 5) as discussed by Ashby (1980), phase transformations may contribute significantly to driving forces for boundary migration. For the 1500 MPa and 700°C experiments, CaCO_3 goes through two phase transformations, Calcite I Aragonite Calcite II, before it reaches the heat-treatment conditions (Wyllie and Boettcher, 1969).

It is not possible to delineate which mechanism(s) dominated grain growth in Solenhofen limestone at high pressures. But the observations that pressure has a major effect below 800°C , decreasing to a negligible effect at 1000°C , and that added water at 1500 MPa increased the growth

rate at all temperatures, indicate the importance of a liquid on the relative mobilities of second phases.

Applications to paleopiezometry

These results will also contribute significantly towards improving the calibration of the dynamically recrystallized grain size paleopiezometer. Without second phases at high strains, a steady-state grain size is reached when the internal free-energy due to dislocations in a strained grain is equal to the interfacial energy of the surrounding grain-boundary area. Just as a boundary migrating to lower its total interfacial energy may be pinned or break away from an immobile second phase particle, a boundary migrating in an internal strain energy gradient (against its radius of curvature) will continue to migrate if the driving pressure due to the combined effects of the internal strain energy, P_δ , and the second phases, P_φ , is less than that due to the grain boundary curvature. Following Ashby (1980) this condition is satisfied when:

$$P_\delta + P_\varphi \leq P_{gg} \quad (7)$$

where P_δ and P_{gg} are given by Equations 4 and 3 and:

$$P_\varphi = 3f\Gamma/d \quad (8)$$

combining these equations and re-arranging:

$$\alpha(\mu b^2 \delta / 2 + 3f/d) = D^{-1} \quad (9)$$

As an example, a reasonable tectonic stress of 20 MPa would produce a steady-state dislocation density on the order of 10^{13} m^{-2} (Eqn.

6) in limestone. Without a second phase, D would equal $1.0 \mu\text{m}$ for α equal to 1. With 5% mica plates with 'effective' diameter of $1 \mu\text{m}$, there would be a 25% reduction in equilibrium grain size. Therefore, the grain-size paleopeizometer might overestimate the deformation stress. The true effect of second phases on dynamic recrystallization is undoubtedly more complicated than this and requires further experimental work.

If grain growth was induced by post-tectonic high temperatures, second phases might pin grain boundaries near their stress-equilibrated size. Relatively pure regions would have larger grain sizes and would thus underestimate the deformation stress.

SUMMARY AND CONCLUSIONS

Grain growth in geologic materials is affected by second phases in ways analogous to those described extensively in the ceramics and metallurgical literature. The most important results of this study for synthetic marbles are:

- 1) Grain growth in wet samples followed a kinetic law appropriate for a pore drag or liquid film controlled mechanism.
- 2) Calcite grain boundaries separated from, were pinned by, and/or were possibly even dragged along by mica plates. A limiting grain size was reached, which was a function of the plate diameter and the volume fraction.
- 3) The effect of pores inhibiting grain boundary migration was analogous to that of particles. Pores were very small when found in grain interiors and coarsen with increasing grain size at grain boundaries.

4) Water increased the rate of grain growth by inducing partial melting along grain boundaries, and decreased the growth rate by increasing the initial sample porosity.

5) Impurity ions both enhanced and suppressed the rate of grain growth.

When these results were applied to grain growth data for Solenhofen limestone, it was found that second phases inhibited boundary migration and that a melt phase was probably present at all temperatures and pressures where significant grain growth occurred. An important application of the data is to the effects of second phases on dynamic recrystallization. Second phases may pin grain sizes below their stress-equilibrated value, and thus, paleostresses may be overestimated in two-phased rocks.

BIBLIOGRAPHY

- Anand, L., and J. Gurland, The relationship between the size of cementite particles and the subgrain size in quenched-and-tempered steels, Metall. Trans. A, 6A, 1975.
- Ashby, M.F., The influence of particles on boundary mobility, in Recrystallization and Grain Growth of Multi-Phase and Particle Containing Materials, edited by N. Hansen, A.R. Jones, and T. Leffers, Proceedings of the 1st Riso International Symposium on Metallurgy and Materials Science, 325-336, 1980.
- Ashby, M.F., and R.M.A. Centamore, The dragging of small oxide particles by migrating grain boundaries in copper, Acta Met., 16, 1081-1092, 1968.
- Barber, D.J., and H.R. Wenk, The microstructure of experimentally deformed limestones, J. Mater. Sci., 8, 500-508, 1973.
- Barber, D.J., and H.R. Wenk, On geological aspects of calcite microstructure, Tectonophysics, 54, 45-60, 1979.
- Bennison, S.J., and M.P. Harmer, Effect of MgO solute on the kinetics of grain growth in Al₂O₃, J. Am. Ceram. Soc., 66, C-90-92, 1983.
- Bennison, S.J., and M.P. Harmer, Grain-growth kinetics for alumina in the absence of a liquid phase, J. Am. Ceram. Soc., 68, C-22-24, 1985.
- Bernabe, Y., W.F. Brace, and B. Evans, Permeability, porosity and pore geometry of hot-pressed calcite, Mechanics of Materials, 1, 173-183, 1982.
- Briegel, U., and C. Goetze, Estimates of differential stress recorded in the dislocation structure of Lochseiten limestone (Switzerland), Tectonophysics, 48, 61-76, 1978.
- Brook, R.J., Controlled grain growth, in Treatise on Materials Science and Technology, edited by F.F.Y. Wang, 9, 331-364, Academic Press, 1976.
- Buerger, M.J., Translation-gliding in crystals, Am. Mineral., 15, 45-64, 1930.
- Buerger, M.J., and Washken, E., Metamorphism of minerals, Am. Mineral., 32, 296-308, 1947.
- Burke, J.E., and D. Turnbull, Recrystallization and grain growth, Progress in Metal Physics, 3, 220-292, 1952.
- Caristan, Y., R.J. Harpin, and B. Evans, Deformation of porous aggregates of calcite and quartz using the isostatic hot-pressing technique, Tectonophysics, 78, 629-650, 1981.
- Caristan, Y.D., High temperature mechanical behavior of Maryland diabase, Ph.D. thesis, Massachusetts Institute of Technology, 155p., December, 1980.
- Chai, B.H.T., Mass transfer of calcite during hydrothermal recrystallization, in Geochemical Transport and Kinetics, edited by A.W. Hofmann, B.J. Gilletti, H.S. Yoder, Jr., and R.A. Yund, Carnegie Institute, Washington, 205-218, 1974.
- Chopra, P.N., and D.L. Kohlstedt, The influence of wet basaltic melt on the flow properties of fine grained polycrystalline olivine, EOS Trans. Am. Geophys. Union, 64, 323, 1983.
- Christie, J.M., and A. Ord, Flow stress from microstructures of mylonites: example and current assessment, J. Geophys. Res., 85, 6253-6262, 1980.

- Cotterill, P., and P.R. Mould, Recrystallization and grain growth in metals, John Wiley and Sons, New York, 409p., 1976.
- Etheridge, M.A., and J.C. Wilkie, Grain-size reduction, grain boundary sliding and the flow strength of mylonites, Tectonophysics, 58, 159-178, 1979.
- Evans, B. and R.S. Hay, Characteristics of chemically induced grain boundary migration: applications to geologic materials, EOS Trans. Am. Geophys. Union, 65, 1106, 1984.
- Evans, B., M. Rowan, and W.F. Brace, Grain-size sensitive deformation of a stretched conglomerate from Plymouth, Vermont, J. Struc. Geol., 2, 411-424, 1980.
- Gee, L.S., The kinetics of grain growth in calcite, B.A. thesis, Harvard University, 27p., April, 1982.
- Griggs, D.T., M.J. Paterson, H.C. Heard, and F.J. Turner, Annealing recrystallization in calcite crystals and aggregates, Geol. Soc. Amer. Mem., 79, 21-37, 1960.
- Hansen, S.C., and D.S. Phillips, Grain boundary microstructures in a liquid-phase sintered alumina ($\alpha\text{-Al}_2\text{O}_3$), Philos. Mag. A, 47, 209-234, 1983.
- Haroun, N.A., and D.W. Budworth, Modifications to the Zener formula for limitation of grain size, J. Mater. Sci., 3, 326-328, 1968.
- Hay, R.S., and B. Evans, Experimental evidence for chemically induced grain boundary migration in calcite, EOS Trans Am. Geophys. Union, 65, 1106, 1984.
- Hellman, P., and M. Hillert, On the effect of second-phase particles on grain growth, Scand. J. Metallurgy, 4, 211-219, 1975.
- Hillert, M., On the theory of normal and abnormal grain growth, Acta Met., 13, 227-238, 1965.
- Hobbs, B.E., Recrystallization of single crystals of quartz, Tectonophysics, 6, 353-401, 1968.
- Hobbs, B.E., W. D. Means, and P.F. Williams, An Outline of Structural Geology, John Wiley and Sons, New York, 571p., 1976.
- Hsu, C.Y., Grain-growth mechanisms in rapidly solidified matrix steels, Ph.D. thesis, Massachusetts Institute of Technology, 138p., February, 1984.
- Hsueh, C.H., A.G. Evans, and R.L. Coble, Microstructure development during final/intermediate stage sintering - I. Pore/grain boundary separation, Acta Met., 30, 1269-1279, 1982.
- Janczuk, B., E. Chibowski, and P. Staszczuk, Determination of surface free energy components of marble, J. Colloid Interface Sci., 96, 1-6, 1983.
- Karato, S., and M.S. Paterson, Rheology of synthetic olivine aggregates, EOS Trans. Am. Geophys. Union, 65, 1107, 1984.
- Kern, H., Texture development in calcite and quartz rocks deformed at uniaxial and real triaxial states of strain, Bull. Mineral., 102, 290-300, 1979.
- Kingery, W.D. and B. Francois, Grain growth in porous compacts, J. Am. Ceram. Soc., 48, 546-547, 1965.
- Knipe, R.J., Distribution of impurities in deformed quartz and its implications for deformation studies, Tectonophysics, 64, T11-T18, 1980.

- Kronenberg, A.K., R.A. Yund, and B.J. Gilletti, Carbon and oxygen diffusion in calcite: effects of Mn content and P-H₂O, Phys. Chem. Minerals, 11, 101-112, 1984.
- Lay, K. W., Grain growth in UO₂-Al₂O₃ in the presence of a liquid phase, J. Am. Ceram. Soc., 51, 373-376, 1968.
- Mercier, J.-C.C., D.A. Anderson, and N.L. Carter, Stress in the lithosphere: inferences from steady state flow of rocks, Pure Appl. Geophys., 115, 199-266, 1977.
- Molodov, D.A., B.B. Straumal, and L.S. Shvindlerman, The effect of pressure on migration of <001> tilt grain boundaries in tin bicrystals, Scripta Met., 18, 207-211, 1984.
- Nes, E., N. Ryum, and O. Hunderi, On the Zener drag, Acta Met., 33, 11-22, 1985.
- Nichols, F.A., Further comments on the theory of grain growth in porous compacts, J. Am. Ceram. Soc., 51, 468-469, 1968.
- Paterson, M.S., The melting of calcite in the presence of water and carbon dioxide, Am. Mineral., 43, 603-606, 1958.
- Rosenholtz, J.L., and D.T. Smith, Linear thermal expansion of calcite, var. Iceland spar, Yule marble, Am. Mineral., 34, 846-854, 1949.
- Rossi, G., and J.E. Burke, Influence of additives on the microstructure of sintered Al₂O₃, J. Am. Ceram. Soc., 56, 654-659, 1973.
- Rutter, E.H., The influence of interstitial water on the rheological behaviour of calcite rocks, Tectonophysics, 14, 13-33, 1972.
- Rutter, Ernest H., The influence of temperature, strain rate and interstitial water in the experimental deformation of calcite rocks, Tectonophysics, 22, 311-334, 1974.
- Rutter, E.H., Experimental static recrystallization and grain growth of calcite, J. Geol. Soc. London, 140, 161, 1983.
- Schmid, S.M., J.N. Boland, and M.S. Paterson, Superplastic flow in finegrained limestone, Tectonophysics, 43, 257-291, 1977.
- Schwenn, M.B., and C. Goetze, Creep of olivine during hot-pressing, Tectonophysics, 48, 41-60, 1978.
- Shewmon, P.G., Transformations in Metals, McGraw-Hill, New York, 394p., 1969.
- Skinner, B.J., Thermal expansion, in Handbook of Physical Constants, edited by S.J. Clark, Jr., Geol. Soc. Amer., Mem., 97, 75-96, 1966.
- Spears, M.A., and A.G. Evans, Microstructure development during final/intermediate stage sintering - II. Grain and pore coarsening, Acta Met., 30, 1281-1289, 1982.
- Spry, A., Metamorphic Textures, Pergamon Press, Oxford, 350p., 1969.
- Tullis, J., and R.A. Yund, Grain growth kinetics of quartz and calcite aggregates, J. Geology, 90, 301-318, 1982.
- Twiss, R.J., Theory and applicability of a recrystallized grain size paleopiezometer, Pageoph., 115, 227-244, 1977.
- Weathers, M.S., J.M. Bird, R.F. Cooper, and D.L. Kohlstedt, Differential stress determined from deformation-induced microstructures of the Moine thrust zone, J. Geophys. Res., 84, 7495-7509, 1979.
- Wenk, H.R., C.S. Venkatasubramanian, and D.W. Baker, Preferred orientation in experimentally deformed limestone, Contr. Mineral. and Petrol., 38, 81-114, 1973.
- White, S.H., Difficulties associated with paleo-stress estimates, Bull. Mineral., 102, 210-215, 1979.

- Wilson, C.J.L., Boundary structures and grain shape in deformed multi-layered polycrystalline ice, Tectonophysics, 57, T19-T25, 1979.
- Wold, K.G., and F.M. Chambers, Grain-size control by dispersed phases, J. Australian Inst. Met., 13, 79-87, 1968.
- Wong, T.-F., and W.F. Brace, Thermal expansion of rocks: some measurements at high pressure, Tectonophysics, 57, 95-117, 1979.
- Wyllie, P.J., and A.L. Boettcher, Liquidus phase relationships in the system CaO-CO₂-H₂O to 40 kilobars pressure with petrological applications, Am. J. Sci., 267-A, 489-508, 1969.
- Yan, M.F., R.M. Canon, and K.K. Bowen, Grain boundary migration, in Ceramic Microstructures - 76, 276-307, edited by Fulrath and Pask, Westview Press, 1977.
- Zener, C., private communication to C.S. Smith, Grains, phases and interfaces: an interpretation of microstructure, Trans. AIME, 175, 15-51, 1948.
- Zeuch, D.H., and H.W. Green II, Experimental deformation of an "anhydrous" synthetic dunite, Bull. Mineral., 102, 185-187, 1979.

TABLE 1. Kinetics of grain growth for various mechanisms
(reprinted from Brook, 1976)

$$n \text{ in } D^n - D_0^n = Kt$$

Pore control

Surface diffusion	4
Lattice diffusion	3
Vapor transport ($P = \text{const}$) [*]	3
Vapor transport ($P = 2S \cdot r$) [†]	2

Boundary control

Pure system	2
Impure system	
coalescence of second phase by lattice diffusion	3
coalescence of second phase by grain boundary diffusion	4
solution of second phase	1
diffusion through continuous second phase	3
impurity drag (low solubility)	3
impurity drag (high solubility)	2

^{*} P = driving pressure

[†] S = grain boundary energy, r = radius of curvature of boundary

TABLE 2. Mica and CaCO₃ powder diameters

<u>Technique</u>	<u>CaCO₃</u>	<u>biotite</u>	<u>phlogopite</u>
Optical microscope	4.9 ± 4.3 μm 3.1 ± 0.5 (cold-pressed)	5 ± 3.5 μm	2.5 ± 2 μm 4.0 ± 3
TEM			
Max.			1.3 ± 0.5
Min.			0.37 ± 0.2
Int.			0.39
BET			
(after mixing)	0.80		0.15, 0.26
(before mixing)	3.2		
X-ray sedimentation			
diameter at 50 mass %	5.8		4.2
at 50 vol. %	0.65		0.0023

Optical Microscope: Diameter of particles intersecting a test line

TEM: Diameters measured from micrographs. Particles are plate-like. Max. = diameter of plate
Min. = thickness of plate. Int. = average dimension of intragranular particles.

BET: Equivalent spherical diameter calculated from measurement of surface area.

X-ray sedimentation: Equivalent spherical diameter; see Appendix 2.

TABLE 3. Grain growth data - Pure

Experiment #	P _c / P _p (MPa) 400/100 or 300/2	time (x10 ⁻³ s)	+ above [†] - on		\bar{L} (μm)	\bar{D} (μm)	range
			0	below			
CA-10	550°C	(500/2)	3.6	(1 hr.)	10.6	15.9	11.1-25.1
CA-2-4	650°	(500/2)	3.6		7.1	10.7	8.7-13.1
2024	800°	x	0.01		10.0	15.0	13.5-17.7
2034		x	0.01		8.6	12.9	11.3-15.2
2039		x	0.01		5.1	7.6	6.2-10.4
2049		x	0.30		7.1	10.6	8.1-14.9
1009		x	2.1		8.2	12.3	10.9-13.7
2006		x	3.6		11.8	17.7	14.1-23.4
CA-13*		x	3.6		14.9	22.3	14.4-37.7
2020		x	3.8		15.7	23.5	20.9-26.1
1007		x	7.2		12.5	18.8	15.8-21.8
2033		x	7.2		20.9	31.4	28.2-35.1
2037		x	7.2		12.4	18.7	15.0-23.6
2042		x	7.2		14.3	21.5	18.0-24.3
2045		x	7.2		26.4	39.6	30.9-46.8
4003		x	7.2		15.4	23.1	13.1-33.2
2021		x	7.3		23.3	35.0	30.2-39.2
2022		x	9.3		22.1	33.1	26.3-41.7
1008		x	10.8		24.0	36.0	-
2026		x	10.8		17.5	26.4	24.2-29.6
2023		x	12.6		32.0	48.0	39.5-57.5
2004		x	14.4		11.3	16.9	15.9-18.3
2028		x	14.4		15.3	23.0	19.2-27.2
2025		x	16.6		16.8	25.2	22.4-30.3
2005		x	20.5		26.8	40.2	29.9-59.9
2053		x	27.0		15.8	23.8	17.7-34.4
2048		x	36.0		18.7	28.0	22.4-42.6
2054		x	36.0		28.6	42.9	27.0-71.3
CA-12*		x	36.0		42.1	63.1	33.3-91.7
2007		x	38.0		15.5	23.3	19.7-28.0
2047		x	86.4		29.5	44.3	38.6-50.1
CA-11*		x	86.4		54.0	68.8	61.1-97.7
CA-15*		x	86.4		43.9	65.9	41.4-95.4
CA-18*	900°C	x	36.0		41.8	62.7	55.7-67.5
2027	900°	x	3.6		22.2	33.3	28.2-40.8
CA-22*	800°(dry)	(300/0)	36.0		29.4	44.1	32.0-48.2

*Initially hot pressed in CA-2-4 or -10 at 550°/650°C and P_c = 500 MPa for 1 hour.

†Indicates that rate of grain growth is faster (+), slower (-) or equal to (0) the rate defined by the CA-series data.

TABLE 4. Grain growth data - 1% and 5% mica, 0.6M MnCl₂ solution and Solenhofen limestone

Experiment #	P _c / P _p (MPa)	P _c / P _p (MPa)		phl/bio [†]	time (x10 ⁻³ s)	L (μm)	\bar{D} (μm)	range
		400/100	or 300/2					
<u>1%</u>								
2039	800°C	x		p	0.01	6.7	9.9	9.8-10.4
2049			x	p	0.30	4.8	7.2	± <0.1
2002		x		b	0.5	4.3	6.5	5.9-7.1
2006		x		b	3.6	10.5	15.7	15.2-17.5
2003		x		b	7.2	8.8	13.2	11.3-15.2
2037		x		p	7.2	10.5	15.8	15.2-15.9
2004		x		b	14.4	9.3	13.9	12.2-15.2
2005		x		b	20.5	21.5	32.3	27.9-39.9
2053			x	p	27.0	14.2	21.3	19.8-22.8
2007		x		b	38.0	17.6	26.4	22.4-31.9
<u>5%</u>								
CA-9	650°C		(500/2)	p	3.6	6.1	9.2	8.7-9.9
2024		x		p	0.01	8.1	12.2	11.1-12.8
2034			x	p	0.01	5.8	8.7	8.3-9.2
2039		x		p	0.01	5.1	7.6	6.9-8.3
2049			x	p	0.30	4.2	6.3	±<0.1
2006		x		b	3.6	7.6	11.4	10.8-12
CA-13*			x	p	3.6	8.0	12.0	11.0-13.4
2020		x		p	3.8	10.4	15.6	14.9-16.5
2033			x	p	7.2	9.1	13.7	12.9-14.1
2037		x		p	7.2	7.0	10.5	9.4-11.5
2021		x		p	7.3	15.4	23.1	21.6-24.3
2022		x		p	9.3	14.8	22.2	19.5-23.4
2026		x		p	10.8	12.8	19.2	18.3-21.2
2023		x		p	12.6	15.9	23.9	23.1-24.6
2028		x		p	14.4	9.6	14.4	14.1-14.7
2025		x		p	16.6	11.5	17.3	16.2-18.5
2005		x		b	20.5	11.7	17.6	15.0-21.9

Table 4. (cont'd.)

Experiment #	P_c / P_p (MPa)		phl/bio [†]	time ($\times 10^{-3}$ s)	\bar{L} (μm)	\bar{D} (μm)	range	
	400/100	or 300/2						
<u>5%</u>								
2053	800°C		x	p	27.0	8.0	12.0	11.0-13.1
2048			x	p	36.0	10.9	16.3	13.1-18.6
CA-12*			x	p	36.0	9.1	13.6	12.6-14.7
2007		x		b	38.0	10.5	15.8	13.4-18.9
2047			x	p	86.4	11.7	17.5	14.4-24.2
CA-11*			x	p	86.4	11.3	16.9	15.0-20.1
CA-15*			x	p	86.4	11.6	17.4	16.1-18.2
<u>Solenhofen limestone</u>								
start					4.2	6.5		<0.1
2054	800°C		x		36.0	6.8	10.1	8.9-13.1
CA-18	900°C		x		36.0	10.8	16.2	13.2-20.7
<u>0.6M MnCl₂ soln.</u>								
CM-2			x		3.6	67.6	101.4	78.5-114.2

*Initially hot pressed in Ca-9 at 650°C and $P_c = 500$ MPa for 1 hour.

[†]Phlogopite/biotite as second phase particles.

TABLE 5. Porosity and pore size measurements

Experiment [#] #	time (x10 ⁻³ sec)	\bar{D} (μm)	Porosity (vol. fraction)	Method of measurement*	Pore size† (μm)
1007 P	7.2	18.8	.063	IM	3.1±2 T (SEM)
			.13	OPT	4.2±2.5 T
				"	1.2±0.5 I
			.14	SEM	6.01 E
1008 P	10.8	36.0	-	-	2.93±1.4 I
1009 P	2.1	12.3	.055	IM	
2004 P	14.4	16.9	.03	"	
1		13.9	.03	"	
2005 P	20.5	40.2	.023	"	
1		32.3	.012	"	
			.002	"	
5		17.5	.022	"	
2006 P	3.6	17.7	.019	"	
1		15.7	0	"	
5		11.4	.017	"	
2007 P	38.0	23.3	.042	"	
			.027	"	
1		26.4	.02	"	
5		15.8	.014	"	
2021 P	7.3	35.0	.027±.005	OPT	1.43±0.48 I
			.05	SEM	3.52±2.01 E
5		23.1	.155±.01	OPT	1.0±.57 I
				"	2.99±1.53 E
2022 P	9.3	33.1	.032±.006	"	
5		22.2	.15±.02	"	
2023 P	12.6	48.0	.038	OPT	
			.05	SEM	
5		23.9	.113±.01	OPT	
2024 P	0	15.0	.103	"	4.3±3.8 E
				"	1.72 I
5		12.2	.10±.01	"	2.5±1.1 E
			.07	SEM	0.88±0.31 I
2025 P	16.6	25.2	.083	OPT	
5		17.3	.083±.009	"	1.07±0.6 I
				"	2.4±0.8 E
2026 P	10.8	26.4	.08±.01	"	

All data collected by Brian Evans (pers. comm.)

[#]P - pure, 1 - 1% mica, 5 - 5% mica.

*OPT - optical microscopy, SEM - scanning electron microscopy, IM - immersion in CCl₄

†I - intragranular, E - grain boundary, T - all pores

Measured from optical micrographs unless otherwise specified.

TABLE 6. K values for synthetic marbles and Solenhofen limestone

Experiment	Temperature	Confining pressure	K(m ³ /s)
<u>Synthetic Marble</u>			
Pure 20XX Series	900°C	400/300 MPa	6x10 ⁻¹⁸ - 10 ⁻¹⁷
" "	800	"	3x10 ⁻¹⁹ 8x10 ⁻¹⁸
" "	700	"	(0.93 - 6.8)x10 ⁻¹⁹
" CA-XX Series	800	300	5x10 ⁻¹⁸
" "	650	"	4x10 ⁻¹⁹
" dry	800	"	2x10 ⁻¹⁸
0.6M MnCl ₂ solution	800	"	3x10 ⁻¹⁶
<u>Solenhofen Limestone</u>			
(Tullis and Yund, 1982)	1000 Wet	1500	2x10 ⁻¹⁷
"	1000 Dry	1500	1.5x10 ⁻¹⁸
"	950 D	1500	1.1x10 ⁻¹⁸
"	900 W	1500	(2-3)x10 ⁻¹⁸
"	900 D	1500	(8-9)x10 ⁻¹⁹
"	800 W	1500	(1-9)x10 ⁻¹⁹
"	800 D	1500	5x10 ⁻²⁰ - 6x10 ⁻¹⁹
"	700 W	1500	4x10 ⁻²⁰
"	700 D	1500	1.2x10 ⁻²⁰
"	700 W	200	10 ⁻²¹
"	650 W	200	2x10 ⁻²²
(Schmid et al., 1977)	1000	300	2x10 ⁻¹⁸
"	950	300	7x10 ⁻¹⁹
"	900	300	1.5x10 ⁻²⁰ - 4x10 ⁻¹⁹
"	800	300	10 ⁻²⁰ 2x10 ⁻¹⁹
"	700	300	5x10 ⁻²¹ - 2x10 ⁻¹⁹
"	600	300	7x10 ⁻²¹ - 9x10 ⁻²⁰

TABLE 7. Activation energies for grain growth

Experiment	Q (KJ/mole)*
<u>Synthetic marbles</u>	
Wet (300 MPa)	175
Dry (300 MPa)	164
<u>Solenhofen limestone</u>	
Tullis & Yund: Wet (700-1000°C; 1500 MPa)	252
Dry (700-900°C; 1500 MPa)	239
Dry (700-1000°C; 1500 MPa)	196
Schmid: (700-900°C; 300 MPa)	142
(700-1000°C; 300 MPa)	187
Diffusion of carbon in calcite	360
Diffusion of oxygen in calcite (Kronenberg et al., 1984)	340-380

* 1 KJ/mole = 0.24 Kcal/mole

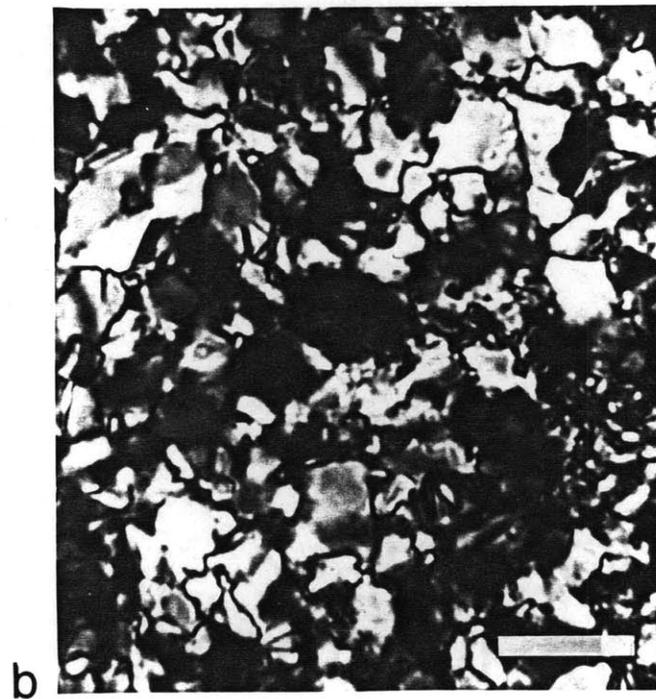
FIGURE CAPTIONS: CHAPTER 3

- FIGURE 1. a) SEM micrograph of initial CaCO_3 powder. Note wide range of particle sizes. b) Optical micrograph of hot-pressed synthetic marble prior to the onset of grain growth. The specimen was heat-treated at 500°C and 500 MPa for 1 hour.
- FIGURE 2. Optical micrographs showing the progressive development of grain size and grain-boundary microstructures in synthetic marbles. a) heat-treated at 550°C and 500 MPa for 1 hour. The microstructure after recrystallization but before significant grain growth has occurred is shown. The grain size from this sample was chosen as the initial grain size, D_0 . b) heat-treated at 800°C and 300 MPa for 1 minute. Polygonal grains, near-equilibrium triple junctions, and included porosity are shown. c) heat-treated at 800°C and 300 MPa for 3.5 hours. Large grains are associated with a very low porosity. d) heat-treated at 800°C and 300 MPa for 4 hours. Grain-size reduction is due to porosity. e) same experiment as c. Grain-size reduction is due to 5% phlogopite particles. It is difficult to distinguish particles from pores. f) heat-treated at 800°C and 300 MPa for 1 hour. Accelerated grain growth is due to a 0.6M MnCl_2 solution. Note the lower magnification.
- FIGURE 3. a) Illustration of the process by which pore clusters form in the middle of grains by secondary recrystallization (reprinted from Rossi and Burke, 1973). Small, first generation structure is pinned by pores. Then secondary recrystallization (exaggerated grain growth) occurs, creating a second generation of grains which have included porosity. These second generation grains then grow until they mutually impinge, creating a third generation structure. b) Optical micrograph showing a similar structure in a synthetic marble. Compare to Figure 2d.
- FIGURE 4. SEM and TEM micrographs showing various microstructures. SEM: a) shapes and relative sizes of pores that are distributed in triple junctions, on grain edges, and in the interior of grains. TEM: b) clusters of mica particles in "glassy" grain-boundary phase (dark-field image); c) mica particles along grain boundary (dark-field image). The orientation of mica particles relative to the boundary, the particle in the grain interior, and the boundary film are shown; d) mica particles in the interior of a grain and in an included pore, (bright-field image). Dislocations are present in all TEM micrographs.

- FIGURE 5. Grain-growth data for pure calcite synthetic marbles are compared to the normal growth law (Equation 1) for n equal to 2, 3, and 4 fit to the CA-XX data. The scatter in the X0XX data is presumably due to porosity variations.
- FIGURE 6. Grain-growth data for synthetic marbles containing mica particles. The data deviate from the n equals 3 reference line. The stable, limiting grain-size is approximately 30 and 24 μm for the 1 and 5% specimens, respectively.
- FIGURE 7. Comparison of D_{max}/d vs $1/f$ data for specimens containing mica particles to the alumina data and the models from Chapter 2. (1) Zener (1948), (2) Hellman and Hillert (1975), (3) Anand and Gurland (1975), and (4) this study (Appendix 1). Models are defined in Chapter 2, Table 1. Compare to Chapter 2, Figure 10. Two values of d are given: the BET diameter and the TEM diameter (Table 2). The dependence of D_{max}/d on $1/f$ is less than 0.5, in agreement with the alumina data.
- FIGURE 8. Grain-growth data for the wet and dry synthetic marbles from this study compared to dry data from Gee (1982) and the 0.6M MnCl_2 data (CM-1). The line is for $n = 3$ as in Figure 5.
- FIGURE 9. Grain-growth data for Solenhofen limestone from this study, from Tullis and Yund (1982), and from Schmid (unpublished data for experiments in Schmid *et al.*, 1977). Reference curve from synthetic-marble data, for Equation 1 with n equals 3, has been included for comparison.
- FIGURE 10. Optical and TEM micrographs of Solenhofen limestone. Optical: a) initial material; b) sample heat-treated at 800°C and 300 MPa for 10 hours (compare to synthetic marbles in Figure 2); TEM: c) dark-field image showing pores and detrital second-phase material. Optical: d) composite from Schmid (unpublished micrographs) illustrating pockets of fluid in sample heat-treated at 1000°C and 300 MPa for 4 hours. This sample showed significant grain growth ($D = 20 \mu\text{m}$).
- FIGURE 11. Plot of synthetic marble and Solenhofen limestone data as the normal grain-growth law (Eqn. 1) for n equals 3.
- FIGURE 12. Arrhenius plot of the growth-rate constant, K , for the normal grain-growth law (Eqn. 1) assuming n equals 3. Activation energies for the grain-growth mechanisms are given in Table 7.



a CaCO_3 powder



b CA-19 10 μm

Figure 1

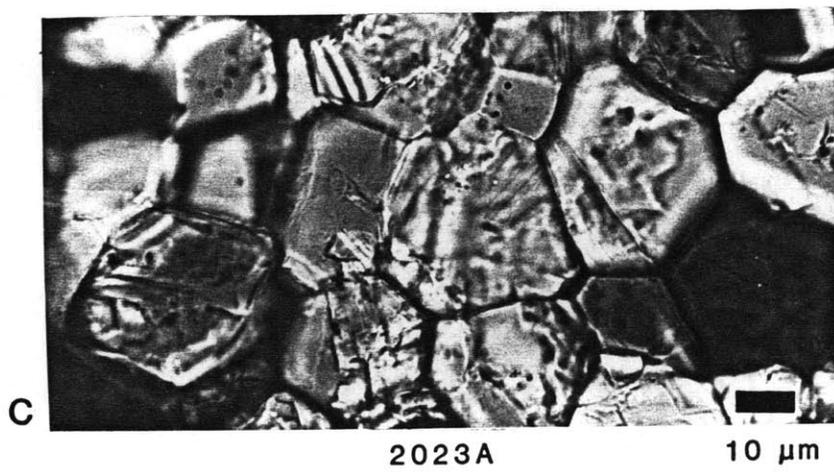
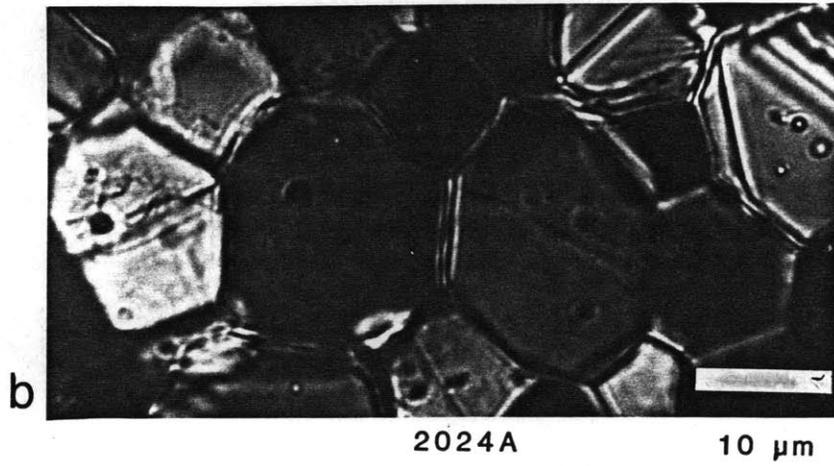
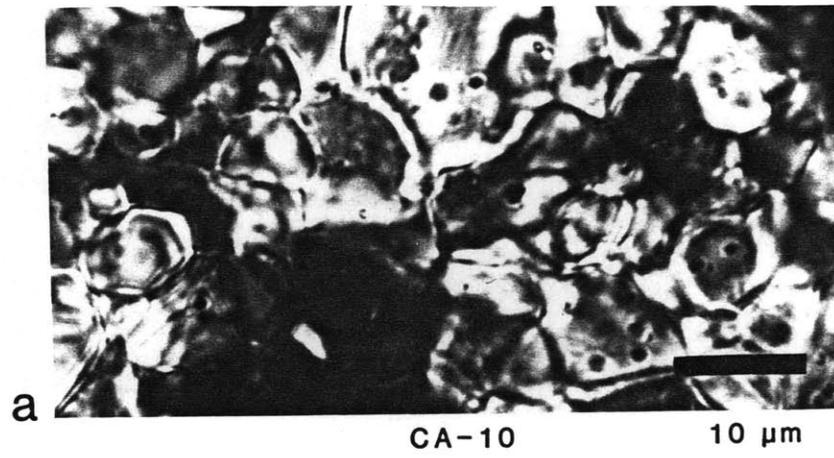


Figure 2

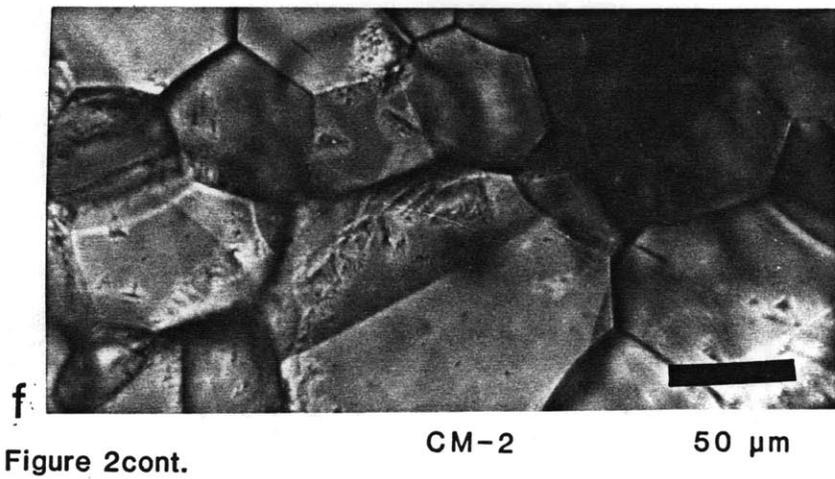
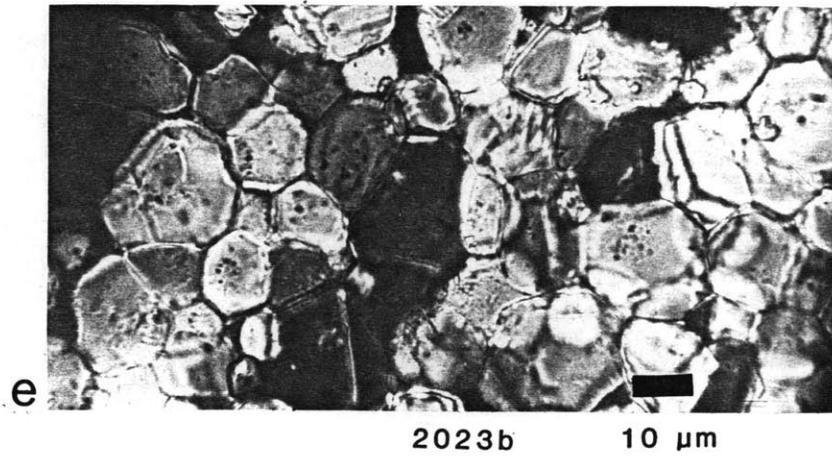
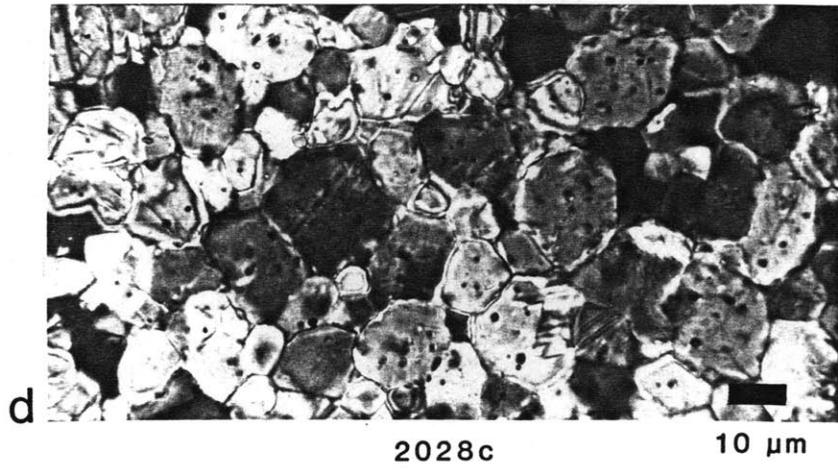
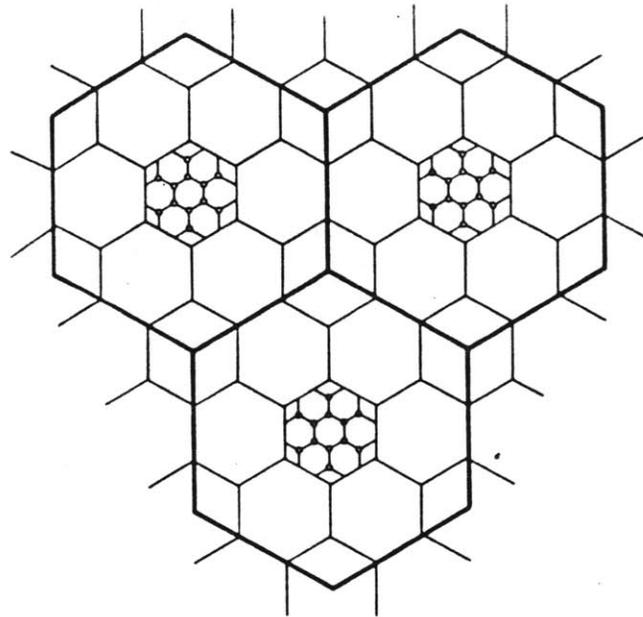
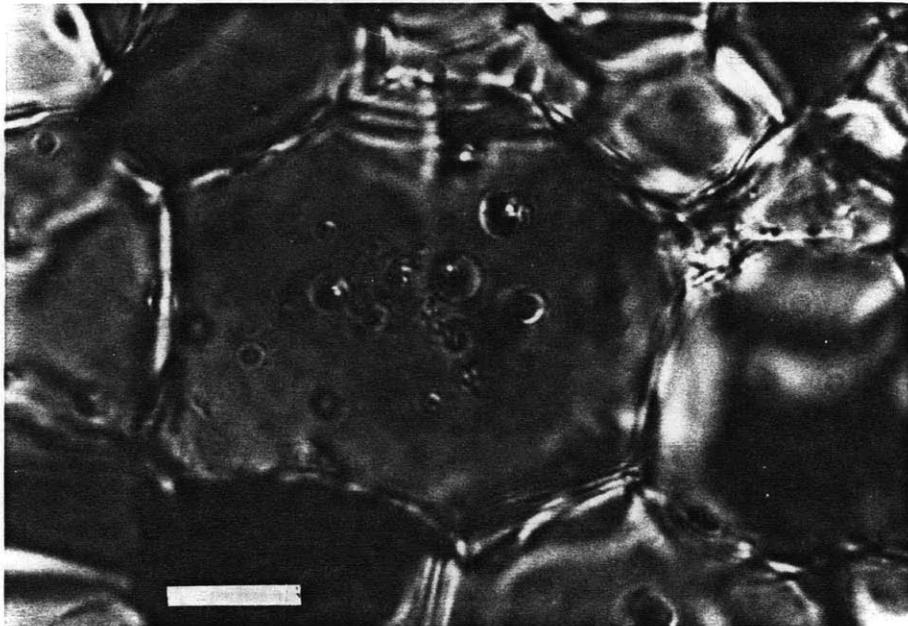


Figure 2cont.



a



b

10 μ m

2028A

Figure 3

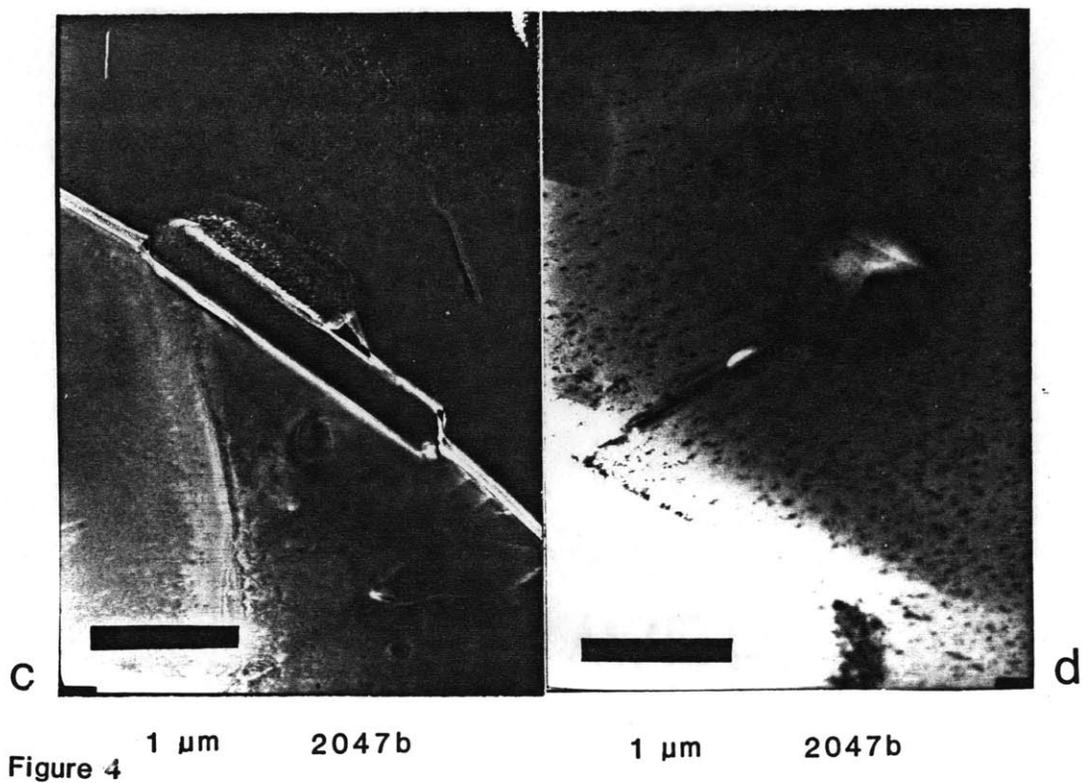
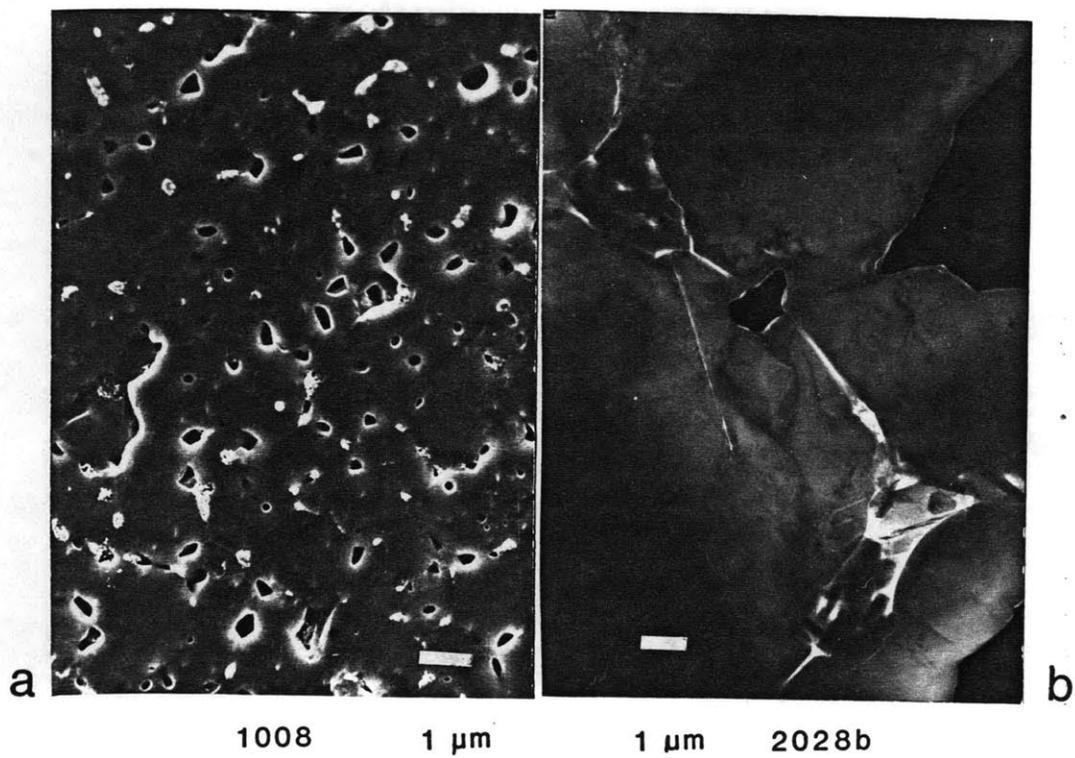
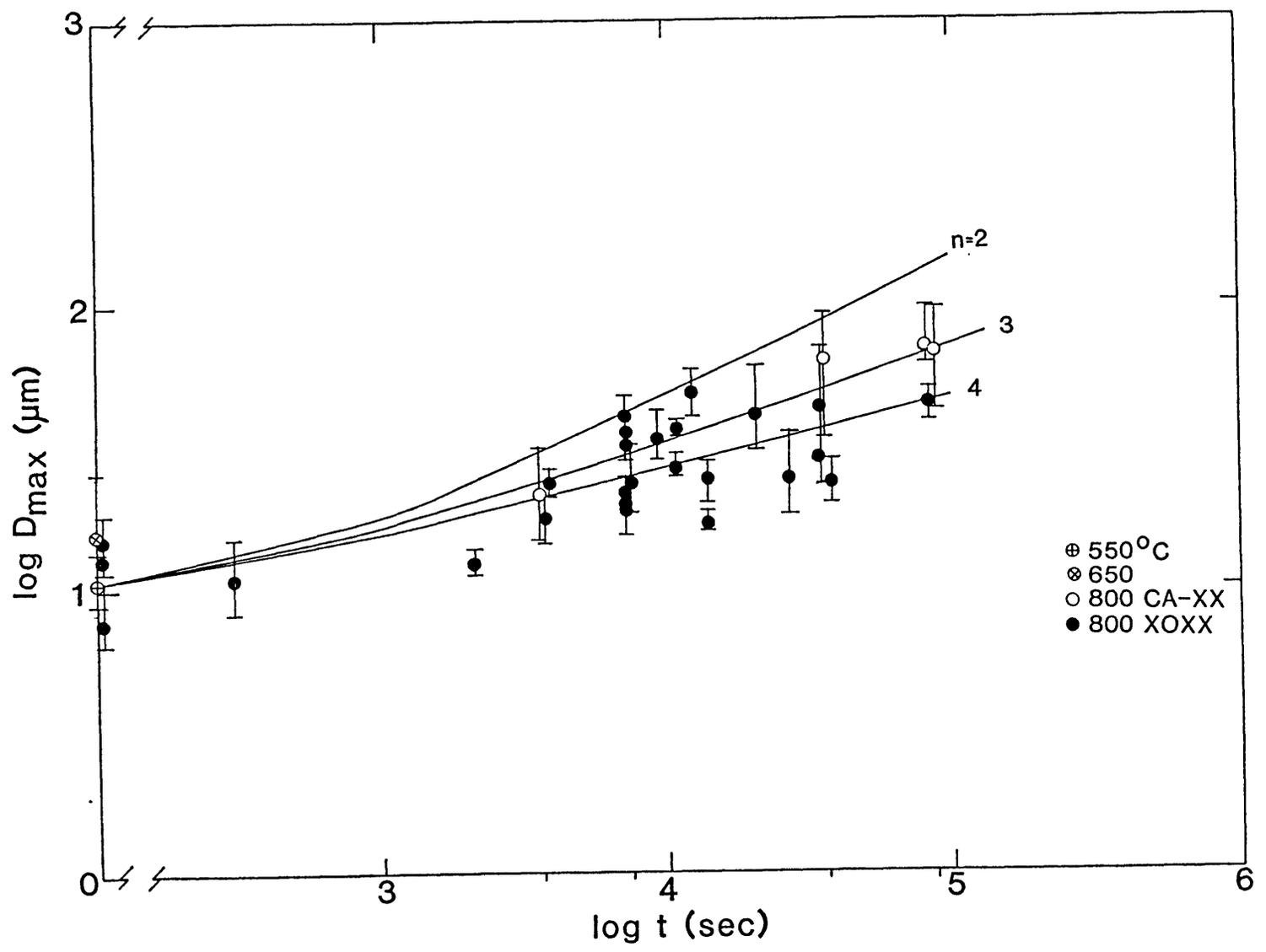
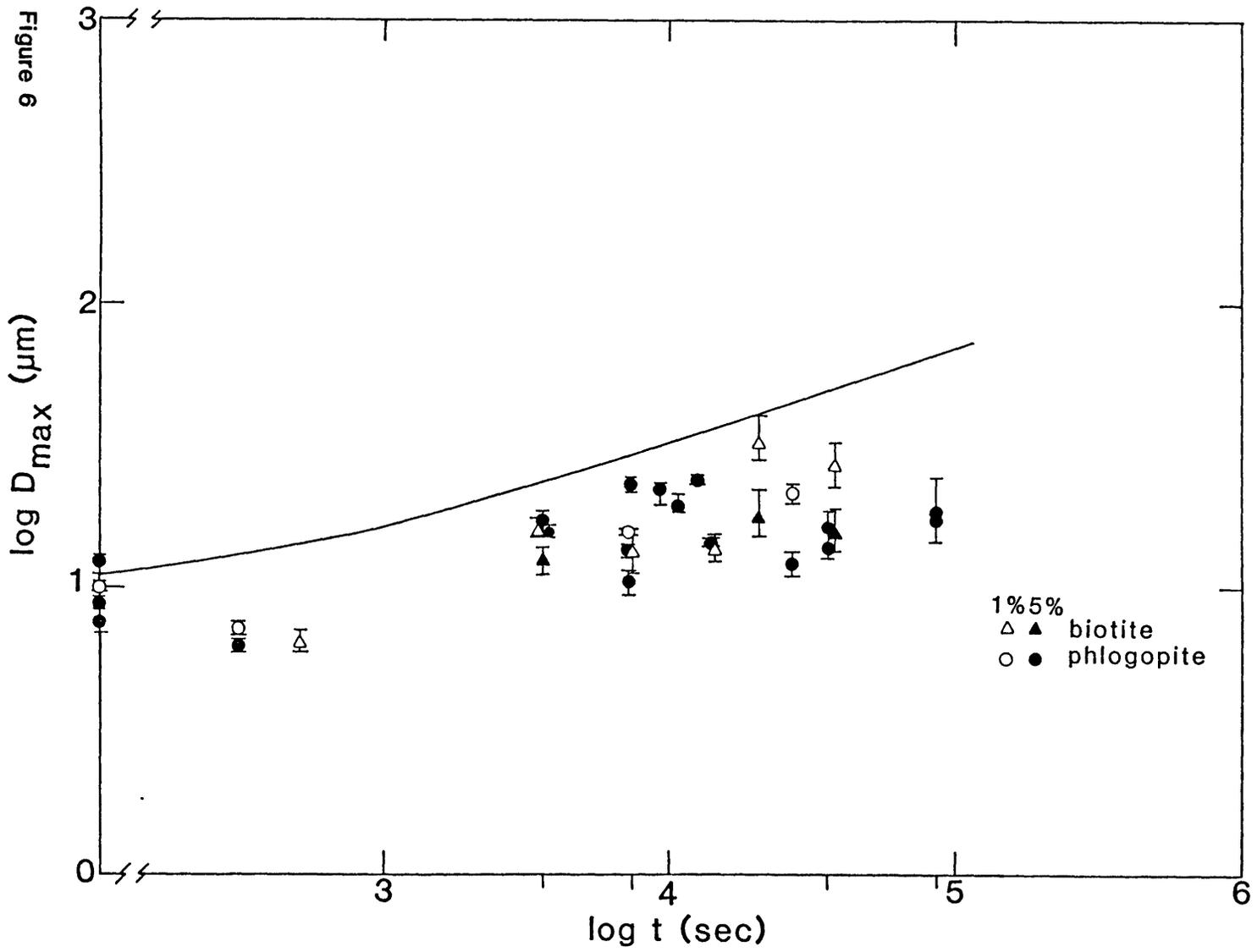


Figure 4

Figure 5





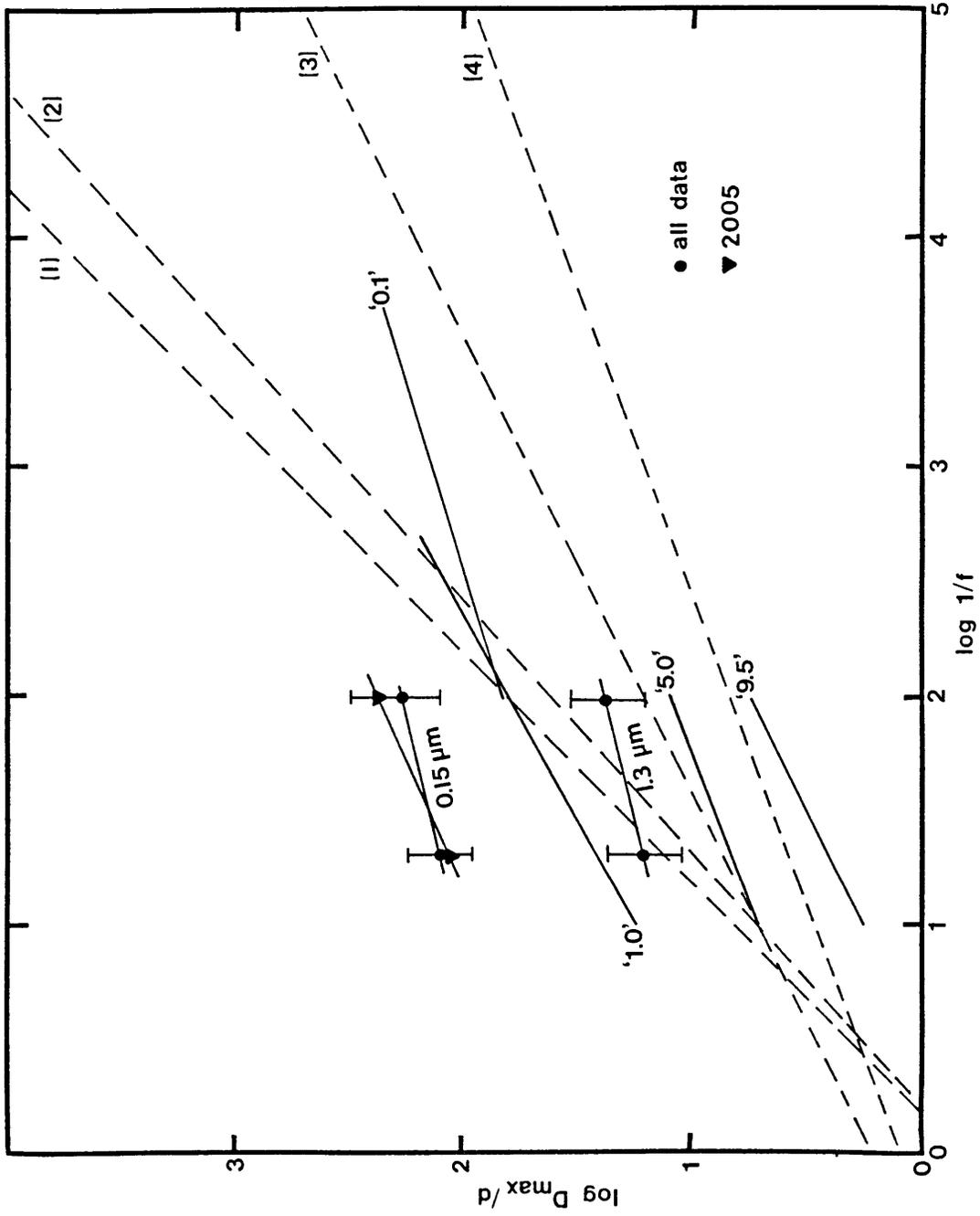


Figure 8

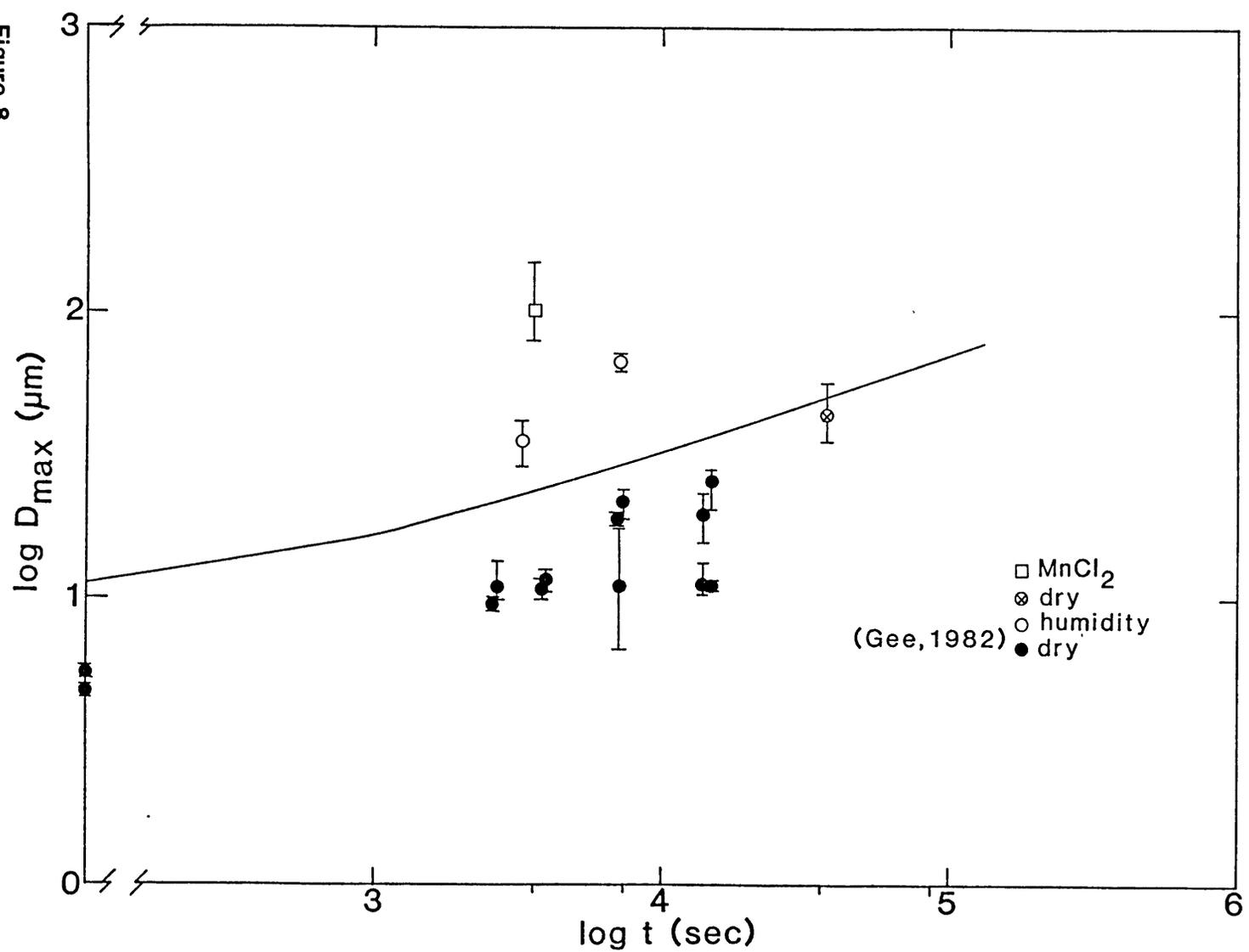
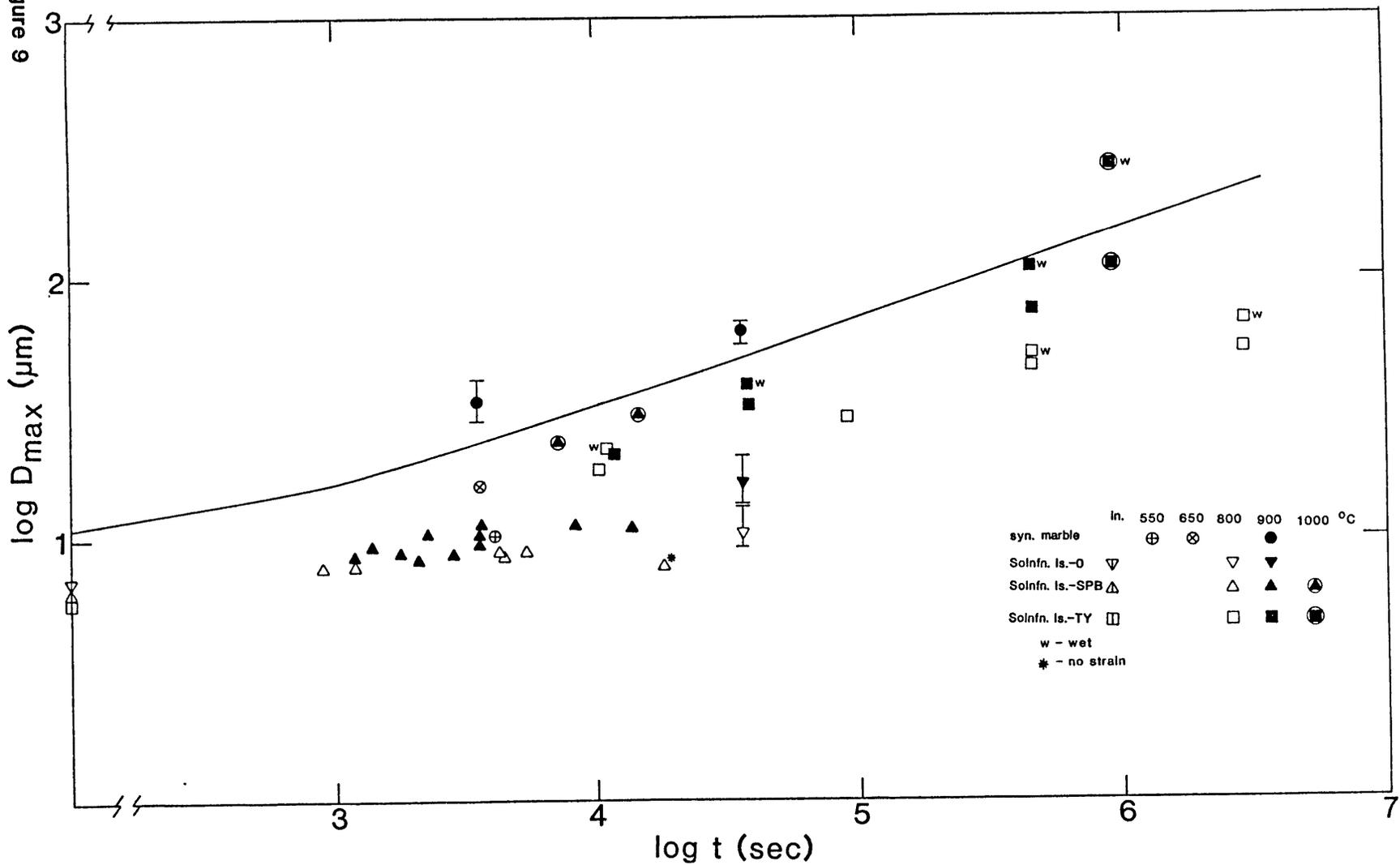


Figure 9



Solenhofen limestone

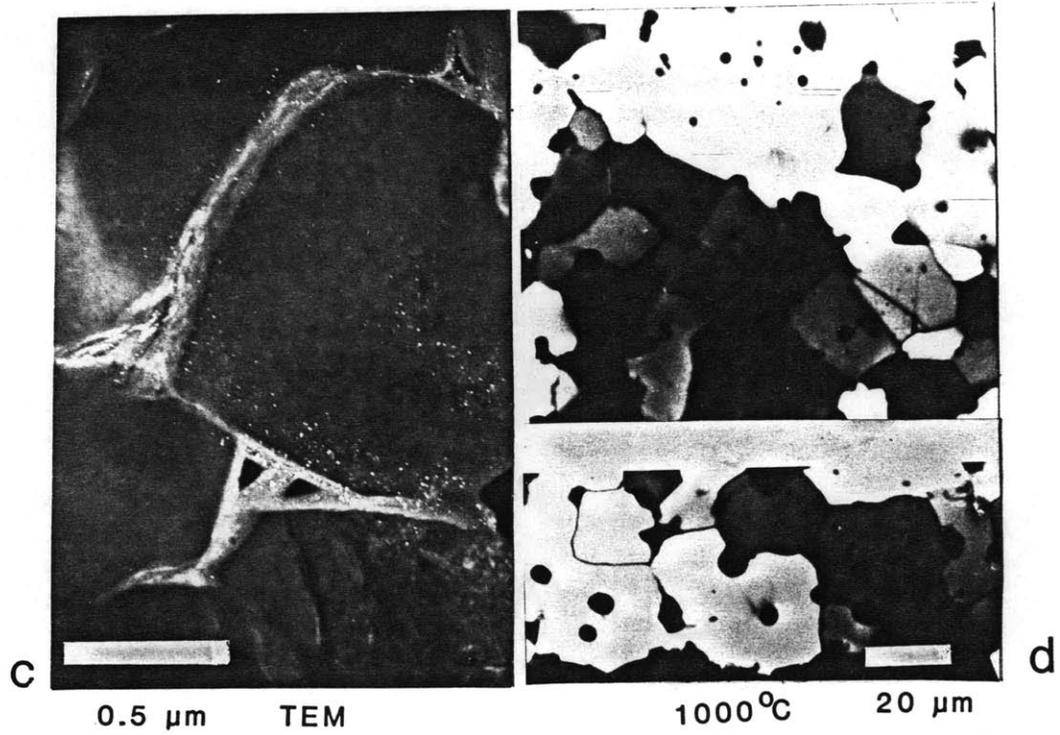
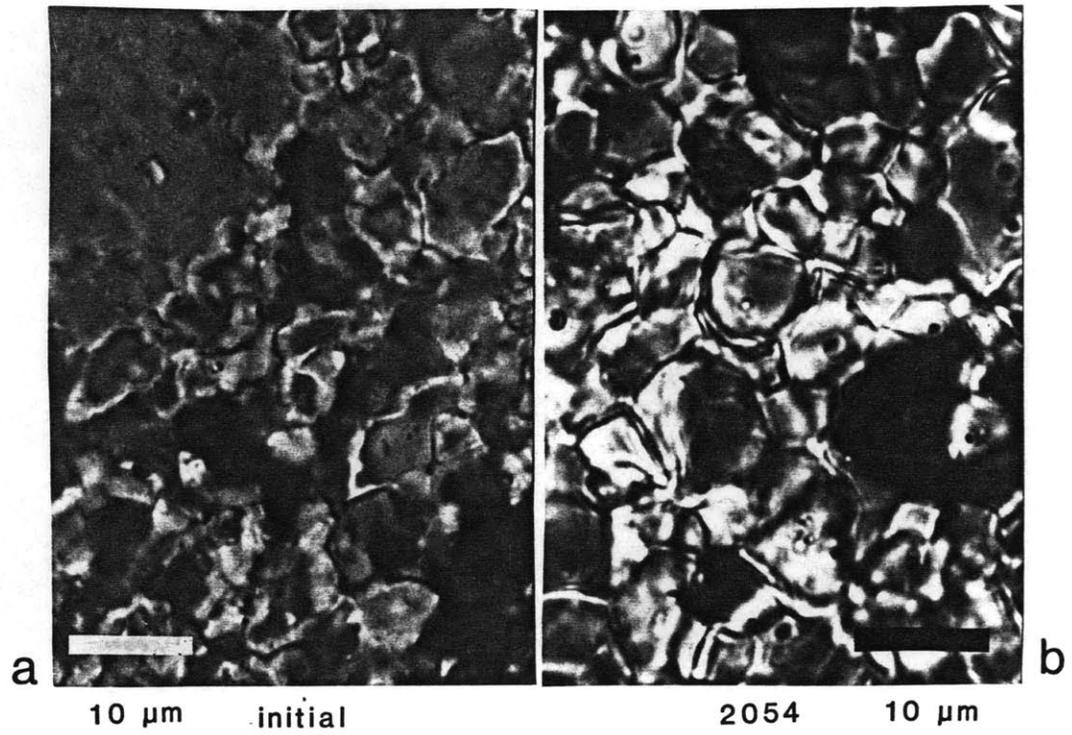


Figure 10

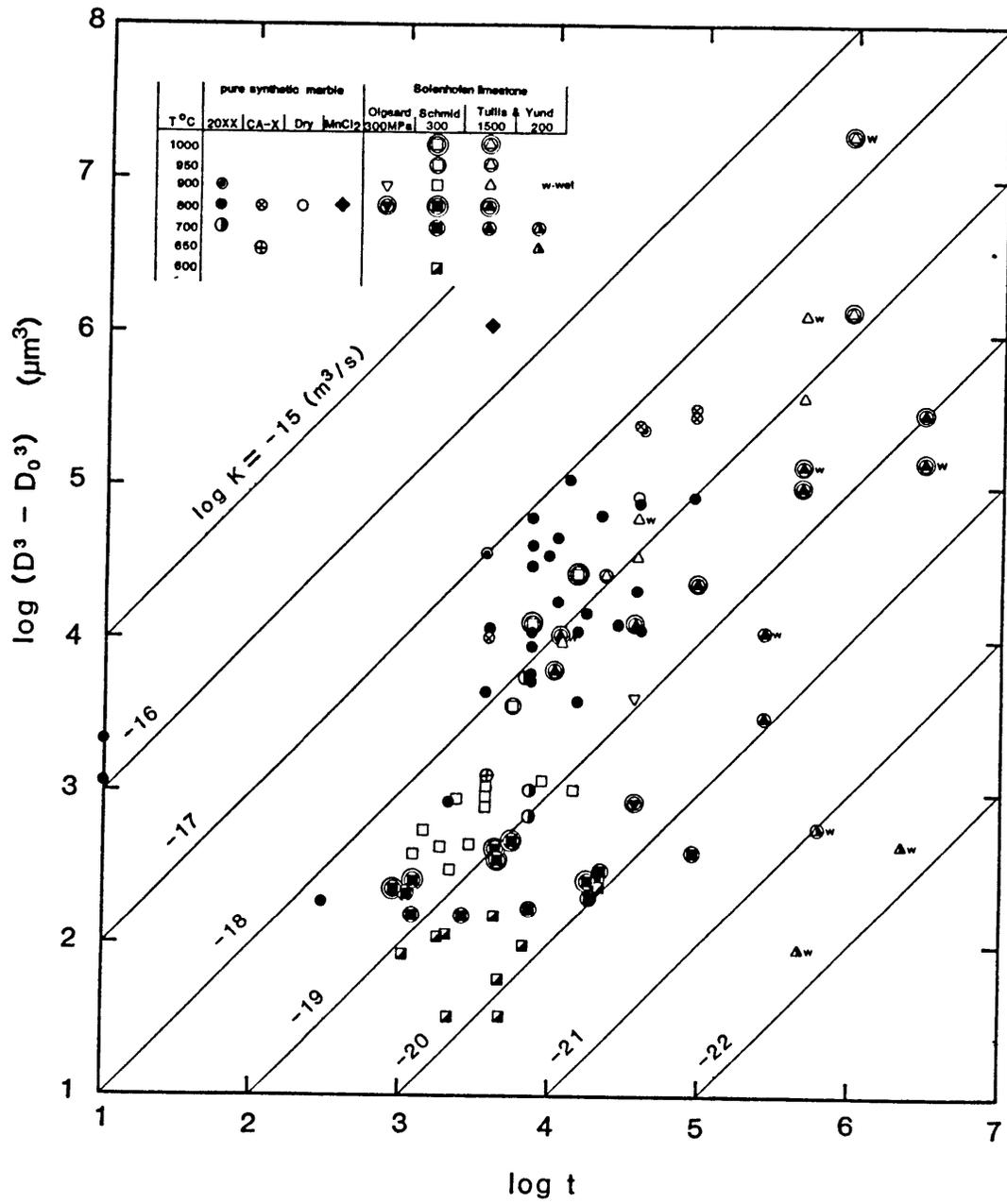


Figure 11

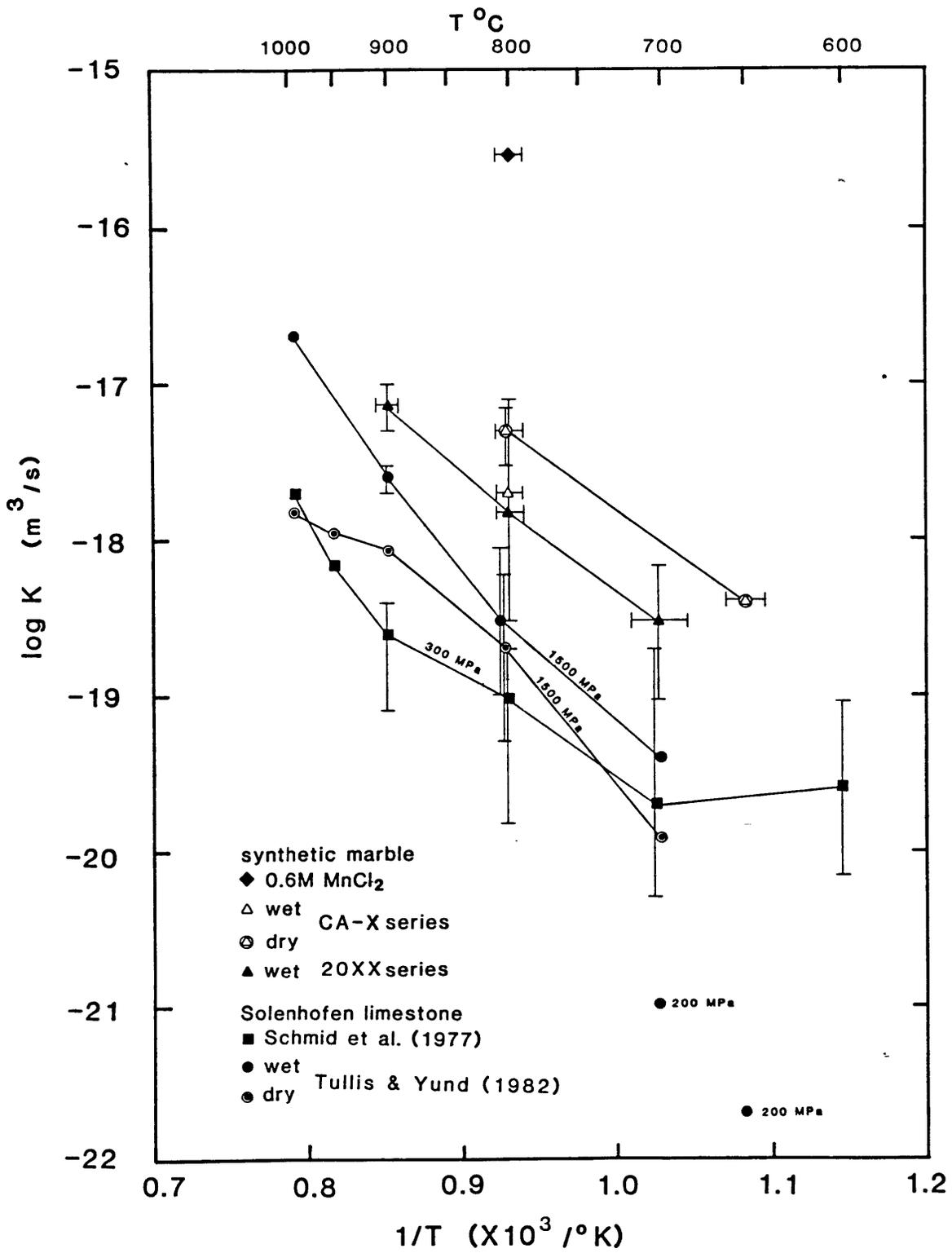


Figure 12

CHAPTER 4

EFFECTS OF VARIATIONS IN GRAIN SIZE, SECOND-PHASE PARTICLE CONTENT
AND WATER ON THE MECHANICAL PROPERTIES OF SYNTHETIC MARBLE

INTRODUCTION

Grain-size sensitive deformation mechanisms may be important at intermediate to high temperatures in the earth. Prior to the experimental study of Schmid et al. (1977) on Solenhofen limestone, it was generally believed that ductile flow in the earth's crust was governed by dislocation processes, which are relatively grain-size insensitive, and could be described by a power-law flow equation (Heard, 1976). Schmid et al., (1977) explored the low-stress regime of ductile flow and showed that fine-grained Solenhofen limestone deformed by a mechanism analogous to superplasticity (Edington et al., 1976). They showed evidence that indicated that the process involved a significant component of grain-boundary sliding. Similar behavior has not been recognized in coarser grained marbles (Schmid et al., 1980, and Heard and Raleigh, 1972), which are significantly stronger than Solenhofen at comparable temperatures and strain-rates.

The importance of superplasticity in a geologic context has been reviewed by Twiss (1976) and Zeuch (1982). To explain "ductile faulting", Twiss (1976) proposed a diffusion-accommodated grain-boundary sliding model and Zeuch (1982) proposed a model based on recovery by dynamic recrystallization with no change in creep mechanism. Since Schmid et al.'s (1977) study, strain softening due to a reduction in

grain size has been demonstrated for anhydrite (Muller et al., 1981) and feldspar (Tullis and Yund, 1985). In both cases, the weakening and strain localization with decreasing grain size were attributed to dynamic recrystallization as opposed to grain-boundary sliding. Karato and Paterson (1985) found that the creep strength of synthetic olivine aggregates increased markedly as the grain size increased and that the stress/strain rate relationship of these fine-grained aggregates was nearly linear. Both of these observations are consistent with superplastic-style behavior. Evidence for superplasticity in naturally deformed mylonites was first inferred by Boullier and Gueguen (1975) and has since been described by several others, including Etheridge and Wilkie (1979), Etheridge and Vernon (1981), and Evans et al. (1980).

If deformation occurs by grain-size sensitive mechanisms, then relatively minor amounts of second phases, such as water and/or rigid particles, and ionic impurities may strongly influence strength. In Chapters 2 and 3, the effects of second phases on thermally-activated solid-state metamorphic processes were investigated using synthetic marbles. These rocks were produced by hot isostatically pressing fine powders into dense composites with microstructures that were very similar to natural, fine-grained limestones. It was shown that the rate of grain growth was sensitive to water content and the chemical environment, and that even minor amounts of second-phase particles limited the grain size to a very small value.

Second phases may also affect the mechanisms of deformation: 1) Particles may promote grain-size sensitive mechanisms by limiting the matrix grain size. 2) Particles may strengthen fine-grained materials by acting as obstacles to grain-boundary sliding. 3) Grain boundary fluids

or melt phases would increase grain boundary diffusion rates or promote grain boundary sliding by decreasing restraining forces between grains. And 4) at high temperatures, water has been shown to promote melting (Chapter 2), and therefore may explain dramatic strength decreases below the bulk melting temperatures but above the temperature where grain-size sensitive flow would be expected.

The initial goal of our experiments was to compare ductile flow properties of our synthetic rocks to Solenhofen limestone discussed by Schmid et al. (1977), and to explore the effects of variations in second-phase content and grain size on the strength of samples with carefully controlled chemistries.

The deformation regime that has been explored appears to be one of intracrystalline plasticity. We have not observed superplastic behavior, as characterized by near-linear dependence of strain rate on reciprocal flow stress, in the synthetic marbles. However, there is evidence to suggest an increased involvement of grain-size sensitive mechanisms with decreasing grain size.

EXPERIMENTAL METHOD

The wet and dry synthetic marbles used in this investigation were fabricated by the method described in Chapter 2. The CAD-series specimens were densified and recrystallized at 500°C, 500 MPa confining pressure (P_c), and 2 MPa pore pressure (P_p) for one hour. The 4000 series specimens were prepared by heat-treating at 750° or 800°C, P_c equal to 300 MPa, and P_p equal to 2 MPa for two hours. Dry samples were prepared as in Chapter 3 and wrapped in a thin (0.03 mm) silver foil. Samples were cut from the middle of each hot-pressed specimen and

machined into cylinders about 12 mm in diameter by 25 mm long.

All specimens were deformed in compression in the high-temperature, high-pressure triaxial-stress apparatus shown schematically in Figure 1 (reprinted from Caristan, 1980). Experiments have been completed at $700^{\circ} \pm 5^{\circ}\text{C}$, P_c equal to 100 ± 2 MPa, P_p equal to 2 ± 2 MPa, and constant displacement rates which correspond to strain rates of approximately 10^{-3} , 10^{-4} , and $2 \times 10^{-5} \text{ s}^{-1}$. The apparatus was particularly suited for low-stress experiments for several reasons. 1) The confining medium (argon) provided a uniform hydrostatic pressure. 2) The internal furnace consisted of two separately controlled coils which could be adjusted to minimize temperature variations over the length of the sample to $\pm 5^{\circ}\text{C}$. 3) Although the load was measured externally, O-ring friction on the sliding piston accounted for only 2.1 ± 0.3 MPa of the differential stress. Yield stress levels in our experiments were between 40 and 90 MPa. In order to explore very low stress behavior (< 10 MPa), an internal load cell would be required to eliminate this uncertainty. Such a load cell has been tested in our apparatus but was not available for the experiments described here. 4) Thin-walled (0.3 mm) copper jackets (19.2 mm O.D.) were used which had a strength of approximately 15 MPa at 700°C and a strain rate of 10^{-3} s^{-1} (Frost and Ashby, 1982). When the jacket was squeezed down around sample, it accounted for 1.2 ± 0.3 MPa. Although the strength of the copper jacket was not significant in the experiments reported here, it may become significant in very low-stress experiments.

Since coarse grained synthetic marbles were easily disaggregated, they could not be cut or shaped. Therefore, in those experiments where the specimens were heat-treated at 800°C and P_c equal to 300 MPa for

10 hours, the samples were shaped into right cylinders before the heat-treatment and then deformed in the same jacket (temperature and pressure were dropped to room conditions to preserve consistency of preparation with the other samples). The dimensions of the specimens at the onset of deformation were assumed to have been the same as before the heat-treatment. Prior to each deformation test, specimens were annealed at 700°C for 15 minutes to remove defects introduced during the heat-up and the initial preparation, and to homogenize the microstructures. Creep tests lasted from a few minutes to a few hours. Total strains were 20 to 50%. The temperature was dropped under load immediately following straining. Typical heat-up and quench histories for temperature and pressure were similar to those shown in Chapter 2, Figure 3. Grain growth was not expected to have affected the microstructure in the short time experiments.

The method outlined by Caristan (1980) was used to convert the measured load vs. displacement curves to stress vs. strain. For this method, the sample shape is assumed to have a parabolic longitudinal cross-section and deformation is non-homogeneous. For sample shapes typically observed, the mean homogeneous stress is a good approximation to the actual stress in an inhomogeneously deformed sample for strains up to 20% (Caristan, 1980). Since almost all of the specimens deformed in this study were strained to greater than 20%, the method may introduce errors at high strains. The equations used were:

$$e_T = \ln(l_0/l) \quad (1)$$

$$\epsilon = e_T/t \quad (2)$$

$$\sigma = (F/A_0)(1-(l_0-1)/l_0) \quad (3)$$

where e_T , ϵ , and σ , l_0 , l , t , F , and A_0 are, respectively, true strain, strain-rate, differential stress, (i.e. $(\sigma_1-\sigma_3)$, the greatest principal stress minus the least principal stress), initial cylinder length, final cylinder length, time, applied load, and initial cross-sectional area. (Note: After the figures were drafted it was discovered that two different methods were used to calculate strain.)

For microstructural analyses, samples were cut parallel to the maximum shortening direction and prepared as in Chapter 2 for optical microscopy and TEM. Grain sizes were measured with an optical microscope using the linear-intercept method (Underwood, 1970). The linear intercept length, L , was chosen to be the average of the sizes measured parallel (L_{\parallel}) and perpendicular (L_{\perp}) to the direction of maximum shortening. Grain size, D , was chosen equal to $3L/2$, the conversion for spherical particles (Exner, 1972). No correction was made for the grain-shape change(s) that occurred during straining.

The error bars in the stress-strain curves shown in Figures 8 and 9 represent the combined uncertainties of: force measured by the load cell, initial and final specimen dimensions, variations in strength due to variations in thickness of the copper jacket, and O-ring friction. The steady-state yield stresses plotted in Figures 13 and 15 were calculated by subtracting the frictional forces on the piston, and the load carried by the copper jacket from the constant stress value. The error bars for the yield-stresses are the above-mentioned uncertainties in the stress plus the uncertainty in the constant stress value chosen from the curves in Figures 8 and 9. The uncertainties in the

measurement of the local values of L_{\parallel} and L_{\perp} were less than the actual spatial variation of grain size. Thus, the horizontal error bars shown in Figure 13 represent the spread of measured grain size.

RESULTS

Thirteen experiments were performed to investigate the effects of second phase particles, water, and grain size on the mechanical behavior of synthetic marbles. All samples were compressed to high strains (20 to 50%) in order to attain the conditions favorable for dynamic recrystallization. The results are summarized in Table 1.

In most cases, the specimens were barrel-shaped, characteristic of samples constrained at their ends and deformed in compression. In several cases, the ends did not remain parallel due to slight misalignment of the specimen column.

In three experiments, equipment failures led to uncertain results. CAD-1 was inadvertently fractured at room temperature prior to straining. CAD-11 was an attempt to duplicate CAD-2, but was unsuccessful due to an equipment malfunction which resulted in a highly-variable load (gray region in Figure 8). CAD-10 was an attempt to duplicate CAD-7, however the jacket developed a leak during the 15-minute anneal prior to straining. CAD-10 was replete with large, open cracks parallel to the maximum compressive-stress direction and the grain size was too small to be optically measured.

CAD-8, the only dry specimen containing alumina particles, was discolored relative to the comparable wet one, CAD-4. It was, in fact, the only deformed sample, wet or dry, showing such discoloration. The color was similar to the color of the '9.5' data from Chapter 2 which was affected by extraneous impurities. However, the cause of the darkening did not appear to affect grain growth during the 10-hour heat-treatment (compare CAD-8 to CAD-4, Table 1).

Optical and transmission electron microscopy

Optical micrographs of several of the deformed specimens are shown in Figure 2. The grain shape and boundary morphologies in the fine-grained samples (Figure 2a and b) were similar to those in fine-grained, undeformed samples described in Chapters 2 and 3. The macroscopic strain was only partially reflected as intragranular deformation, suggesting that the deformation was, at least in part, accommodated by intergranular sliding or dynamic recrystallization. In coarser-grained samples (Figures 2c and 2d), the grains were elongated perpendicular to the maximum shortening direction, and the boundaries were sutured.

In 4002 (the only sample strained to over 50%, Table 1), dynamic recrystallization occurred throughout the specimen (Figure 3c and d). New grains appeared to nucleate along grain boundaries and comprised less than 10% of the bulk (Figure 3c). In regions of higher strain, near the corners of the sample (Figure 3d) for example, a larger volume fraction had recrystallized, and unrecrystallized grains had elongation ratios of 10:1 or greater.

In the pure dry specimens, there were distinct regions of coarse and fine grains (Figure 4). In CAD-6 (Figure 4a), the coarse grains were scattered in isolated pods and constituted 10 to 20% of the bulk. In CAD-7 and CAD-9 (Figure 4b and c), the coarse grains were distributed in bands (Not shown in photos) perpendicular to the direction of maximum shortening and constituted a significantly larger volume of the specimen. It is not known when this bimodal grain-size structure developed, however, it is unlikely that the bimodal grain-size in CAD-9 developed by

dynamic recrystallization since all grains were similarly strained.

A limited TEM study was conducted to define the mechanisms of deformation and the processes involved in dynamic recrystallization. Dislocations were abundant in all specimens and occurred as isolated individuals, tangled in clusters, and aligned into low-angle boundaries (Figures 5a-c). Preliminary estimates from CAD-9 and CAD-5 indicate that the dislocation densities were 5×10^{12} to 10^{13} m^{-2} ; an order of magnitude higher than the estimated density in undeformed specimens (Chapter 3). Dislocation densities were lower and less uniformly distributed from grain to grain in the fine-grained samples than in the coarse-grained ones (Figures 5a-d). There was no noticeable difference in dislocation arrangements or in densities between wet and dry samples.

Dynamic recrystallization was recognized in almost all specimens analyzed with the TEM. The progressive development of dynamic recrystallization is shown in Figures 6a-f. Dislocations first climb into low-angle subgrain walls, (Figure 6a). These subgrain walls were more prevalent near the grain boundaries than in the grain interiors, and they commonly cut off grain corners (upper right of Figure 6a). Subgrain sizes were typically 0.1 to 1.0 μm in diameter. A subgrain wall that was imaged "edge-on" is shown in Figure 6b. This wall was associated with a jog in the high-angle grain boundary, shown in the upper left, forming a cavity which was visible when the high-angle boundary was imaged "edge-on". Continued misalignment across these low-angle boundaries leads to separate grains, shown in the left side of Figure 6c. An enlargement of this region (Figures 6d-f) revealed several characteristics of these newly-formed grains: 1) Three-grain intersections did not show equilibrium angles ($\approx 120^\circ$) as at the relic triple junction in the upper

left of Figure 6d. 2) Some coherency still existed along a few boundaries as shown in the center of Figure 6e. 3) The cavities at three-grain intersections (Figure 6f) were similar in shape to those that formed when twins or subgrain walls intersected grain-boundaries. However, no twins or subgrain walls were evident, and the cavities were much larger than expected from the few dislocations that were associated with them. Because pores were known to exist in the sample prior to deformation, it is possible that these cavities were deformed relic pores. 4) Free dislocations, i.e. those dislocations not bound in subgrain walls, were rare in recrystallized grains.

The grain boundary "melt" phase, described in detail in Chapter 2 and Appendix 2, was also evident in the wet samples heat-treated at 800°C for 10 hours (Figures 7a) but was not present in similarly treated dry samples (Figures 7b). There was also evidence that the "melt" phase existed in wet samples which were not heat-treated at 800°C prior to shortening. It is possible that the "melt" phase influenced the ease of, or the amount of grain boundary sliding by increasing diffusion rates in the grain boundary plane. However evidence for grain boundary sliding was not detected with the TEM.

The effect of the alumina particles (Figure 3a and b), on deformation was not evident from TEM study. Intragranular particles were not associated with anomalously high dislocation densities, indicating that dislocations could easily climb around these obstacles.

Stress-strain behavior

Stress-strain curves for each of the thirteen experiments are shown in Figures 8 and 9; the most important parameters are summarized in Table 1. Excluding the three experiments in which equipment failures occurred the remaining ten experiments produced several qualitatively consistent trends.

In most of the 'wet' experiments, a steady-state flow stress was reached within 10% strain. The addition of 5% of 1 μm alumina increased the steady-state stress by 10% in samples without prior heat-treatment (CAD-3 vs. CAD-4). The 10 hour heat-treatment at 800°C and 300 MPa confining pressure resulted in an increase in grain size in both the pure and the 5% alumina samples, and a corresponding decrease in strength. None of the wet samples displayed the characteristic oscillating or single peak curves of dynamic recrystallization (reviewed by Sakai and Jonas, 1984). Even in 4002, where homogenous dynamic recrystallization was positively indentified, the oscillatory or single peak behavior was not observed. However, the steady strain-hardening observed in this specimen may be related to dynamic recrystallization.

For the dry specimens, a correlation was seen between alumina content and grain size, and strength. For comparable grain sizes (CAD-8 and CAD-6), 5% alumina increased the strength by up to 25% although the effect of the bimodal grain-size in CAD-6 is not known. The heat-treatment led to a decrease in the flow stress (CAD-9 vs. CAD-7) and to a considerable increase in the grain size. A decrease in strength associated with an increase in grain size was also noted for CAD-6 and CAD-7, neither of which had the prior heat-treatment.

The cause of the oscillating stress levels for CAD-7 at strain rates, $\dot{\epsilon}$, equal to 10^{-3} and 10^{-4} s^{-1} (Figure 9) is not well understood. It is possible that the stress variation at $\dot{\epsilon} = 10^{-3} \text{ s}^{-1}$ was due to temperature, which oscillated nearly in phase with the stress by $\pm 5^\circ\text{C}$ during the three minute period of the experiment. The correlation between temperature and flow stress could not be determined from our study, but analogous studies by Schmid (1976) and Schmid et al. (1977) indicated that a stress variation of 2 to 3 MPa for a temperature fluctuation of $\pm 5^\circ\text{C}$ was reasonable. CAD-4 had a similar temperature fluctuation, however it displayed no cyclic flow stress. At $\dot{\epsilon} = 10^{-4} \text{ s}^{-1}$ CAD-7 also showed the cyclic flow stress behavior with no temperature variation. Therefore it is possible that the temperature fluctuation accounted for the stress fluctuation, but it is unlikely.

In a review of dynamic recrystallization in metals, Sakai and Jonas (1984) observed that cyclic flow behavior signified grain size coarsening. CAD-7 was not heat-treated prior to straining and, therefore, had one of the smallest initial grain-sizes. The grain size after straining was bimodal, (Figure 5b) with the coarser size (17 μm) constituting about 20% of the sample and occurring in bands perpendicular to the maximum stress direction. The other pure, dry specimens (CAD-6 and CAD-9) also had bimodal grain sizes, but did not exhibit oscillating behavior. Most of the dry specimens were deformed at more than one strain rate. Therefore, the relationship between the final microstructure and the stress-strain behavior in the experiments was difficult to interpret both because of the varied lengths of time "at temperature" and

because of overprinting of the microstructures as a result of variations in the strain rate.

Although the presence of water promotes melting along grain boundaries, the effect of water on strength was small. Non-heat-treated wet samples were consistently weaker than the dry ones but by only 5% (Figure 10). In the heat-treated samples, the relationship was complicated by the influence of grain size.

The three stress-strain curves for the marbles containing 5% alumina particles are shown in Figure 11 along with the curve for CAD-2 (pure) for comparison. The final grain sizes of the heat-treated samples were smaller than expected, given the results of Chapter 2, although the grain size after the 10-hour heat-treatment and prior to the straining was not measured. The behavior of the two-phase marbles was consistent with the results of the pure samples, in that water and the heat-treatment caused a decrease in the flow stress. One effect of the alumina particles was to stabilize the grain size, as predicted from the results of Chapter 2, therefore, the grain size was not dependent on the kinetics of grain growth, which have been shown to vary significantly with porosity and with sample preparation (see Chapter 3, Figure 11).

DISCUSSION

The compressive steady-state flow stress increased with second-phase particle content, decreased with water content and decreased with increasing grain size. In Figure 12, stress-strain curves from several of our experiments are compared to those of Schmid (1976) and Schmid et al. (1977) for fine-grained ($\approx 6 \mu\text{m}$) Solenhofen limestone, and Schmid et al. (1980) for coarse grained ($\approx 200 \mu\text{m}$) Carrera marble. The confining pressure in their experiments was 300 MPa instead of 100 MPa, however, the effect of this difference was probably minor, since in all studies the differential stress was less than the confining pressure (Edmond and Paterson, 1972).

Flow stress dependence on alumina particles and water

Additions of 5% of $1.0 \mu\text{m}$ diameter alumina particles increased the flow stress in the wet fine-grained samples by 10% (compare CAD-2 and CAD-3 in Figure 8). The steady-state creep strength of multi-phased composites has been shown to be dependent upon the individual creep strengths and the volume fractions of particles and matrix (Chen and Argon, 1979). The strengthening effect of only 5% of nearly rigid particles (alumina is an order of magnitude stronger than calcite under the conditions of our experiments (Frost and Ashby, 1982)) would primarily be due to the reduction in the effective cross-sectional area of the deforming matrix (Chen and Argon, 1979). The stress-exponents for the single-phase marbles (to be discussed below) indicate that creep was controlled by dislocation glide and climb (for a review, see Takeuchi and

Argon, 1976) and therefore any additional effects of the alumina would have been related to their ability to impede dislocation motion. However, preliminary TEM results showed no evidence of particles pinning dislocations.

The mild weakening effect of water could also be explained by cross-sectional area effect since samples containing water had a few percent higher porosity than those without water (Chapter 3) (pores being a second phase of virtually no strength). One important effect of the water was to promote melting (Chapter 2) particularly in the samples heat-treated at 800°C. If a melt phase did exist, its effect on the strength of the synthetic marbles was minor compared to the effect of particles and grain size.

Flow stress dependence on grain size

The dependence of the steady-state flow stress on grain size is shown in Figure 13. The steady-state flow stress was chosen as the value where the stress was independent of strain (often higher than the value at 10% strain). We assumed that the grain size remained relatively constant during the experiments. This assumption is reasonable for the wet experiments, since they lasted only a few minutes, and for the two-phase dry samples, since the grain size reached a limiting value during the 10-hour heat-treatment, but the grain size of the dry, pure specimens was quite variable in each specimen and it is clear that the size changed during the experiment.

The observed grain-size-dependence of flow stress, shown in Figure 13, is difficult to rationalize. At relatively low temperatures and high strain rates, ductile flow occurs by dislocation glide, and the

grain-size dependence of the yield stress ($\sigma_y \leq \sigma_{SS}$) is governed by the Hall-Petch relation,

$$\sigma_y = \sigma_0 + KD^{-1/2} \quad (4)$$

(σ_0 and K are constants) (Petch, 1953; Hirth and Lothe, 1982). Olsson (1974) has shown that this relation adequately explains yield-stress data for marbles at low temperatures. At higher temperatures and/or lower strain rates, dynamic recovery processes involving dislocation climb becomes important and a steady-state flow stress would eventually be reached which may persist to high strains (e.g. Takeuchi and Argon, 1976). At still higher temperatures or lower strain rates, fine-grained materials may exhibit superplastic behavior where the steady-state flow stress depends inversely on grain size ($\sigma_{SS} = KD^1$ (Edington et al., 1976)). Such behavior has been observed in Solenhofen limestone ($D = 6 \mu\text{m}$) at high temperatures and low strain rates (Schmid et al., 1977), but not in the coarser-grained Yule or Carrera marbles (Heard and Rayleigh, 1972; Schmid et al., 1980).

The inverse dependence of flow stress on grain size for our synthetic marbles is qualitatively similar to a Hall-Petch-type relationship, however, several experimental observations are inconsistent with deformation controlled by glide: 1) In all cases a steady-state flow stress was reached indicating little or no strain-hardening. 2) TEM observations showed considerable evidence for dislocation climb; namely, the presence of subgrain walls and the absence of high concentration, of dislocations associated with grain boundaries, particles or pores. 3) Schmid et al. (1977) observed power-law creep and superplastic behavior under similar conditions in Solenhofen limestone. 4) Olsson

(1974) observed Hall-Petch behavior at much lower temperatures (<300°C) than in our experiments. Superplastic mechanisms were also not realistic because the stress-grain size dependence was the inverse of that expected. The present interpretation based on the microscopic observations and the stress-strain curves shown in Figures 9 and 10 is that dislocation creep was the dominant mechanism of deformation but that the free movement of dislocations was impeded by grain boundaries.

At 700°C and $\dot{\epsilon}$ equal to 10^{-5} s^{-1} , the natural rocks were 35 to 50% stronger than our strongest wet or dry synthetic marbles. The synthetic marbles appeared to deform primarily by dislocation creep at the temperature, confining pressure, strains, and strain rates explored. At $\dot{\epsilon}$ equal to 10^{-5} s^{-1} , Solenhofen limestone appeared to deform by a superplastic mechanism and was considerably weaker than Carrera which deformed by dislocation creep. For our synthetic marbles, the fine-grained samples were always stronger than the coarser-grained ones. At 10% strain, the one pure synthetic marble which was deformed at $\dot{\epsilon}$ equal to 10^{-5} s^{-1} (CAD-6) was weaker than Carrera by almost a factor of 3 but was 25% stronger than Solenhofen. The transition to superplasticity, as recognized in Solenhofen limestone was not observed in our specimens.

Strain accommodation

In order to identify the partitioning of strain between grain boundary process and intracrystalline processes, we measured the grain shapes and compared them to the macroscopic specimen strain (Figure 14). According to Schmid et al. (1977), if it is assumed that the original grains were spherical, the amount of grain flattening (e_g) is defined

as the strain in the direction of shortening:

$$e_g = R^{2/3} - 1 \quad (5)$$

where R is the average aspect ratio of the grains defined as the grain size measured parallel to the maximum shortening direction over that measured in a perpendicular direction ($R = D_{\parallel}/D_{\perp}$). For the macroscopic strain we chose e_T as the true specimen strain. The values used for D_f and e_g/e_T are listed in Table 1. All experiments in which the grain size was measured, including CAD-1 and CAD-11, were plotted. For the three pure, dry samples, e_g/e_T was calculated for each of the two grain sizes listed in Table 1 with e_T equal to the total macroscopic strain. We ignored the possibility of inhomogeneous straining, although it is likely that the coarser-grained regions strained proportionally more.

The data shown in Figure 14 are consistent with strain accommodation by a grain-size sensitive mechanism for both the wet and dry specimens, if it is assumed that no recrystallization occurred. In the wet specimens, most of the strain was due to intracrystalline slip, but for the smallest grain sizes, 50% of the strain may have been accommodated by other mechanisms. Using this interpretation, intracrystalline slip in the dry sample accounted for much less of the total strain than in the wet.

The mechanism of grain-boundary sliding was not consistent with several aspects of our data: 1) In the wet samples, the grain boundary "melt" phase observed in TEM would presumably have weakened grain boundaries and promoted sliding relative to the dry samples. And 2)

where grain-boundary sliding dominated, the flow stress should have decreased with increasing grain size.

The relationship shown in Figure 14 may be due to dynamic recrystallization since recrystallized grains would show less internal deformation than unrecrystallized grains. Homogeneous dynamic recrystallization was optically observed in specimen 4002 and dynamic recrystallization appeared to occur in several of the other samples that were analyzed in TEM (Figure 6). Only one specimen, CAD-7, exhibited the characteristic stress-strain curves of dynamic recrystallization (Sakai and Jonas, 1984); of course, small oscillations below the experimental resolution could have gone unnoticed. According to Roberts and Ahlblom (1978), although the steady-state stress and the final size of dynamically-recrystallized grains are independent of the initial grain size, in specimens with finer grain sizes, the recrystallization kinetics may be accelerated, and the strain required to initiate dynamic recrystallization may be reduced. Therefore, it is possible if not highly probable, that dynamic recrystallization occurred in the pure fine-grained synthetic marbles. Since the recrystallized grain size achieved in 4002 was approximately the same as the grain size in the fine-grained synthetic marbles (5-10 μ m) (Figure 3), dynamic recrystallization may not have been noticed optically.

Comparison to Solenhofen limestone

The data from the multiple strain-rate experiments of this study are shown in Figure 15 along with the data for 700°C from Schmid et al. (1977) and the boundary between Schmid's Regime 2 (power-law creep) and Regime 3 (superplasticity) which was determined at several temperatures.

The strain-rate dependence on flow stress has the form $\epsilon = A\dot{\epsilon}^n$ where A is a constant and n is dependent on the deformation mechanism. The stress exponent, n , was 4 to 5 for our pure data, and 7 for our 5% alumina data. Schmid et al. (1977) found n equal to 4.3 to 5 in Regime 2 and equal to 1.5 to 1.8 in Regime 3 for Solenhofen limestone. For two coarser grained marbles, Carrera (Schmid et al., 1980) and Yule (Heard and Rayleigh, 1972) marbles, n values of 7 to 8 were observed under similar conditions. These values of n are consistent with creep being controlled by dislocation climb (Takeuchi and Argon, 1976). Within the uncertainty in the data, synthetic marbles, both pure and two-phased, agree rather well with Solenhofen limestone deformed in Regime 2. We did not observe the transition to superplasticity in our samples, although three of our experiments were in Schmid's Regime 3. These results indicate that the Solenhofen experiments may not be generally applicable to all marbles, as was discussed by Schmid et al. (1980) for Carrera marble.

The effects of a grain boundary "melt" phase on deformation mechanisms requires further study. Melting along grain boundaries (Figure 7) might have a significant effect on grain-size sensitive deformation mechanisms. As previously discussed, (Chapter 3), a melt phase may have promoted grain growth in wet and dry Solenhofen limestone above 900°C. Therefore, it is also possible that the transition from intracrystalline creep to superplasticity accommodated by grain-boundary sliding observed by Schmid et al. (1977) may have been related to a grain-boundary phase that enhanced sliding. Below 900°C, grain-boundary sliding may still have been enhanced by a "melt" phase, while grain growth was suppressed by second phases such as detrital clay and quartz particles, and pores.

SUMMARY

Although our results were based on only a few experiments, several trends have been established showing the effect of three parameters: second phase particle content, water content, and grain size, on the steady-state flow stress of fine-grained synthetic marbles. At 700°C, 100 MPa confining pressure and strain rates ranging from 10^{-3} to $2 \times 10^{-5} \text{ s}^{-1}$ our results showed that:

- 1) Additions of 5% of 1.0 μm diameter alumina particles increased the flow stress by 10% in wet samples with average grain sizes of 8 μm .
- 2) Wet specimens were a few percent weaker than similarly treated dry ones.
- 3) There was a definite inverse dependence of flow stress on grain size for both wet and dry samples with and without alumina particles. The dependence was weaker than expected for Hall-Petch behavior and indicated that the major mechanism of deformation was power-law creep with dislocation movement being impeded by grain boundaries.
- 4) Grain-strain was found to be grain-size dependent. We offer two explanations: grain boundary sliding and dynamic recrystallization.
- 5) The addition of water also affected the mechanism(s) of strain accommodation. However, we did not observe that the grain-boundary fluid phase promoted grain-boundary sliding.
- 6) Dynamic recovery by dislocations climbing into subgrain walls was prevalent (Figure 6) and dynamic recrystallization may have been partly responsible for the behavior described in 4) and 5) above.

- 7) Our synthetic marbles were significantly weaker than both Carrera marble and Solenhofen limestone deformed in the power-law creep regime.
- 8) Although the critical strain-rate for the transition from power-law creep to superplasticity, recognized by Schmid et al. (1977) in Solenhofen limestone, was crossed in three multiple strain-rate experiments, no change in the stress sensitivity of strain-rate was recognized in the synthetic marbles.

RECOMMENDATIONS FOR FUTURE WORK

Due to the limited number of experiments, only general conclusions are drawn. We can suggest a number of further experiments to help explain differences between synthetic and natural calcite rocks:

- 1) The uncertainties in the stress-strain curves need to be resolved by duplicating some of the experiments already performed.
- 2) The grain size should be measured in each sample before straining in order to determine the extent of dynamic recrystallization and the cause or effect of size heterogeneities.
- 3) Samples with similar grain sizes should be tested with and without the prior 800°C heat-treatment to determine if the heat-treatment effected the flow stress in ways other than by increasing the grain size. This check could be accomplished by using higher concentrations of smaller alumina particles (Chapter 2) which would pin the grain sizes at very small values.

4) The low stress (<10 MPa) regime should be explored to establish under what conditions strain rate becomes grain-size sensitive. An internal load cell which eliminates the uncertainty of O-ring friction would be required for these experiments. Such a cell is currently being tested for the system used in this study.

Such experiments should improve our understanding of the plastic flow behavior of marbles under geologic conditions of significantly lower temperatures and much lower strain rates. We believe that synthetic marbles are the most suitable materials for such experiments because of the range of grain sizes available and the controllable second phases.

BIBLIOGRAPHY

- Boullier, A.M., and Y. Gueguen, SP-mylonites: origin of some mylonites by superplastic flow, Contrib. Mineral. Petrol., 50, 93-104, 1975.
- Caristan, Y.D., High temperature mechanical behavior of Maryland diabase, Ph.D. thesis, Massachusetts Institute of Technology, 155p., December, 1980.
- Chen, I.W., and A.S. Argon, Steady state power-law creep in heterogeneous alloys with coarse microstructures, Acta Met., 27, 785-791, 1979.
- Edington, J.W., K.N. Melton, and C.P. Cutler, Superplasticity, Prog. in Mats. Sci., 21, 61-158, 1976.
- Edmond, J.M., and M.S. Paterson, Volume changes during the deformation of rocks at high pressures, Int. J. Rock Mech. Min. Sci., 9, 161-182, 1972.
- Etheridge, M.A. and R.H. Vernon, A deformed polymeric conglomerate - the influence of grain size and composition on the mechanism and rate of deformation, Tectonophysics, 79, 237-254, 1981.
- Etheridge, M.A., and J.C. Wilkie, Grain size reduction, grain boundary sliding and the flow strength of mylonites, Tectonophysics, 58, 159-178, 1979.
- Exner, H.E. Analysis of grain- and particle-size distributions in metallic materials, Int. Metall. Rev., 17, 25-42, 1972.
- Frost, H.J., and Ashby, M.F., Deformation-Mechanism Maps: The Plasticity and Creep of Metals and Ceramics, Pergamon Press Inc., Oxford, 166p., 1982.
- Heard, H.C., Comparison of the flow properties of rocks at crustal conditions, Phil. Trans. R. Soc. Lond. A., 283, 173-186, 1976.
- Heard, H.C., and C.B. Raleigh, Steady-state flow in marble at 500 to 800°C, Geol. Soc. Am. Bull., 83, 935-956, 1972.
- Hirth, J.P., and J. Lothe, Theory of Dislocations, John Wiley, New York, 857p., 1982.
- Kingery, W.D., H.K. Bowen, and D.R. Uhlmann, Introduction to Ceramics, John Wiley, New York, 1032p., 1976.
- Muller, W.H., S.M. Schmid, and U. Briegel, Deformation experiments on anhydrite rocks of different grain sizes: rheology and microfabric, Tectonophysics, 78, 527-543, 1981.
- Olsson, W.A., Grain size dependence of yield stress in marble, J. Geophys. Res., 79, 4859-4862, 1974.
- Petch, N.J., The cleavage strength of polycrystals, J. Iron Steel Inst., 174, 25-28, 1953.
- Roberts, W., and B. Ahlblom, A nucleation criterion for dynamic recrystallization during hot working, Acta Met., 26, 801-813, 1978.
- Sakai, T., and J.J. Jonas, Dynamic recrystallization: mechanical and microstructural considerations, Acta Met., 32, 189-209, 1984.
- Schmid, S.M., Rheological evidence for changes in the deformation mechanism of Solenhofen limestone towards low stresses, Tectonophysics, 31, T21-T28, 1976.
- Schmid, S.M., J.N. Boland, and M.S. Paterson, Superplastic flow in finegrained limestone, Tectonophysics, 43, 257-291, 1977.

- Schmid, S.M., M.S. Paterson, and J.N. Boland, High temperature flow and dynamic recrystallization in Carrara marble, Tectonophysics, 65, 245-280, 1980.
- Takeuchi, S., and A.S. Argon, Review: Steady-state creep of single-phase crystalline matter at high temperature, J. Mater. Sci., 11, 1542-1566, 1976.
- Tullis, J., and Yund, R.A., Dynamic recrystallization of feldspar: A mechanism for ductile shear zone formation, Geology, 13, 238-241, 1985.
- Twiss, R.J., Structural superplastic creep and linear viscosity in the earth's mantle, Earth Planet. Sci. Lett., 33, 86-100, 1976.
- Underwood, E.E., Quantitative Stereology, Addison-Wesley, Reading, Mass., 274p., 1970.
- Zeuch, D.H., Ductile faulting, dynamic recrystallization and grain-size-sensitive flow of olivine, Tectonophysics, 83, 293-308, 1982.

TABLE 1. Results of mechanical experiments

Experiment #	Comp.+/ Prep.#	$\dot{\epsilon}$ (s^{-1})	$\sigma_{10\%}$ and σ_{ss} (MPa)	e_T	\bar{D}_i^* (μm)	D_f (μm)	$D_{ }$ (μm)	D_{\perp} (μm)	e_g/e_T	Comments
<u>Wet</u>										
4001	P A	1.8×10^{-4}	40.7 (41)	.225	11.9-14.4 ^a	19.1	16.0	22.1	.86	
4002	P B	2.1×10^{-3}	65.5	.508	11.7, 39.6 ^a	19.1	13.6	24.6	.85	
CAD-1	P C	1.1×10^{-3}	68.5 (58)	.22	10.0 ^b	7.1	6.6	7.7	.47	fractured prior to heat up; $\sigma_{10\%}$ is peak value.
CAD-2	P C	1.2×10^{-3}	76.8 (78)	.334	10.0 ^b	7.6	6.7	8.5	.43	
CAD-3	5/5 C	1.3×10^{-3}	79.5 (88)	.353	7.7 ^b	8.2	6.9	9.6	.56	
CAD-4	5/5 CD	1.3×10^{-3}	69 (73)	.323	20.0 ^b	12.3	10.5	14.1	.55	
CAD-5	P CD	1.2×10^{-3}	54.5 (60)	.373	49.6 ^b	28.2	21.0	35.4	.79	
CAD-11	P C	1.0×10^{-3}	51±4	.13	10.0 ^b	12.8	12.0	13.7	.64	mechanical malfunction
<u>Dry</u>										
CAD-6	P C	1.1×10^{-3}	57 (57.5)	.163	24.1 ^a	22.4	20.0	24.8	.249 ^δ	bimodal grain size smaller size is dominant
		1.2×10^{-4}	(35)	.134		11.8	11.0	12.6	.161 ^δ	
		2.8×10^{-5}	(25)	.169						
		1.5×10^{-3}	(47)	.071						
CAD-7	P C	1.0×10^{-3}	85 (83±2)	.222	5.7-8.2 ^c	17.0	16.1	18.2	.20 ^δ	oscillating stress-strain; bimodal grain size
		1.2×10^{-4}	45 (48±2)	.162		8.7	8.4	9.0	.12 ^δ	
CAD-8	5/5 CD	0.93×10^{-3}	76.5 (78)	.172	12.8-13.7 ^c	12.3	10.4	14.1	.49	high strain rate estimated
		1.0×10^{-4}	(58)	.118						
		2.6×10^{-5}	(45)	.085						
CAD-9	P CD	0.93×10^{-3}	50.5 (51)	.239	44.2-47.1 ^c	117.	86.7	147.	.91 ^δ	bimodal grain size
		2.0×10^{-2}	(~80)	.089		48.4	37.5	59.4	.70 ^δ	
CAD-10	P C	1.2×10^{-3}	68.5 (73)	.425	-	<5	-	-	-	jacket rupture; grain size too small to measure

$\dot{\epsilon}$ - strain rate, $\sigma_{10\%}$ and σ_{ss} - flow stress at 10% strain and steady-state, respectively, e_T - true strain, D_i - initial grain size, D_f - final grain size, $D_{||}$ and D_{\perp} - grain size measured parallel to and perpendicular to the direction of maximum shortening, respectively and e_g - amount of grain flattening.

† Composition: P - pure CaCO₃; 5/5 - 5% of '5.0' alumina polishing grit with $d \sim 1.0 \mu m$ (see Chapter 2).

‡ Preparation procedure (temperature, confining pressure, time): A - 750°C, 300 MPa, 2 hours; B - 800°C, 300 MPa, 2 hours; C - 500°C, 500 MPa, 1 hour; D - 800°C, 300 MPa, 10 hours.

* Initial grain size inferred from: a - measurement of sizes at sample ends, b - the grain growth experiments of Chapter 2, and c - a separate static grain growth experiment at 700°C, 100 MPa, 15 minutes.

δ e_g/e_T calculated for each grain size using the total specimen strain.

FIGURE CAPTIONS: CHAPTER 4

- FIGURE 1. Experimental assembly inside pressure vessel used for the deformation experiments (reprinted from Caristan, 1980). The load and the displacement were measured externally. The pore pressure was added through the thermocouple hole. The schematic is approximately 1/2 true scale.
- FIGURE 2. Optical micrographs of synthetic marbles following deformation: a) wet, fine-grained; b) dry, fine-grained; c) wet, coarse-grained; d) dry, coarse-grained. The grain morphologies between wet and dry are similar, and the grain elongation is greater in the coarse grains. The maximum shortening direction was horizontal.
- FIGURE 3. Optical micrographs of samples containing 5% alumina particles heat-treated at 800°C and 300 MPa for 10 hours: a) wet and b) dry. Grain elongation and dynamic recrystallization in sample 4002: c) in the middle of the sample and d) near the region of highest strain where the sample extruded around a corner of the alumina spacer.
- FIGURE 4. Optical micrographs of three dry samples which show bimodal grain sizes. Examples of the fine (left) and the coarse (right) grained regions are shown. a) Coarse grains were isolated in pods in a matrix of fine grains. b) Coarse grains occurred in bands perpendicular to the maximum shortening direction. c) Coarse grains also occurred as bands perpendicular to the maximum shortening direction. The intracrystalline strain in c is significantly larger than in the others.
- FIGURE 5. TEM micrographs of dislocations and boundary structures in samples following deformation: a) wet, fine-grained; b) dry, fine-grained; c) wet, coarse-grained; and d) dry, coarse-grained. The dislocation densities are higher in the coarse-grained samples even though the flow stresses were higher in the fine-grained ones.
- FIGURE 6. TEM micrographs showing the sequential development of dynamic recrystallization: a) low-angle boundaries at grain corners and edges; b) low-angle boundary viewed edge-on; c) small grains which have formed at the corner of a large grain; and d-f) higher magnification of the region in the lower left of c. Grain-boundary cavities or pores, and a "semi-coherent" boundary are shown in d.
- FIGURE 7. Bright-field (left) and dark-field (right) TEM micrographs: a) wet sample showing melt-phase along grain boundaries and in pores; and b) dry sample with no melt phase.

- FIGURE 8. Stress vs. strain curves for wet synthetic marbles (see Table 1 for the conditions of each experiment). All strain rates are approximately 10^{-3} s^{-1} unless otherwise indicated. Error bars are explained in text.
- FIGURE 9. Stress vs. strain curves for dry synthetic marbles. For the multiple strain-rate experiments, the stress was dropped to near zero between each stage (see Table 1 for the conditions of each experiment). Approximate strain rates (s^{-1}) are indicated. Error bars are explained in the text.
- FIGURE 10. Stress vs. strain curves comparing wet and dry, fine-grained synthetic marbles. The flow stress decreased with water for similar grain sizes for both pure calcite (solid lines) and for samples containing 5% alumina (dashed lines). Error bars are given in Figures 8 and 9.
- FIGURE 11. Stress vs. strain curves for samples containing 5% alumina particles and one pure sample (dot-dashed line) at strain rates equal to 10^{-3} s^{-1} (see Table 1 for the conditions of each experiment). The flow stress decreased with water and with increasing grain size. Error bars are given in Figures 8 and 9.
- FIGURE 12. Stress vs. strain curves comparing the synthetic marbles to Solenhofen limestone and Carrera marble from Schmid *et al.* (1977) and Schmid *et al.* (1980), respectively. Approximate strain rates (s^{-1}) are as indicated. Error bars are given in Figures 8 and 9.
- FIGURE 13. Steady-state flow stress, σ_{SS} , vs. grain size, D , for synthetic marbles at strain rates equal to approximately 10^{-3} . Dashed, horizontal tie-lines are for samples with bimodal grain sizes. The value of the grain size exponent, n , in a Hall-Petch-type equation (see text) is given for each line. A line whose slope agrees with Hall-Petch-type behavior is shown. The uncertainties contained in the error bars are explained in text.
- FIGURE 14. Grain size, D , vs. relative shortening, e_g/e_T , for dry and wet synthetic marbles.
- FIGURE 15. Steady-state flow stress, σ_{SS} , vs. strain rate, ϵ , for synthetic marbles and Solenhofen limestone deformed under similar conditions by Schmid *et al.* (1977). Also included is the line for the transition from Regime 2 (power-law creep) to Regime 3 (superplasticity) for Solenhofen limestone. The uncertainties contained in the error bars for σ_{SS} are given in the text. The uncertainty in ϵ is estimated to be $\pm 15\%$.

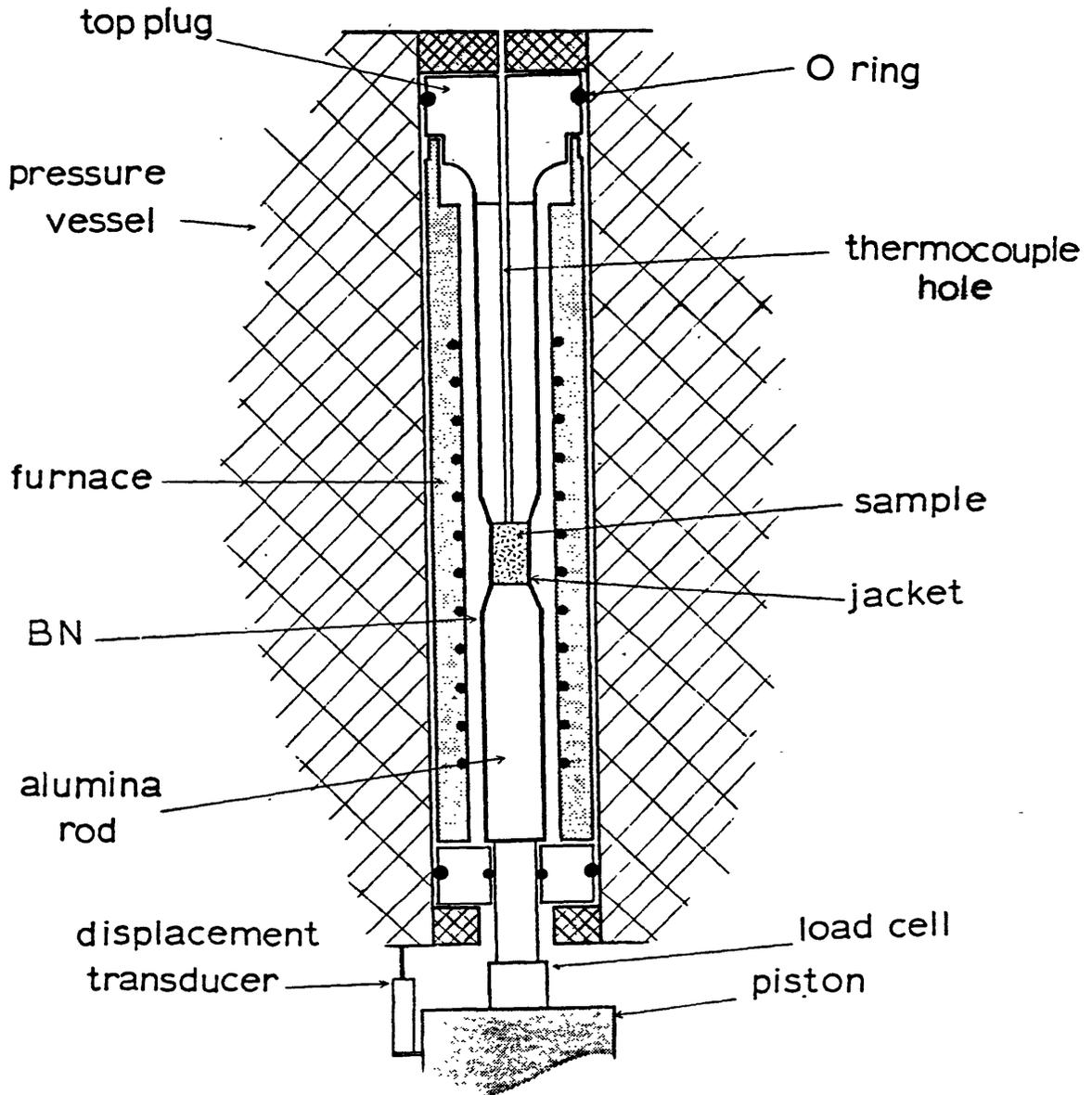


Figure 1

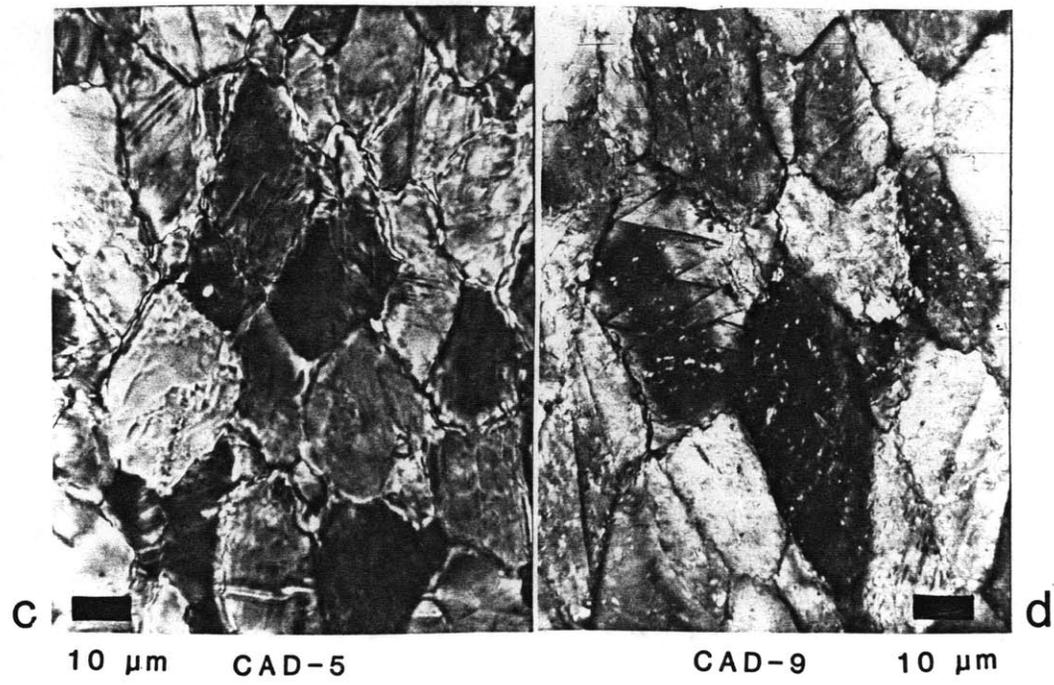
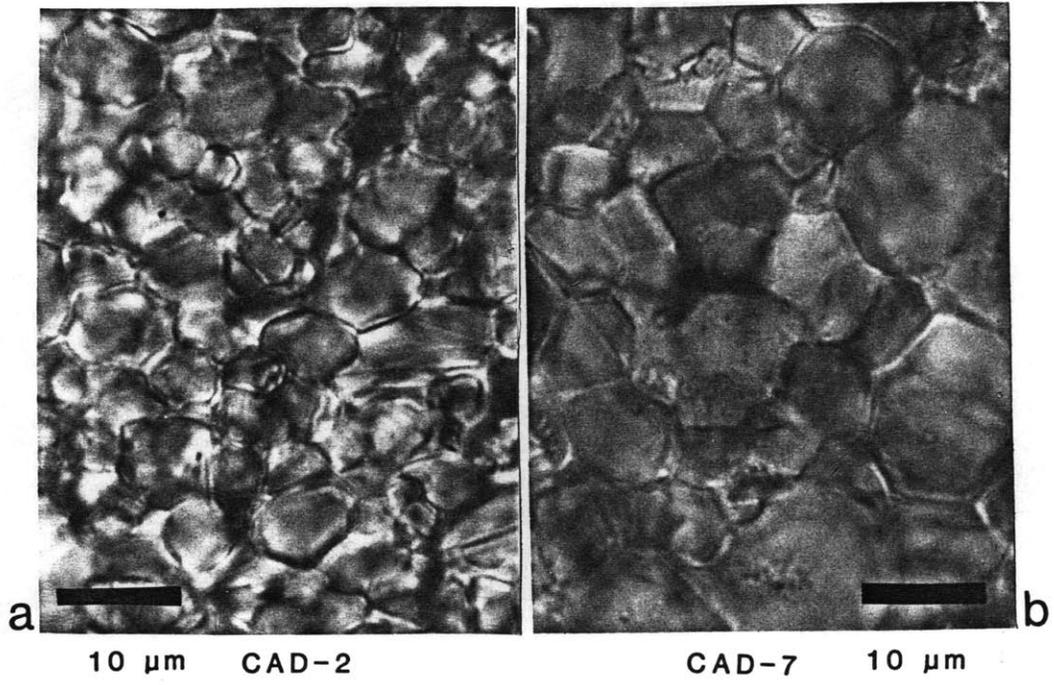


Figure 2

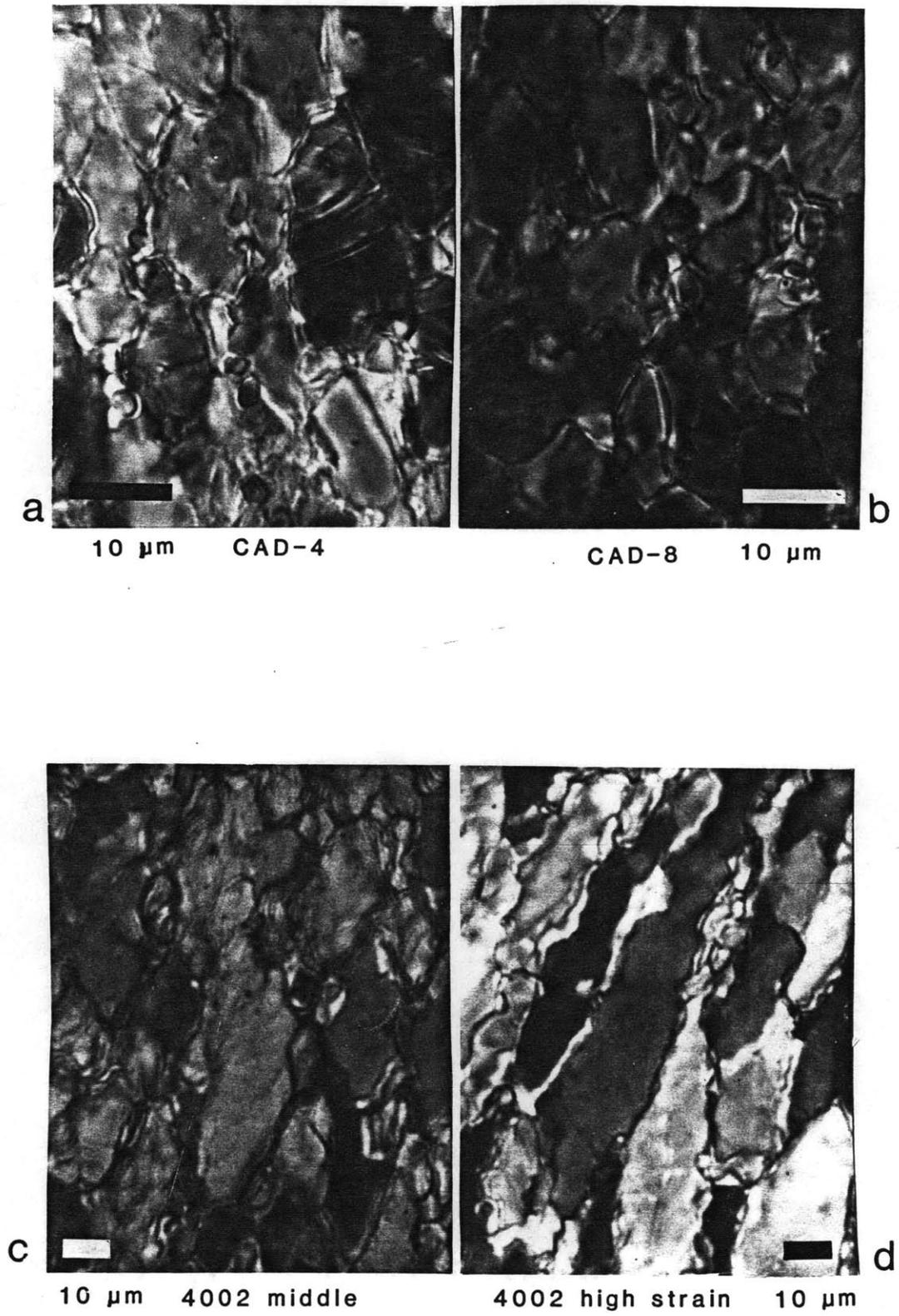


Figure 3

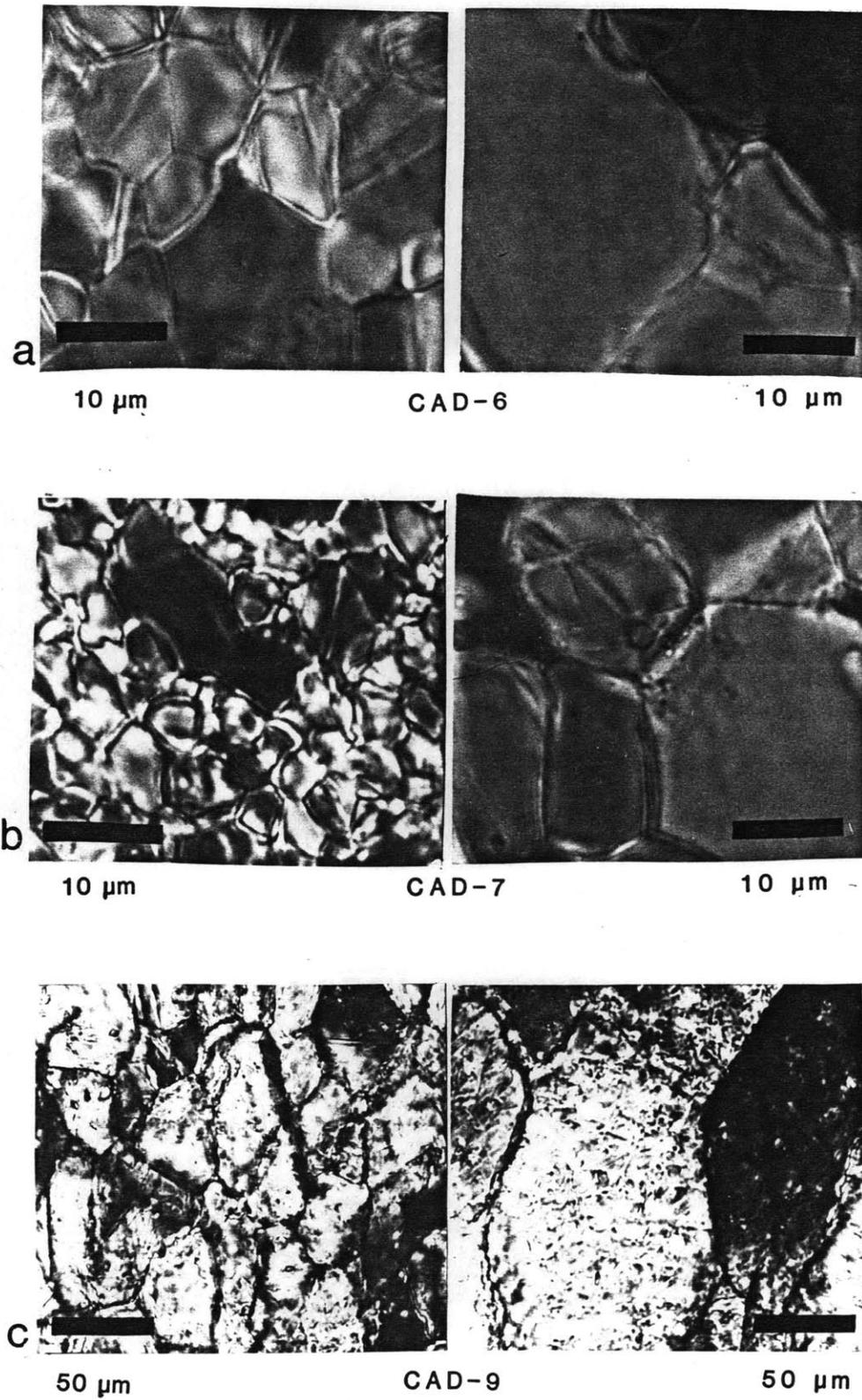


Figure 4

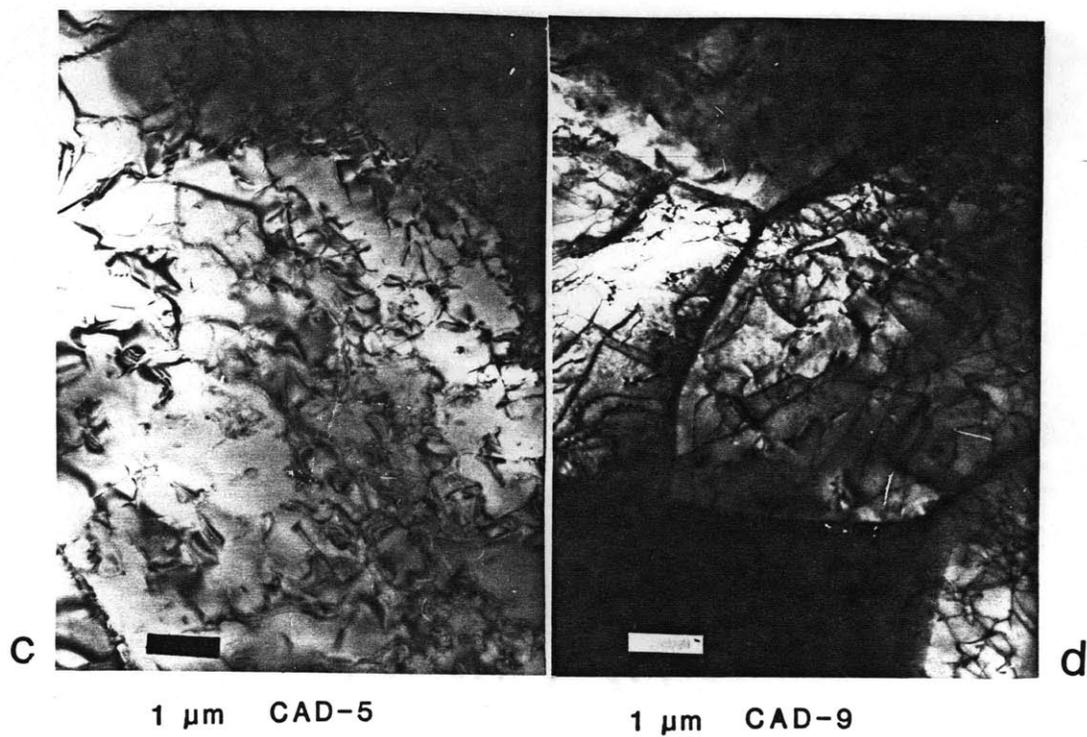
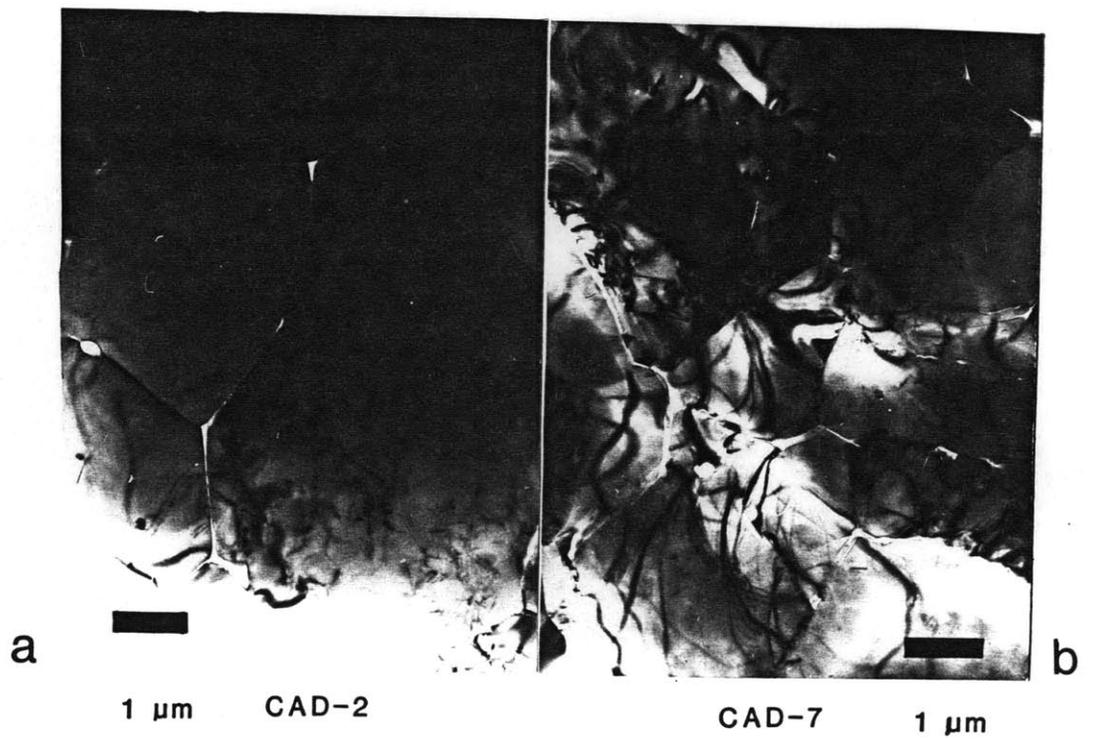


Figure 5

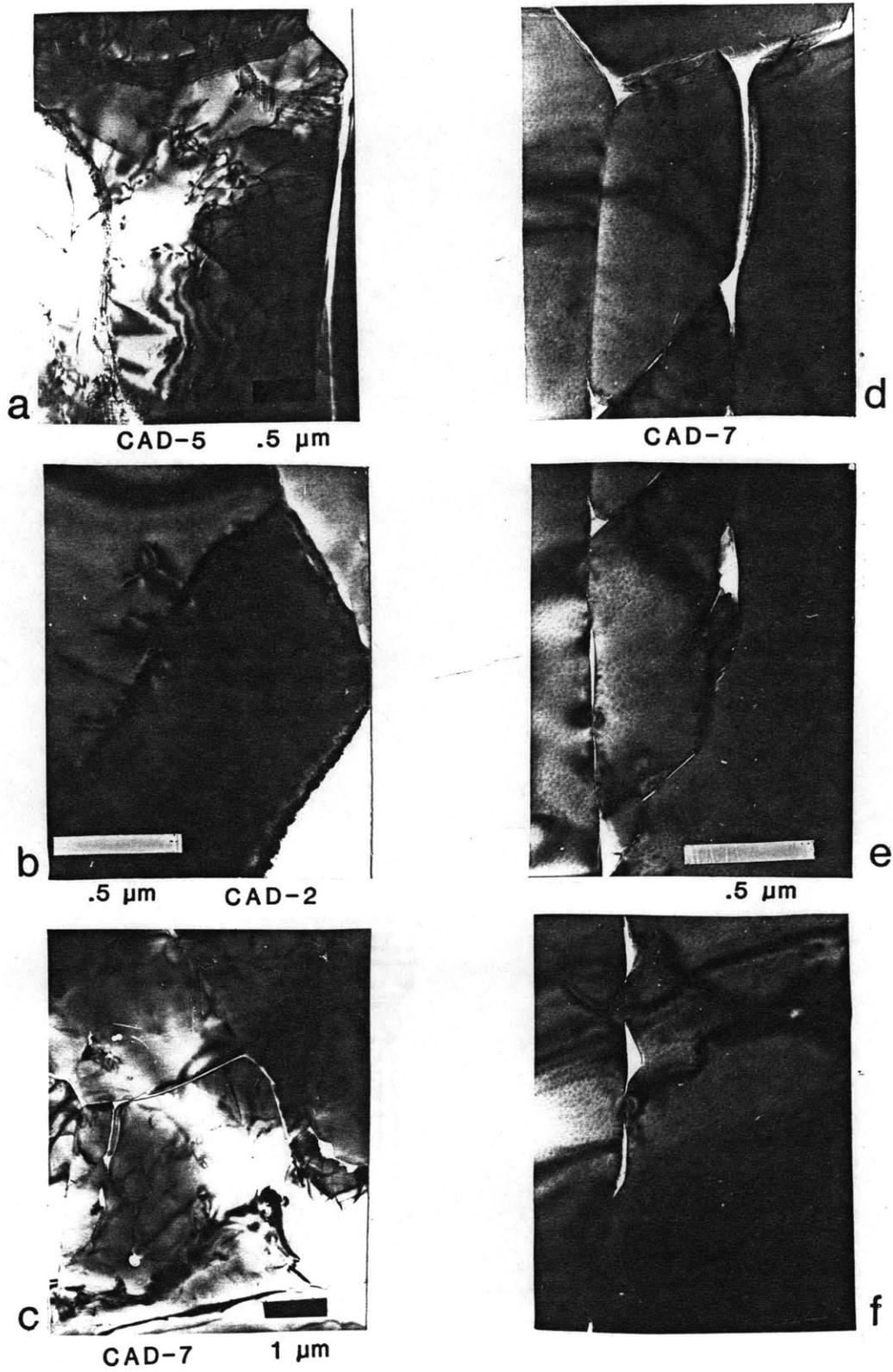
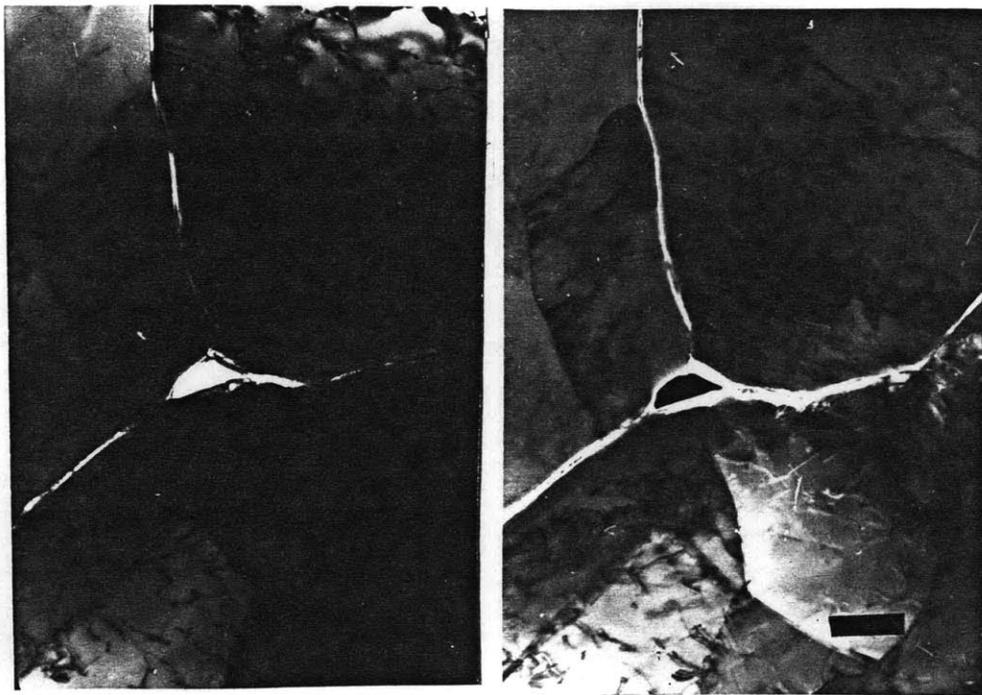


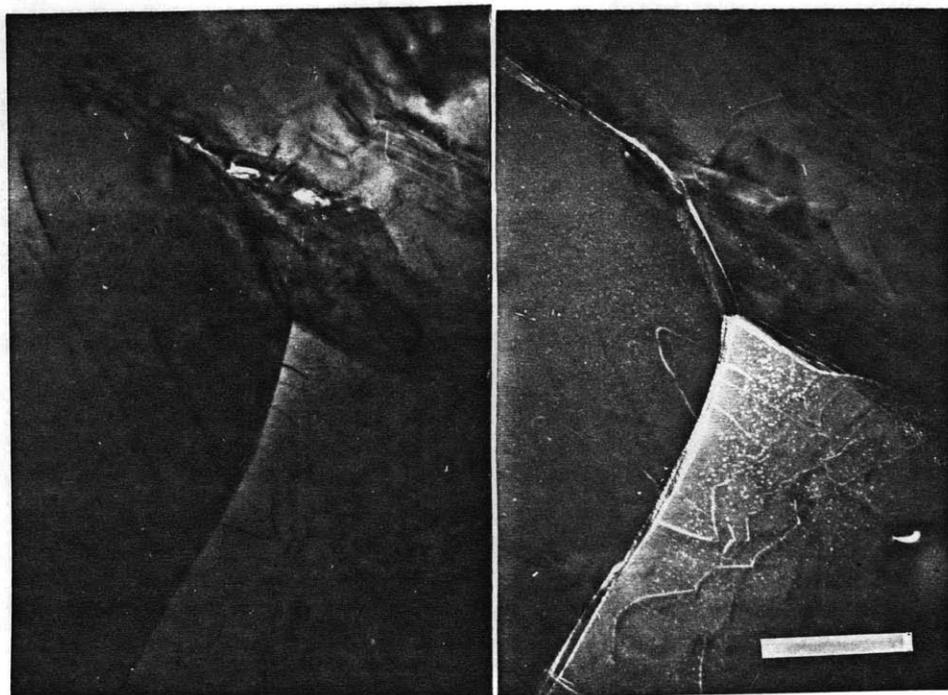
Figure 6



a

CAD-5

1 μ m



b

CAD-9

.5 μ m

Figure 7

Figure 8

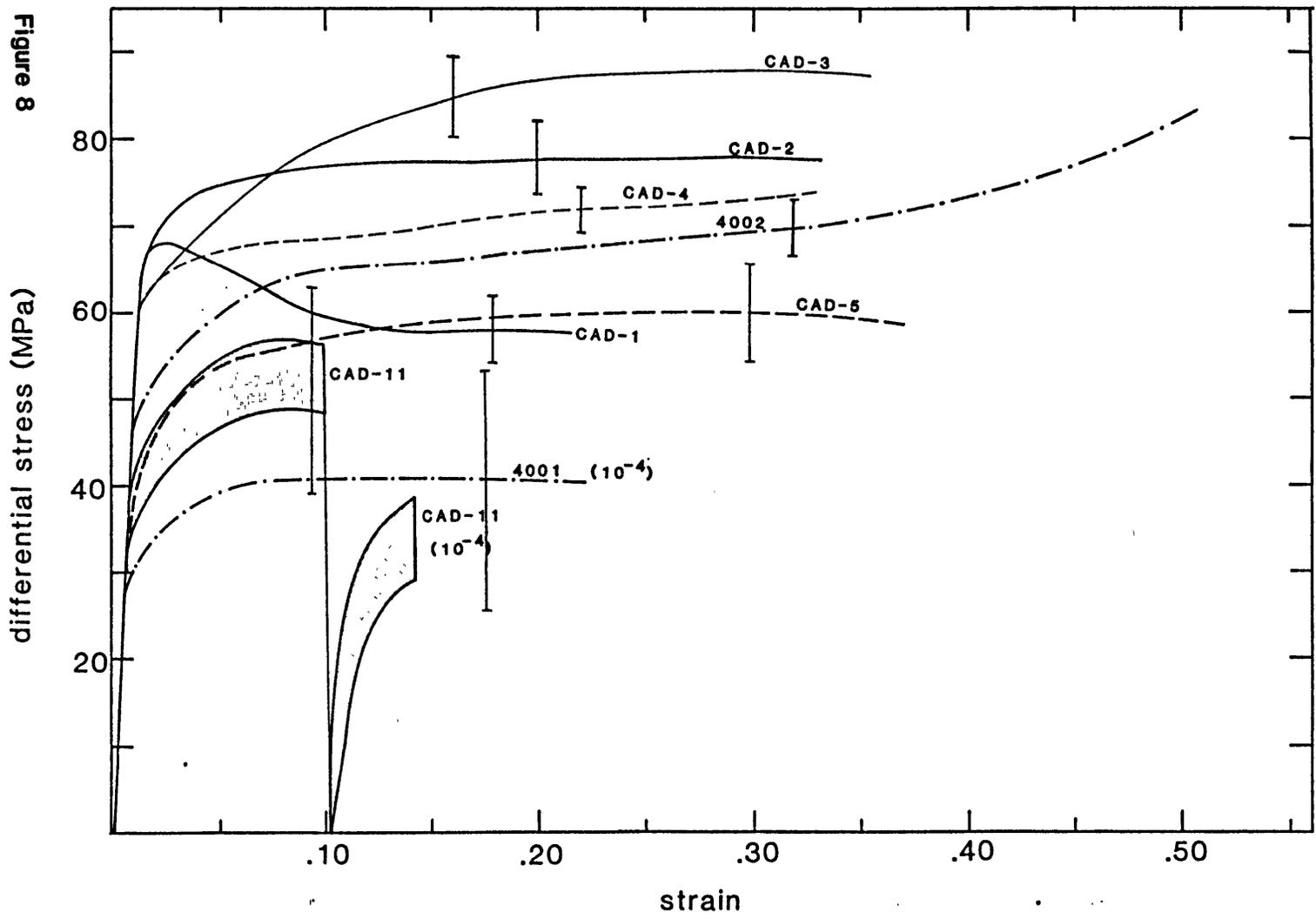


Figure 9

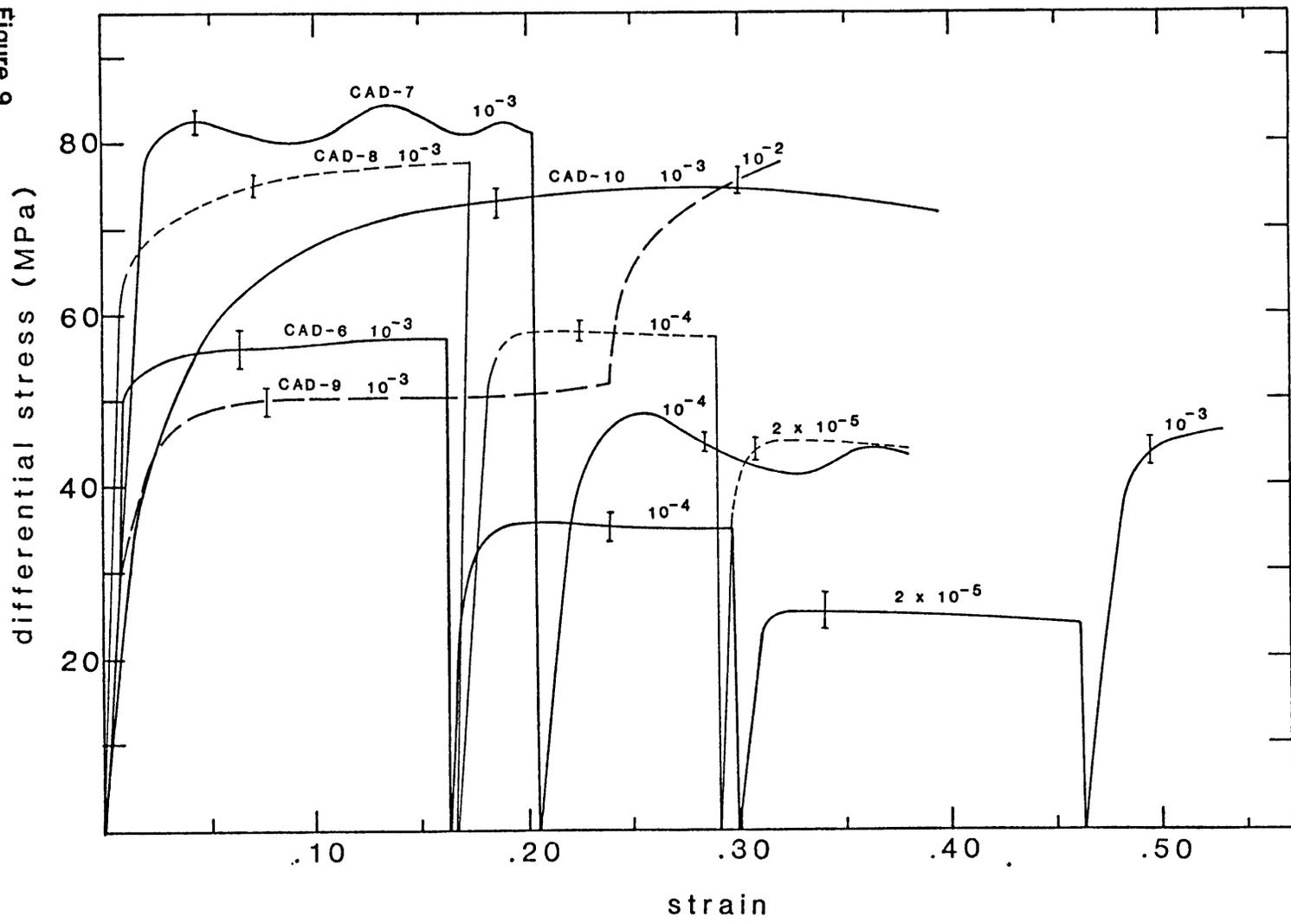


Figure 10

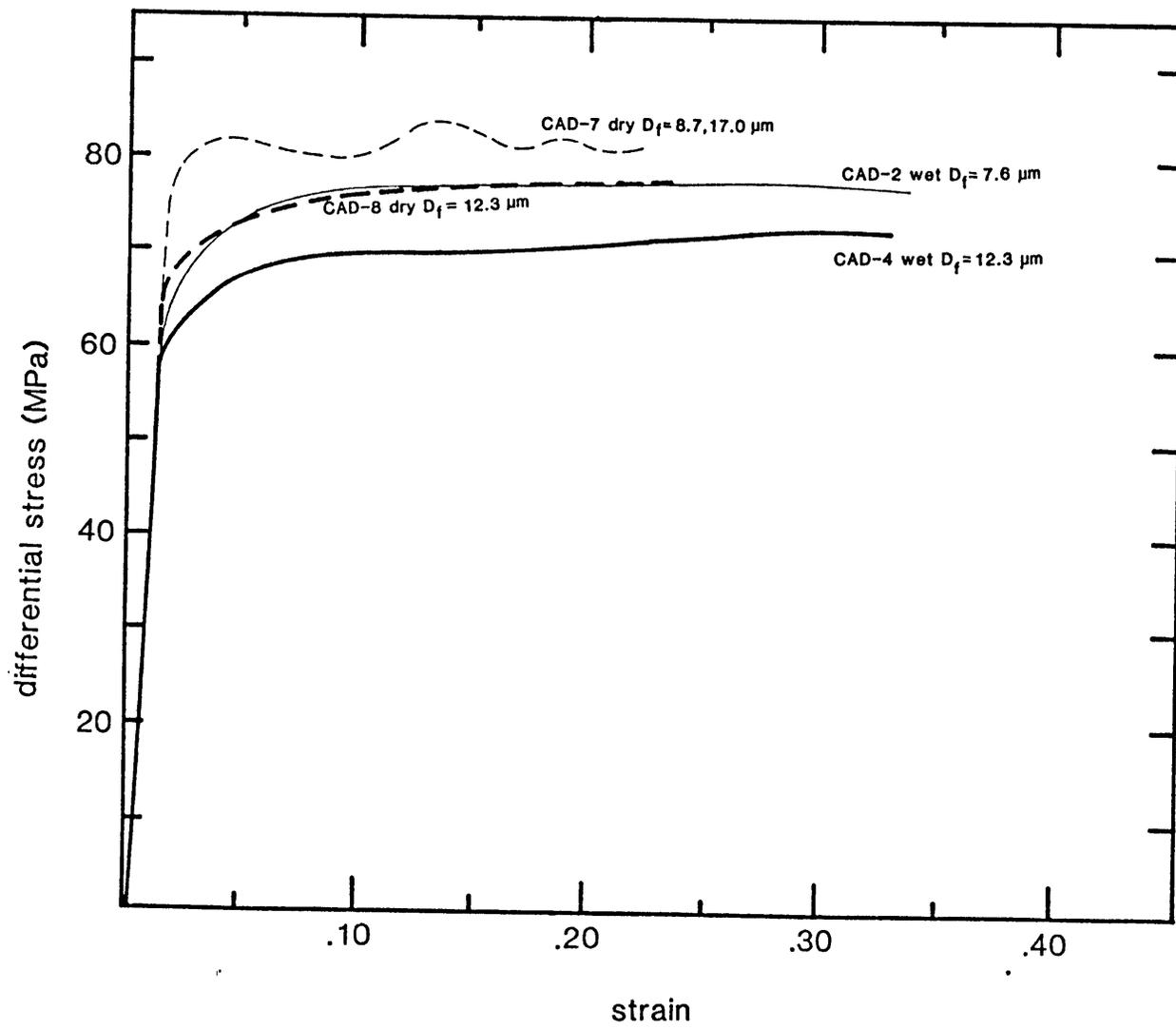
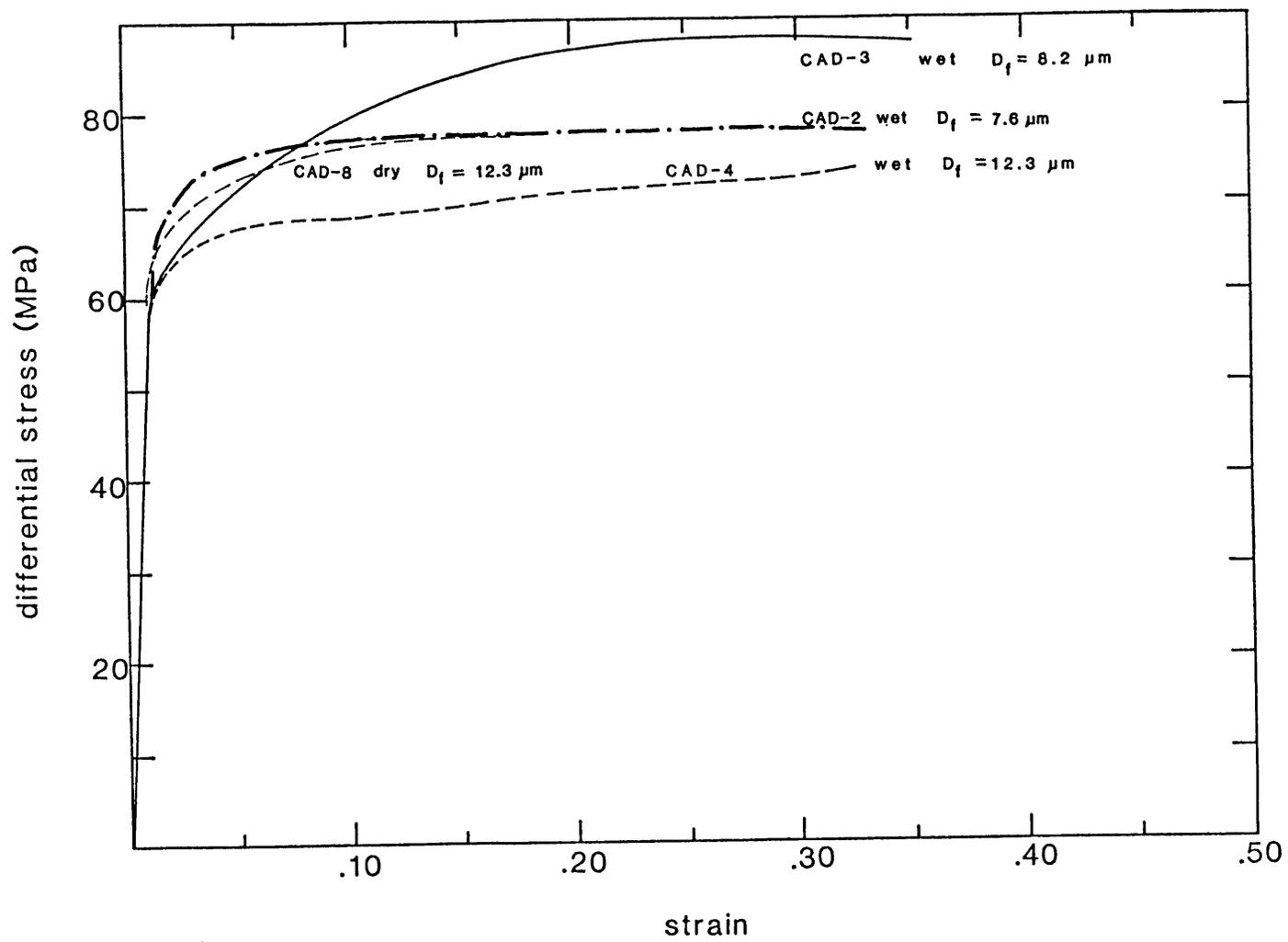


Figure 11



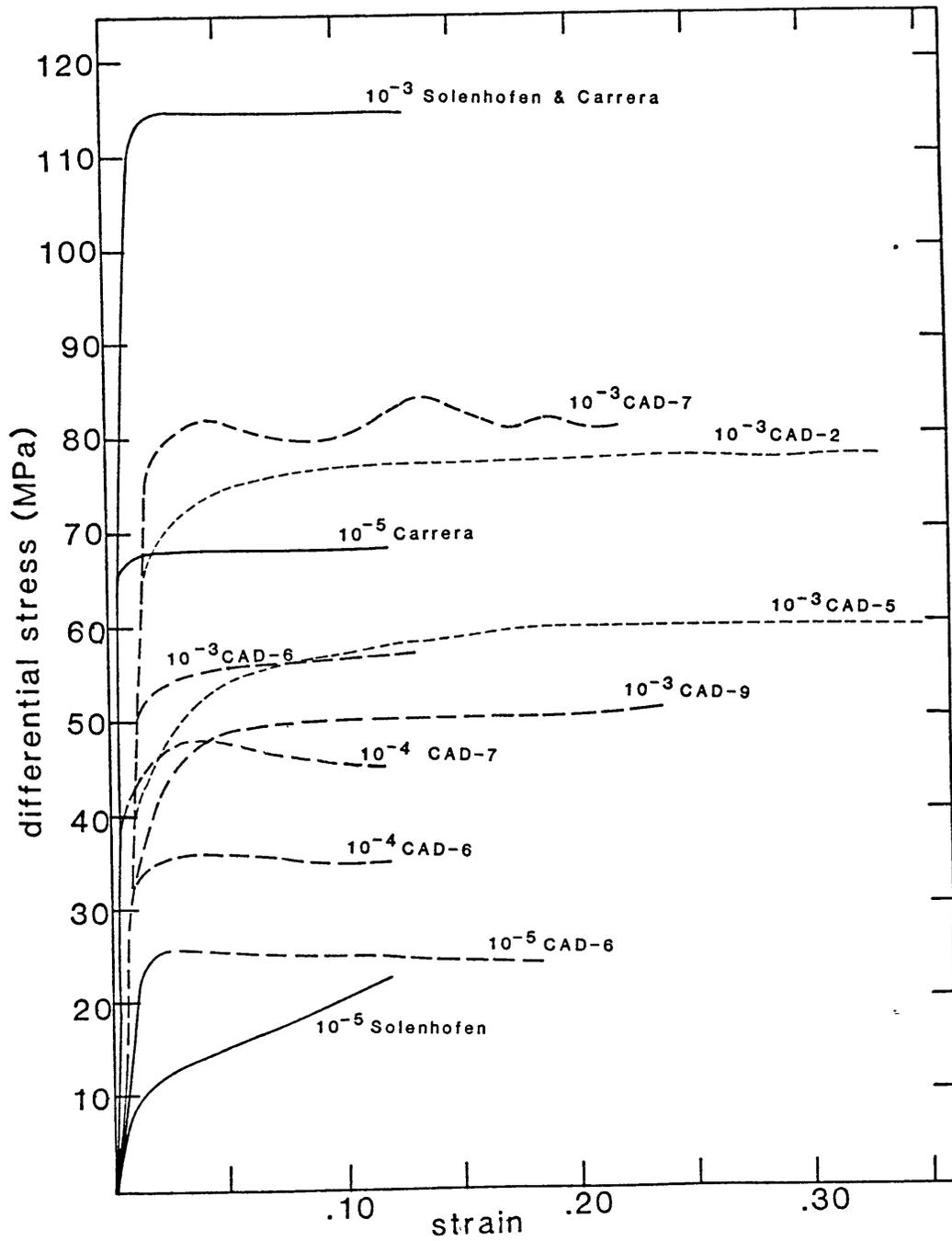
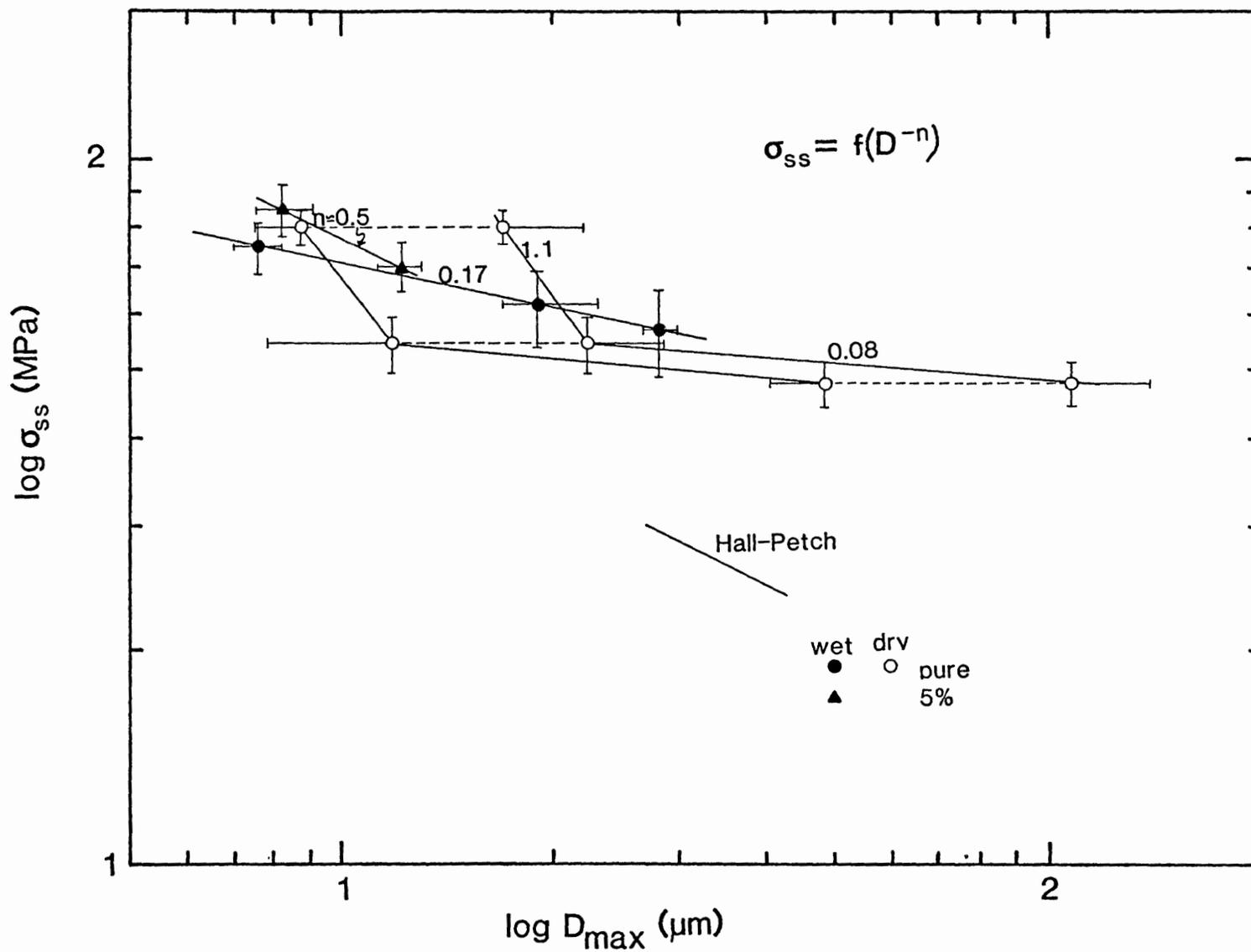


Figure 12

Figure 13



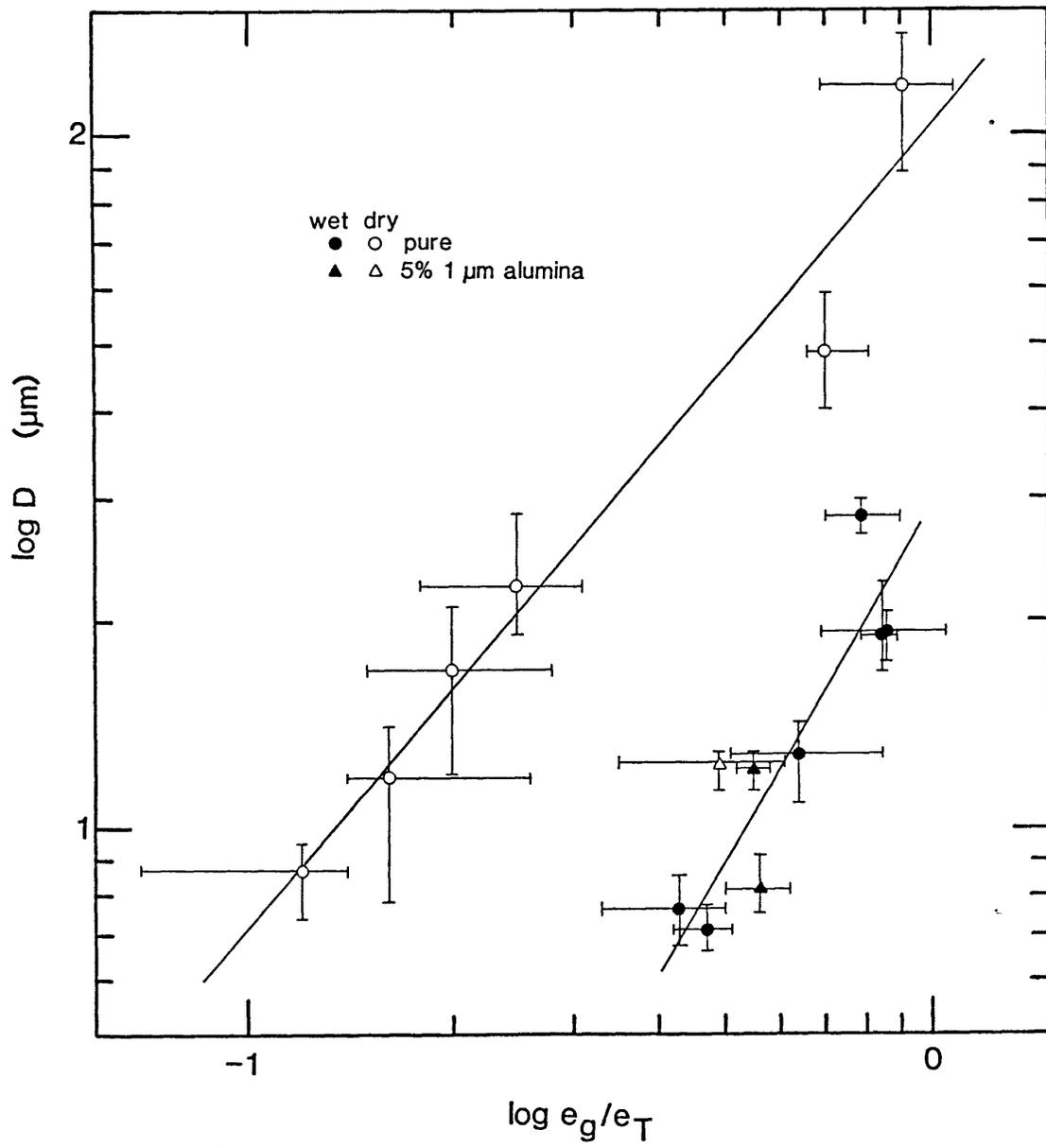
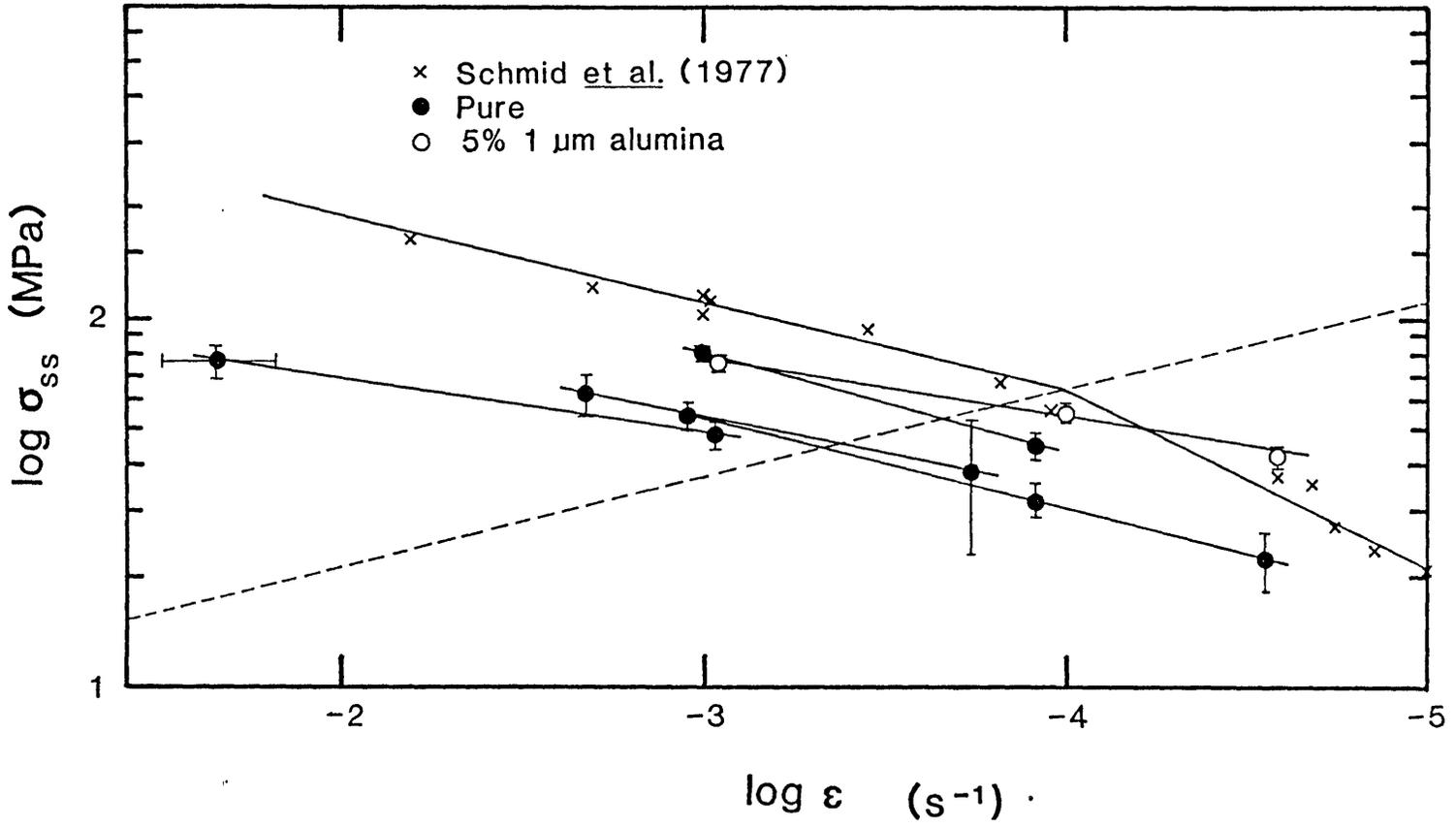


Figure 14

Figure 15



APPENDIX 1

THE DEPENDENCE OF D_{\max} ON d AND f

WHEN ALL GRAINS LIE ON GRAIN CORNERS

Grain boundaries can be pinned by particles at the center of the grain boundary, along grain edges, or at four-grain corners. If particles (or pores) are able to migrate with moving boundaries, the second-phase concentration at four-grain corners will increase with increasing grain size. Therefore, the limiting grain size, D_{\max} , will eventually be dependent on the pinning ability of second phases at corners.

Based purely on geometric considerations, the dependence of D_{\max} on d and f is derived for the case where all particles lie on grain corners. Similar geometric derivations have been made by Anand and Gurland (1975) and Haroun and Budworth (1968) for the case where particles lie on grain edges, and by Hellman and Hillert (1975) for the case where particles lie on grain corners. As with the other studies, it is assumed that the pinning force of a particle is large enough to prevent a boundary from breaking away.

The following derivation was provided by Brian Evans (personal communication). Assuming that the angles at grain corners are fixed by interfacial equilibrium and that the grain shape remains constant, the minimum number of second phase particles required to pin every boundary is one at every other grain corner. If all grains in a material had the same size and were homogeneously packed, they would be shaped like tetrakaidecahedra (Figure 1) and the number of corners would be six times

the number of grains. Therefore the number of particles required to stabilize the grain size would be three. The necessary volume fraction, f , of spherical second-phase particles of radius r is then given by:

$$f = (3) \frac{4/3\pi r^3}{11.314 a^3}$$

where a is the edge length of a tetrakaidecahedron. The mean intercept length is:

$$1.69a = L \quad (\text{Underwood, 1970})$$

Therefore:

$$L = 1.75 r/f^{1/3}$$

The diameter of a tetrakaidecahedra, defined as the distance between two parallel hexagonal faces (Figure 1), is:

$$D_{\max} = 1.44L \quad (\text{Underwood, 1970})$$

Therefore:

$$D_{\max} = 2.52 r/f^{1/3}$$

This equation is given in Chapter 2, Table 1 as Equation 11. The most important relation is the inverse cubic dependence of D_{\max} on f when particles are restricted to grain corners.

FIGURE CAPTIONS: APPENDIX 1

FIGURE 1. Tetrakaidekahedron. A regular space filling shape which approximates those of a grain in a polycrystalline material, $R_0 = 1/2\sqrt{6}(l)$ (reprinted from Gladman, 1966).

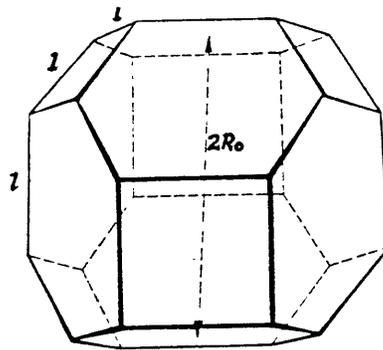


Figure 1

APPENDIX 2

CALCULATION OF THE NUMBER DISTRIBUTION CURVES FOR GRAIN SIZE FROM
X-RAY SEDIMENTATION DATA

X-ray sedimentation, a technique for measuring small-particles, has been briefly described in Chapter 1. This technique has been used to characterize all of the powders used in the experiments of this thesis. In Chapter 1, this technique was used to estimate the surface area of fault gouge. In Chapters 2 and 3, it was used to estimate the average diameter of the calcite, alumina, and phlogopite particles used to make the synthetic marbles. It is a technique which avoids the tedium of microscopy analyses and eliminates errors due to surface topography. However, it is sensitive to particle shape and particle clustering, and is limited to particles in the size-range of $1.0 \mu\text{m} < d < 100 \mu\text{m}$ (Chapter 1). For the two finest alumina sizes in our study ('0.1' and '1.0' see Chapter 2) the lower end of the size range has been extended to $0.1 \mu\text{m}$.

The particles were ultrasonically dispersed in air and then classified. The uncorrected data are shown in Figures 1 and 2 for the fault gouge and for the CaCO_3 , Al_2O_3 and phlogopite particles, respectively. Distributions of fine particles are most commonly governed by the log-normal law (Herdan, 1960). Therefore all of the uncorrected data have been plotted on log-probability graphs (Figure 3; Chapter 1, Figure 6; and Chapter 2, Figure 1). A straight-line fit on such a plot indicates a perfect log-normal distribution. With the exception of the '5.0' and the CaCO_3 (Chapter 2, Figure 1), a straight line was a reasonable approximation. Even the '0.1' and '1.0' data below $1.0 \mu\text{m}$

were reasonably represented by a log-normal distribution providing evidence to support the extension of the lower bound on the particle size. The shape of the '5.0' curve is indicative of a bimodal distribution. The shape of the CaCO_3 curve indicates a skewed distribution.

For the purposes of the surface area calculations of Chapter 1, the data required no further manipulation. In order to determine the particle diameters presented in Chapters 2 and 3, the "mass percent" data needed to be converted to "number percent". A distribution diagram (Figure 4) was plotted for values determined directly from Figure 2 for the CaCO_3 and the Al_2O_3 data. Since the number-averaged diameter is inversely proportional to the cube of the mass-averaged diameter, the small mass fractions of the smallest particles constitute the majority of the number fraction (compare Figures 2 and 4). Therefore, slight errors in choosing the concentration of the smallest particles will lead to large errors in the number-averaged particle diameter. A simpler, more direct conversion can be made if it is assumed that the data is best fit by a log-normal distribution. Following Herdan (1960, pg. 94-96) if the mass percent is log-normally distributed, then the number percent is also log-normal with the same standard deviation, $\log \sigma_g$, but around different means. If the weight distribution is known, then the number distribution follows from:

$$\log X_g = \log X'_g - 6.908 \log^2 \sigma_g$$

where X_g is particle size at the number fraction, g , X'_g is the particle size at the equal mass fraction, and $\log \sigma_g$ is the standard

deviation given by:

$$\log \sigma_g = \log X_{50} - \log X_{16}$$

where X_{50} and X_{16} are the particle sizes at 50% and 16% mass (or number) fraction, respectively. In Figure 3 and Chapter 2, Figure 1, the number distributions have been plotted with the mass distributions. The slopes of the lines are the same (since $\log \sigma_g = \log \sigma_g'$) and the curves with large $\log \sigma_g$ (flatter slopes) have larger differences between the mass-averaged particle size and the number-averaged particle size.

Reasonable agreement was found between the X-ray sedimentation diameters calculated using this method and the diameters calculated from the BET method for the CaCO_3 and Al_2O_3 particles (Chapter 2, Table 2). The bimodal grain size of the '5.0' and the skewed distribution of the CaCO_3 powders have no effect on the number-averaged diameter. The agreement between the X-ray sedimentation and the other measurement methods for the phlogopite particles, however, is very poor (Chapter 3, Table 2); the sedimentation diameter is unreasonably small. The reason for this small diameter is probably related to the flakiness of the phlogopite particles (Figure 6) which would not follow Stoke's law of particle setting. The relation between particle shape and the applicability of the X-ray sedimentation method is discussed in Chapter 1.

To determine the ability of a dispersion of particles to inhibit grain-boundary migration, the shape of the size distribution as well as the average particle-size should be accounted for. A summation method proposed by Flowers (1979) has been used.

The "effective" size of a distribution is:

$$d_F = \frac{\sum_i (Y_i d_i^3)}{\sum_i (Y_i d_i^2)}$$

where Y_i is the fraction of the total particles with diameter d_i ,
and d_F is defined as the "Flowers" diameters.

FIGURE CAPTIONS: APPENDIX 2

- FIGURE 1. Uncorrected X-ray sedimentation data for fresh (F) and old (O) fault gouge.
- FIGURE 2. Uncorrected X-ray sedimentation data for calcite, alumina, and phlogopite powders. Numbers indicate alumina grit sizes.
- FIGURE 3. X-ray sedimentation results for phlogopite and calcite plotted on log-probability graph. The data were collected as mass percent, M, and converted to number percent (#).
- FIGURE 4. Particle size (number) histogram for the alumina and calcite powders. The small mass fractions of the smallest particles constitute an overwhelming majority of the number fraction.
- FIGURE 5. TEM micrograph of a phlogopite particle. Particles are made up of very thin plates which do not obey Stoke's law of particle settling.

Figure 1

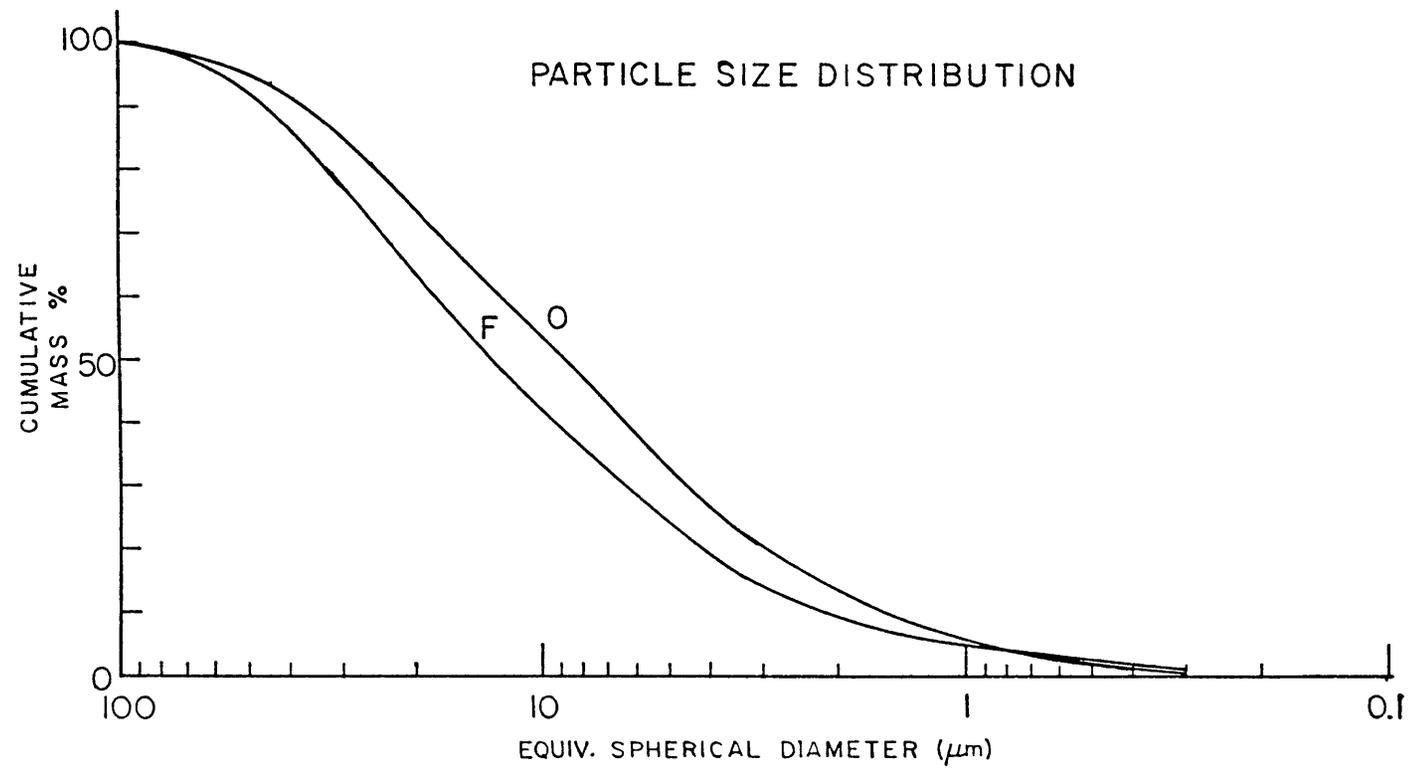


Figure 2

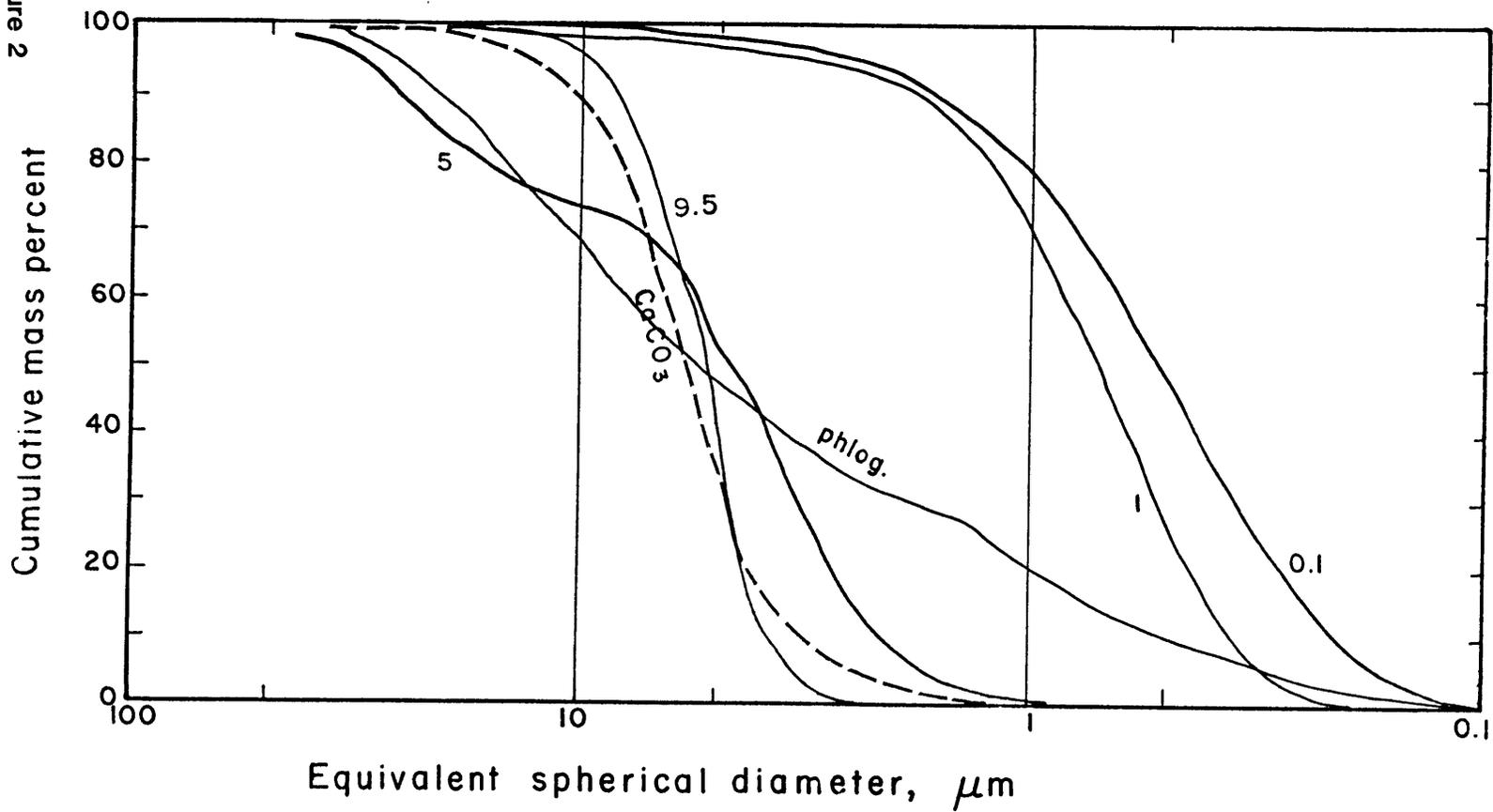


Figure 3

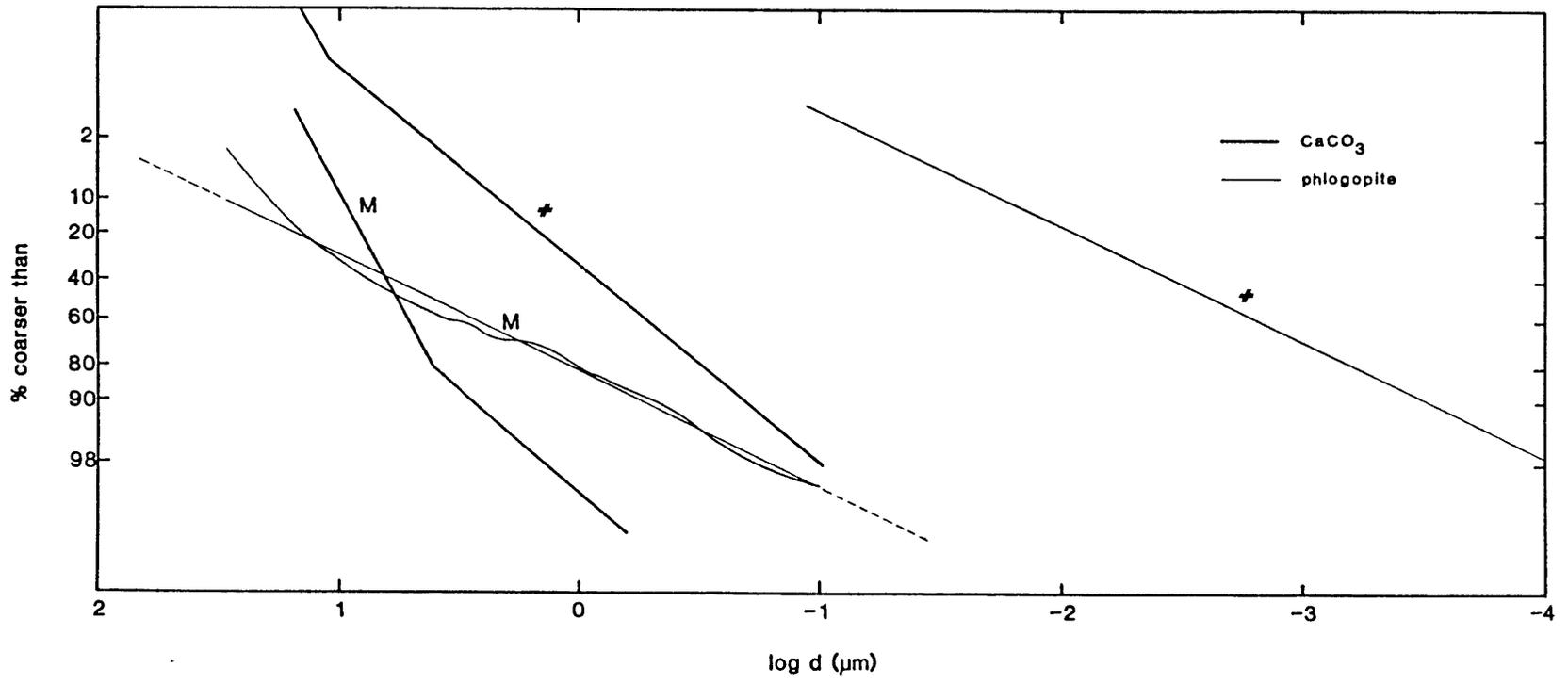
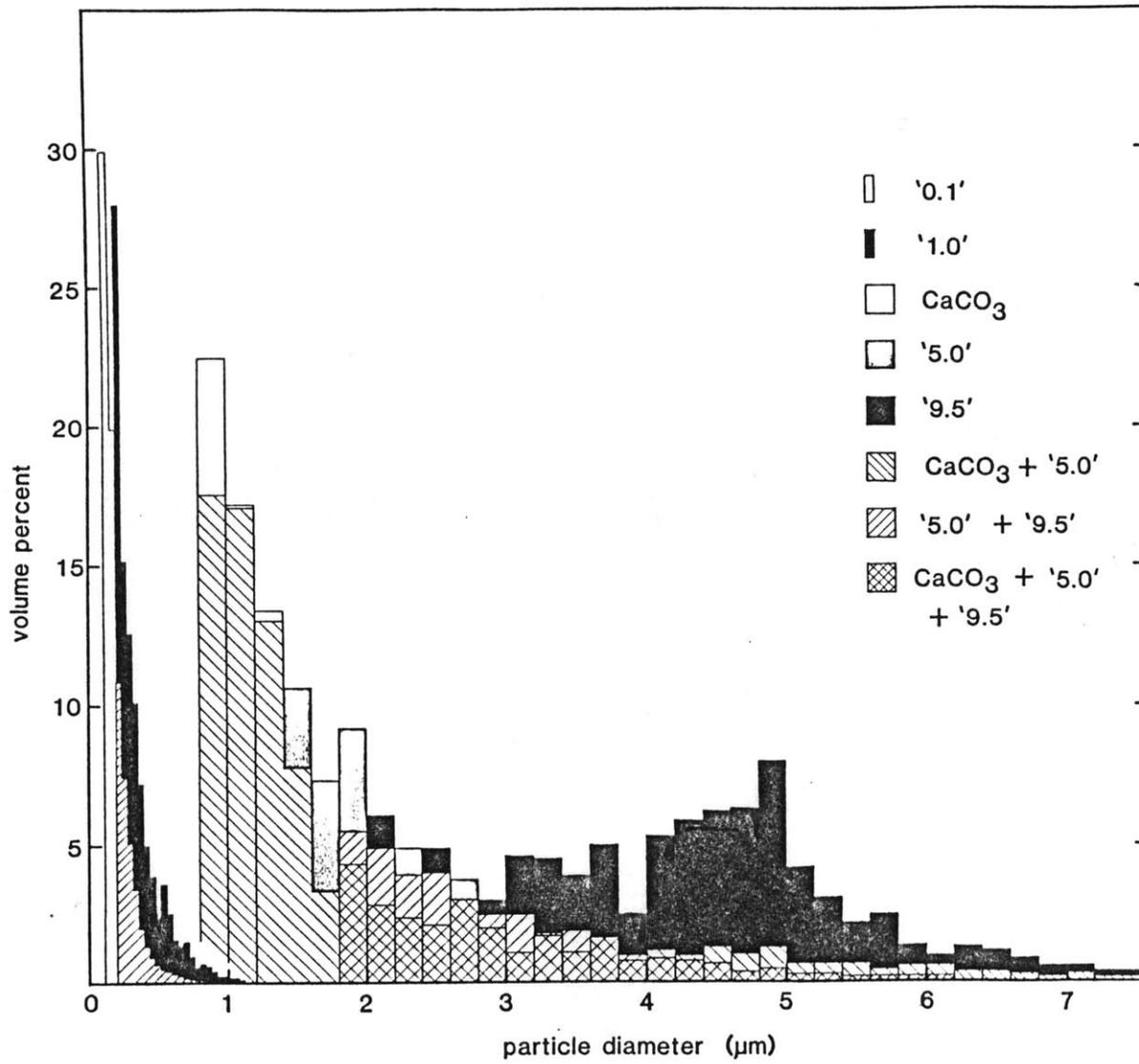


Figure 4



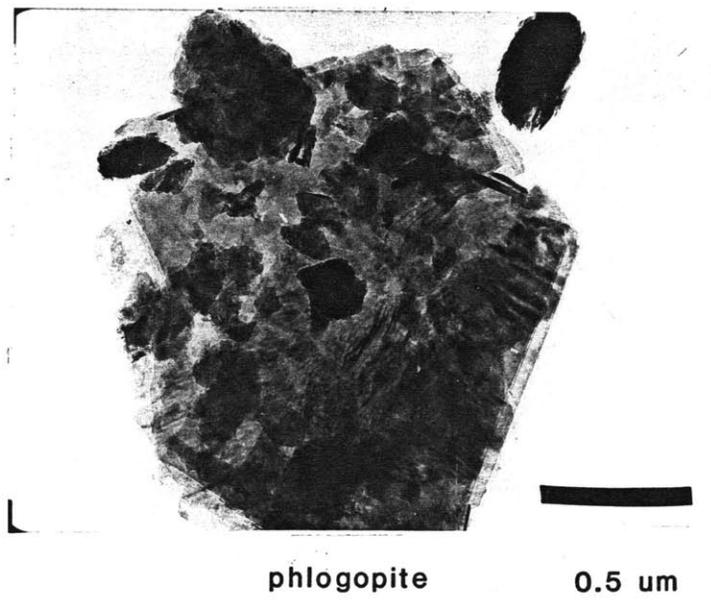


Figure 5

APPENDIX 3

TECHNIQUE USED TO IDENTIFY THIN INTERGRANULAR FILMS

Thin intergranular films are known to affect the mechanism(s) and kinetics of grain-boundary migration in ceramics (Brook, 1976, Yan, et al., 1977; Bennison and Harmer, 1985). However, unambiguous identification of such films is difficult. The most commonly used techniques are lattice-fringe imaging and conventional bright field/dark field microscopy. Lattice-fringe imaging has been used by geoscientists to determine the distribution of intergranular glass-phases as thin as 2 nm in olivine-basalt aggregates (Vaughan and Kohlstedt, 1982) but as yet has only been used to analyze intracrystalline defects in carbonates (Wenk et al., 1983). Mastering this technique requires considerably more time than was available for the present study, therefore conventional bright field/dark field methods, described by Lou et al. (1978), Clarke (1979 and 1980), and Hansen and Phillips (1983), were followed with slight modifications.

The technique used in this study involved setting up two-beam conditions such that "glassy" or very fine-grained regions were illuminated in dark-field. The procedure involved four steps: 1) Triple junctions that appeared to contain a "glassy" phase were located in bright field and centered on the optic axis (Figure 1a). Selected-area-diffraction (SAD) patterns from such regions showed the characteristic "amorphous" ring pattern (Figure 1b). 2) A portion of one of the brighter rings, preferably a portion away from a strongly reflecting spot, was rotated onto the optic axis. When this region was

then imaged in dark field, the "glassy" phase at the triple junction was illuminated. 4) In bright field, specimens were tilted so that the grain boundary of interest was parallel to the electron beam (edge-on). A "glassy" film along the grain boundary was thereby illuminated in dark field relative to the surrounding grains (Chapter 2, Figure 7b).

Complications due to ion-bombardment during the preparation of the specimen, to the conductive carbon-coat, to electron-beam damage, and to the pervasive grain-boundary cracks which resulted from thermal stresses, precluded positive identification of films less than 10 nm in thickness.

The composition of the thin intergranular film was tentatively identified by computing the crystal-lattice spacing, d , from the ring diameter, $2r$, using:

$$(\lambda L)/r = d$$

where, λ , is the electron wavelength dependent upon the accelerating voltage (100 or 200 kV), and L is the camera length which is unique for each electron microscope. The measurements of d from a single ring pattern and from a combination of several ring patterns are compared to the known lattice spacings of possible crystalline substances listed in Table 1. The correlation of the measured lattice spacings from the TEM diffraction patterns to those measured by X-ray methods supports but does not necessarily prove the contention that the intergranular "glassy" phases were derived from a melt with a composition of $\text{CaCO}_3 + \text{Ca(OH)}_2$, consistent with the observations of Wyllie and Boettcher (1969). An SAD pattern was also taken from a polycrystalline region of the sample (Figure 2), and the rings were indexed and found to be very similar to those shown in Figure 1a and listed in Table 1. Several of

the measured lattice spacings also agree with lattice spacings in carbon. However, the rings in the diffraction patterns from carbon-coated grids (Figure 3) were more diffuse than those from the "glassy" film.

Several other observations helped to identify the presence or absence of thin intergranular films: 1) Pores with dihedral angles greater than 60° were present in specimens heat-treated at low temperatures (Chapter 2, Figure 7c). 2) No thin film was detected along the boundary of a calcite bicrystal heated to over 800°C . 3) No thin film was detected in Carrera marble which was not heat-treated.

Using this technique alone, it is not possible to establish whether or not some or all of the grain boundaries in samples heat-treated above the melting temperature were completely wet. Development of a lattice-fringe imaging technique may be required to answer such a question.

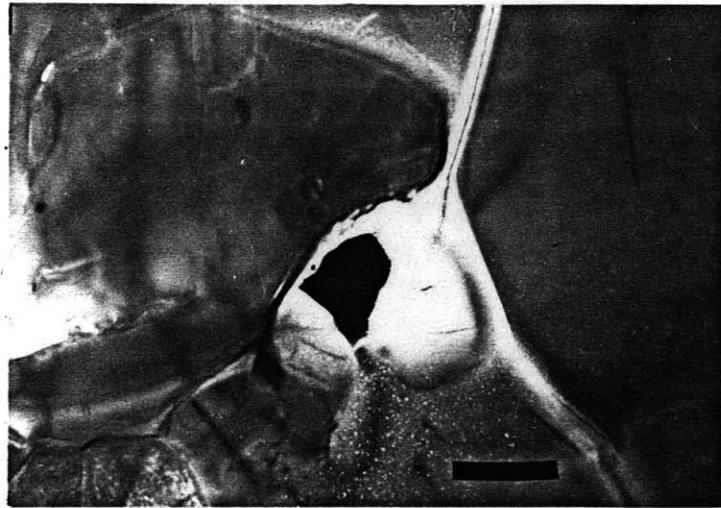
TABLE 1. Comparison of lattice spacings from ring patterns to that from X-ray data* for strongly diffracted lattice planes.

<u>Ring patterns</u>		<u>Lattice spacings</u>			
Single Pattern	Correlation of several patterns	CaCO ₃	Ca(OH) ₂	CaO	C
d(Å)		d(Å)/hkl			
	2.6	2.495/110	2.63/101	2.52	
2.25	2.2	2.28/113		2.28	
1.93	2.0	2.09/202		2.09	
		1.93/024	1.93/102	1.91	2.08/101
				1.88	1.96/012
	1.7	1.63/211	1.79/110		1.67/006
		1.60/122	1.69/111		
1.36	1.4	1.42/00 $\overline{12}$	1.45/112		1.46/015
		1.34/02 $\overline{10}$			
	1.3	1.30/128	1.31/202		
			1.21/113		1.23/110
1.17	1.2	1.18/21 $\overline{10}$	1.18/210		1.19/107
		1.14/226	1.13/203		1.12/009
1.11	1.1	1.06/20 $\overline{14}$			1.08/018
	1.0	1.01/03 $\overline{12}$	1.01/301		.99/116
		0.98/232	.96/302		
.88	.9	.88/11 $\overline{18}$.94/105		
			.90/220		
			.88/221		
.86		.86/31 $\overline{10}$.88/303		.84/00 $\overline{12}$
			.86/310		
.78		.785/41 $\overline{12}$.85/311		.79/122
.74			.81/006		
.64					
.53					

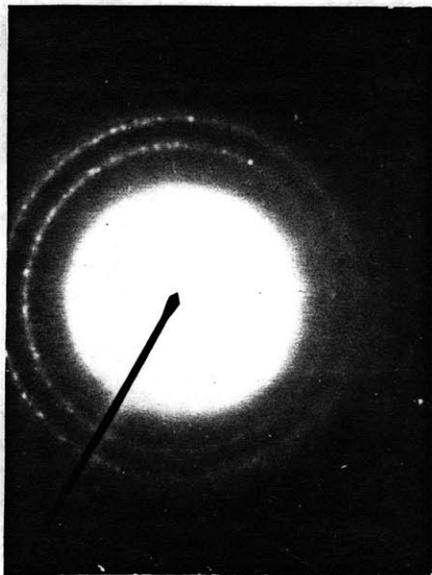
*Collected from Joint Committee on Powder Diffraction standards (JCPDS)

FIGURE CAPTIONS: APPENDIX 3

- FIGURE 1. TEM micrographs of synthetic marble. a) dark-field micrograph of "glassy" region that was used for diffracting conditions; b) the bright-field diffraction pattern from the triple junction in a); c) dark field diffraction pattern with a bright ring rotated onto the optic axis.
- FIGURE 2. TEM micrographs of: a) polycrystalline calcite from a synthetic marble; and b) diffraction pattern from the polycrystalline region in a).
- FIGURE 3. TEM micrographs of carbon. a) dark-field micrograph of carbon film; b) diffraction pattern from film showing the diffuse rings.



a dark field 1 um



b bright field

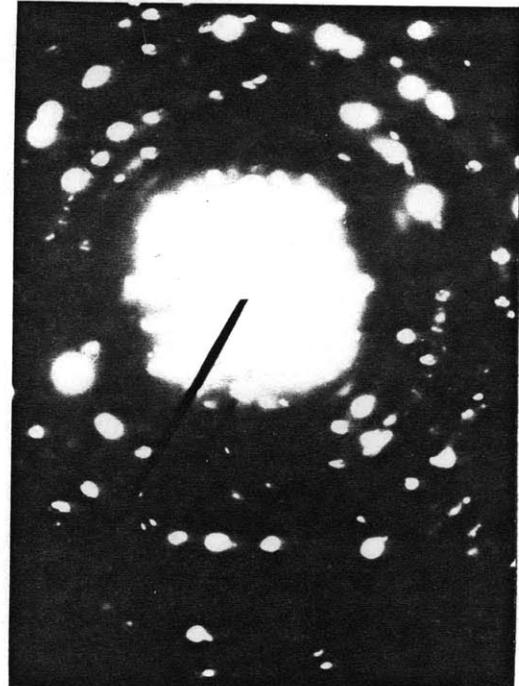


c dark field

Figure 1



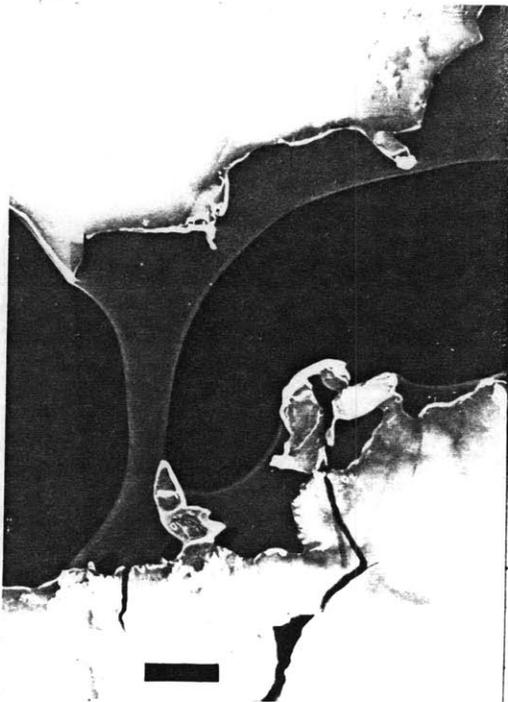
a 0.5 um



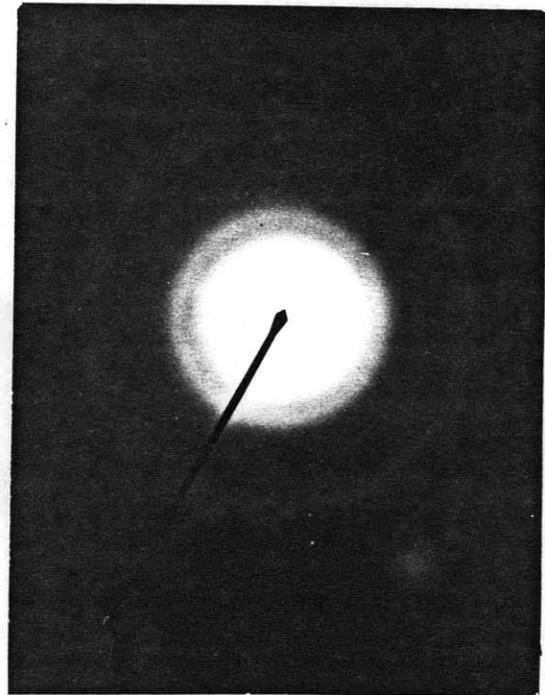
b

synthetic marble

Figure 2



a 1.0 um



b

carbon

Figure 3

BIBLIOGRAPHY

- Anand, L., and J. Gurland, The relationship between the size of cementite particles and the subgrain size in quenched and tempered steels, Metall. Trans. A., 6A, 928-931, 1975.
- Bennison, S.J., and M.P. Harmer, Grain-growth kinetics for alumina in the absence of a liquid phase, J. Am. Ceram. Soc., 68, C-22-24, 1985.
- Brook, R.J., Controlled grain growth, in Treatise on Materials Science and Technology, edited by F.F.Y. Wang, 9, 331-364, Academic Press, 1976.
- Clarke, D.R., On the detecting of thin intergranular films by electron microscopy, Ultramicroscopy, 4, 33-44, 1979.
- Clark, D.R., Observation of microcracks and thin intergranular films in ceramics by transmission electron microscopy, J. Am. Ceram. Soc., 63, 104-106, 1980.
- Flowers, J.W., Grain growth inhibition by spherical particles with a distribution of sizes, IEEE Trans. Magn., 15, 1601-1603, 1979.
- Gladman, T., On the theory of the effect of precipitate particles on grain growth in metals, Proc. R. Soc. London, 294A, 298-309, 1966.
- Hansen, S.C., and D.S. Phillips, Grain boundary microstructures in a liquid-phase sintered alumina (α -Al₂O₃), Philos. Mag. A., 47, 209-234, 1983.
- Haroun, N.A., and D.W. Budworth, Modifications to the Zener formula for limitation of grain size, J. Mater. Sci., 2, 326-328, 1968.
- Hellman, P., and M. Hillert, On the effect of second-phase particles on grain growth, Scand. J. Metallurgy, 4, 211-219, 1975.
- Herdan, G., Small particle statistics, Butterworth, London, 418p., 1960.
- Lou, L.K.V., T.E. Mitchell, and A.H. Heuer, Impurity phases in hot-pressed Si₃N₄, J. Amer. Ceram. Soc., 61, 392-396, 1978.
- Underwood, E.E., Quantitative Stereology, Addison-Wesley, Reading, Mass., 274p., 1970.
- Vaughan, P.J., and D.L. Kohlstedt, Distribution of the glass phase in hotpressed, olivine-basalt aggregates: An electron microscopy study, Contrib. Mineral. Petrol., 81, 253-261, 1982.
- Wenk, H.-R., D.J. Barber, and R.J. Reeder, Microstructures in carbonates, in Carbonates: Mineralogy and Chemistry, Reviews in Mineralogy, 11, edited by R.J. Reeder, Mineralogical Soc. of Amer., Washington, 301-367, 1983.
- Wyllie, P.J., and A.L. Boettcher, Liquidus phase relationships in the system CaO-CO₂-H₂O to 40 kilobars pressure with petrological applications, Am. J. Sci., 267-A, 489-508, 1969.

BIOGRAPHICAL NOTE

The author was born in a blizzard on February 17, 1956 in Cooperstown, North Dakota. Before the age of twelve, he lived in 9 different houses, in 7 different towns, in 3 different states; attended 7 different grade schools; played on 5 different baseball teams; and rooted for 2 different Major League clubs. His family finally settled in Rapid City, South Dakota where, in 1974, he bought a 1962 Mercedes-Benz and graduated from high school.

Thanks to geographical distribution requirements, he was able to attend Cornell University as a prospective engineer. He studied geology because he knew he was destined to be either a scientist or a farmer and didn't want to be simply a chemist, physicist, mathematician, or engineer. To stay afloat in college he gave up his degenerate, free-loading ways and became the nerd that his friends know him as today. A few traits that he did retain, besides his big mouth, were his desire to work outdoors, especially in the summer, and his interest in tinkering with old cars.

He spent two summers in South Dakota and one year deep in the heart of Texas as a tobacco-chewing field geologist chasing drill rigs across the prairie. He changed gears during his last two years in college and became interested in rock mechanics through his contact with materials science and his love to tinker with his old Mercedes. Again benefiting from his Dakota heritage he was accepted at MIT and spent many enjoyable hours, weeks, and months repairing equipment and running experiments.

Through the encouragement and companionship of an irreplaceable group of friends, he was able to rekindle his interest in physical fitness and athletic competition through softball, basketball, soccer, skiing, and especially long-distance running. After nearly twenty years as a loyal Yankee fan, he switched to the Red Sox; they kind of grow on you in Boston.

The results of his research over the last 69 months are summarized in this thesis. Chapter 1 was published in 1983 and almost all of the rest has been presented at meetings of the American Geophysical Union. The last three chapters will be submitted for publication shortly.

ACKNOWLEDGEMENTS

First and foremost, I would like to thank my parents, Senora and Ralph, my sister Janece and my brothers Paul and Roger, for their encouragement, support, and unselfishness throughout my life, particularly over the last 5 years. They continually reminded me that no matter how inflated my head got, I was still just their son or brother David; nothing more, nothing less. My gratitude is not easily expressed.

My research would not have been possible without the guidance, enthusiasm, and support of my principal advisors, Professors Brian Evans and Bill Brace. Brian suggested the main topic of my thesis and worked closely with me from the very beginning. In fact, he was ready to start the project before I had even unpacked my softball glove. My only regret is that more of his optimism and imagination didn't rub off on me. Bill suggested the topic for Chapter 1 and worked closely with me throughout the course of my research. He taught me the importance of careful, safe experimentation. Both Brian and Bill were constructively critical of my work and emphasized simplicity and purpose when performing experiments and presenting results. Bill also taught me the fine art of trail running and coached me through my first marathons; I was always amazed at how well he ran... for his age. I will miss the two-hour runs through the woods of Concord and Lincoln and Peggy's cold beer, homemade bread, and delicious fresh fruit which always followed. Financial support for this work came primarily from the National Science Foundation. NSF has been an integral part of my scientific education; they funded research projects during high school, college, and graduate school and have even funded my post-graduate research (I'm 4 for 4 with NSF research proposals).

Several other faculty members, both at MIT and Cornell, also contributed to this thesis. Bill Travers first sparked my interest in geology. Dave Kohlstedt introduced me to rock mechanics and was a major influence on my decision to attend MIT. He has kept in touch with me and my work over the last several years and has provided valuable advice and instruction on the TEM. Tim Grove gave me full access to his laboratory and tried to teach me about petrology. He and his family provided friendship, food, and beer when I needed them most. Peter Molnar, Clark Burchfiel, and the clones exposed me to tectonics and helped bridge the gap between experimental and field structural geology.

Special thanks to Sarah Luria for word processing most of this thesis and to Leigh Hall for drafting most of the figures. Madge Slavin, Jean Titilah, and Sheila Gardner handled all of the administrative work and always found money for a couple of thermocouples. Jock Hirst, Joe Walsh, and Mike Frongillo provided much needed technical assistance. My work also benefited from interactions with several present and former rock mechanics students, especially Yves Caristan and Teng-Fong Wong during the early years, and Karl Coyner, Yves Bernabe, Randy Hay and Steve Hickman during the later years.

I am fortunate to have the best group of friends anyone could ask for. Whether as teammates, officemates, roommates, or other, I will always be grateful for knowing them. Steve (nice guy) Bratt, Scott (if Ted Williams had been a Rockslider he'd have played right) Phillips, Darby (most loyal fan) Dyar, and Roger (I think I learned more about playing softball and basketball at MIT than I did about geophysics) Buck formed the core of many pick-up and intramural games. The day we beat the "Free agents" and went on to win the intramural softball championship

was the pinnacle of my sporting career. John Blendell and Carol Handwerker not only helped me understand ceramics and materials science, but were also very close friends, running partners and bike fixers. These people along with the other members of the Rocksliders, Post-Glacial Rebounders, Nine Planets, and Riverrats kept me in shape. Tom Wissler spent many hours repairing my lemon-yellow SAAB story, and Sim Wissler cooked the most delicious Chinese dinners I have ever tasted. Lind Gee, Steve Roecker, Christen Lekorenos, Eric Gustafson, Jim Kukla, Brian Wernicke, Joann Stock, Peter Crowley, Tanya Furman, Larky and Kip Hodges, Alex Kagan, Kay Sheddlock, and Michael Baker put up with my temperment day-in-and-day-out, and were always there when I needed help; I admire them for their patience and kindness.

New England is a wonderful place to live and I wish to thank Fenway Park, Maine, Haymarket, and Toscanini's for being what they are.

Finally, I wish to thank Becky and Kelly (she's a good puppy) Cleaver for all of the above... and a lot more. Over the last few years, they have been involved in all aspects of my life and really pulled me through. They showed me that there is more to life than machines and microscopes or even baseball; there are also tummy rubs and puppy-dog kisses.

Thank you all.

Yours truly,

Santa

P.S. And last but not least, to a little drugstore out in the middle of nowhere.....

"TRIPLES"

The Great American Novel
by Phillip Roth



Finish line, JFK 50-mile run, November, 1983